IMPROVEMENTS TO STRAIN COMPUTATION AND RELIABILTY ANALYSIS OF FLEXIBLE PAVEMENTS IN THE MECHANISTIC-EMPIRICAL PAVEMENT DESIGN GUIDE

By

SENTHILMURUGAN THYAGARAJAN

A dissertation submitted in partial fulfillment of
the requirements for the degree of

DOCTOR OF PHILOSOPHY

WASHINGTON STATE UNIVERSITY

Department of Civil and Environmental Engineering

MAY 2009

To the Faculty of Washington State University

The members of the Committee appointed to examine the dissertation of SENTHILMURUGAN THYAGARAJAN find it satisfactory and recommend that it be accepted.

_____
Balasingam Muhunthan, Chair

_____
Nadarajah Sivaneswaran

_____
Haifang Wen

_____
David Pollock

ACKNOWLEDGEMENTS

I would like to thank Dr. Balasingam Muhunthan for serving as the chairman of my dissertation committee and for his extended support throughout my doctoral studies. His continuous encouragement and care in addition to his valuable knowledge on the subject significantly affected the outcome of this study. I feel privileged for having had the opportunity to work and learn under the supervision of Dr. Nadarajah Sivaneswaran at Turner-Fairbank Highway Research Center (TFHRC), Mclean, Virginia

The help and assistance provided by Jim Sherwood, Katherine Petros, Eric Weaver, and members of Pavement Design and Performance Modeling team in Office of Infrastructure at TFHRC is acknowledged with gratitude.

Dr. Laith Tashman is thanked for guiding me through the initial stages of my doctoral degree program. Special thanks are due to Dr. David Pollock and Dr. Haifang Wen for serving as committee members and for their valuable input to this study. Dr. Balasingam Muhunthan, I thank you again for the extra time and attention you spent in helping me achieve my goals.

I would like to thank the Department of Civil and Environmental Engineering for accepting me to continue my education at Washington State University. I am very grateful for the unique atmosphere and the financial support the department provided at my initial stages. I greatly appreciate the financial support provided by the Federal Highway Administration through the Dwight David Eisenhower Transportation Fellowship Program which enabled me to work at TFHRC.

Lastly, but most importantly, I want to thank my parents Sumathy and Thyagarajan, my sister Lakshmi and brother-in-law Venkat for their love, support and encouragement. I am also appreciative to all my friends who made my stay during the course of my study at WSU a happy and memorable one.

IMPROVEMENTS TO STRAIN COMPUTATION AND RELIABILTY ANALYSIS OF FLEXIBLE PAVEMENTS IN THE MECHANISTIC- EMPIRICAL PAVEMENT DESIGN GUIDE

Abstract

by Senthilmurugan Thyagarajan, Ph.D.
Washington State University
May 2009

Chair: Balasingam Muhunthan

The first part of this study evaluates the effect of load-strain linear proportionality assumption employed in the Mechanistic-Empirical Pavement Design Guide (MEPDG) design of flexible pavements. In the design procedure, the strains computed through Jacob Uzan Layered Elastic Analysis (JULEA) are used to accumulate the damage and distresses over the design period. To minimize computing time, the MEPDG makes the assumption that the computed strains are linearly proportional to the applied load and exploits this assumption to extrapolate strains from an 18 kip single axle load and the specified tire pressure to the entire load spectrum in the traffic composition. However, in reality, for truck loads of interest, the contact (tire inflation) pressure remains within a narrow range whereas the contact area changes with axle load. The study showed that this assumption can lead to significant error in the prediction of Hot Mix Asphalt (HMA) rutting. A method that computes strains at three reference axle loads, and extrapolates or interpolates the strain values for other axle loads is shown to provide a suitable alternative to the MEPDG assumption.

The second phase of the study is on the improvements to the reliability analysis currently used by the MEPDG. This procedure relies on the variability of the measured output (distress) obtained from a data base. This does not directly account for the variability of the input parameters that induce such variability in distress in reliability predictions. This study developed a reliability procedure that directly evaluates the effect of uncertainties in the model input parameters of HMA materials on the reliability of flexible pavements using Monte Carlo and Latin Hypercube simulation and Rosenblueth's 2K+1 point estimate method. The proposed reliability procedure also uses some techniques to reduce the extensive computational time involved in simulations. The Latin Hypercube simulation method is found to be an efficient alternative to the computationally intensive Monte Carlo simulation. Rosenblueth's 2K+1 point estimate method is not capable to capture the output distribution type. Robust sensitivity analyses through Tornado plots and extreme tail analyses are used to identify the relative importance of the input variables on the predicted distress.

TABLE OF CONTENTS

Page

LIST OF TABLES

LIST OF FIGURES

CHAPTER 1

INTRODUCTION

The Mechanistic-Empirical Pavement Design Guide (MEPDG) of the NCHRP 1-37A project represented a major advancement to pavement design and analysis. It uses elastic, plastic, viscous, and creep properties of materials to predict the fatigue and rutting performance of pavements. The inclusion of basic material parameters that are obtained from element tests into distress prediction models in the MEPDG has facilitated the design of pavements based on site specific characteristics. The design guide also includes provisions for incorporating rehabilitation procedures of existing pavements. The MEPDG can also accommodate improvements to distress prediction models, changes in construction materials, traffic pattern, vehicle types, and tire types and configuration.

The MEPDG is currently in its evaluation stages with updates from researchers before full implementation into practice by the state departments of transportation. Some of these include the refinement of the distress prediction models, their validation of procedures, and the assumptions involved in the design analysis. One of the key assumptions in the MEPDG involves the determination of strain under different loads. To minimize computing time, the MEPDG makes the assumption that the computed strains are linearly proportional to applied load and exploits this assumption to extrapolate strains from an 18 kip single axle load and specified tire pressure to the entire load spectrum in traffic composition. This load-strain linear proportionality assumption, however, holds true only if the contact area remains the same as the load varies, resulting in similar variation in the contact pressure. However, in reality, for truck loads of

interest, the contact (tire inflation) pressure remains within a narrow range whereas the contact area changes with axle load. This reality is violated by the load-strain linear proportionality assumption. This study first evaluates the effect of non-linearity in strain extrapolation by the MEPDG on rutting prediction and puts forward an alternative scheme to overcome this drawback.

The MEPDG uses a set of mechanistic-empirical models to analyze distresses of flexible pavement structure in response to traffic, climate, and materials. These models include prediction of rutting, fatigue cracking, and thermal cracking. Practically all input variables (traffic, climate and materials) are associated with some level amount of uncertainty in their measurement. For the pavement design to be effective, uncertainty in these variables must be incorporated in a consistent manner through a reliability-based design procedure.

In order to evaluate the reliability of a selected pavement structure, the current MEPDG procedure utilizes the overall standard deviation of the measured distresses, obtained from calibration against distressed pavements, in comparison with predicted values. This technique is relatively simple; however, it is far from accurate (Design Manual, NCHRP 1-37A). It relies on a set of predetermined variability values obtained from a performance database rather than on those based on the site specific input parameters that induce such uncertainty in distress prediction. Some other limitations of the current reliability analysis include standard deviation being calibration-site specific, as well as the assumption of normality of the distribution of measured distress levels.

Thus, the second phase of the study is concerned with the improvement of the reliability analysis currently used in the MEPDG by directly incorporating the effects of

variability and uncertainty of the material inputs on distress prediction with a focus on flexible pavements. The reliability of pavement distress for a given level of uncertainty in material input is evaluated through Monte Carlo and Latin Hypercube simulation techniques and the Rosenblueth's Point Estimate Method.

Current sensitivity analyses of the predicted distresses involve the quantification of their deviation based only on the variation of one input variable at a time. This does not account for the combined influence of the input parameters on distress in the field. Robust techniques that account for their combined effect on the sensitivity of distress prediction are proposed. The sensitivity analyses are performed with the simulated data obtained from the proposed reliability procedures.

1.1 Scope and Outline of the Dissertation

The main objectives of the study are to:

1. Improve the prediction of load-strain behavior in MEPDG,
2. Develop and validate methods to predict pavement distress reliability, and
3. Develop improved methods of sensitivity analysis

Chapter 2 reviews the basics of the flexible pavement design procedure described in the Mechanistic-Empirical Pavement Design Guide (MEPDG). The materials properties, traffic and climatic inputs required for design analysis are discussed. The probabilistic characteristics of the input variables as reported in past literature are reviewed. The distress models and the reliability procedures used in the MEPDG relating to this study are also discussed. This chapter concludes with the review of some simulation techniques that are used in the determination of system reliability and past studies that attempted reliability analysis for pavement design.

The effects of strain extrapolation on distress prediction are studied in Chapter 3. A computer code based on MEPDG design procedure is developed first. The code is then modified to compute the strain at each axle load level. The extent of the deviation by MEPDG procedures in distress prediction as a result of non-linearity is determined. An alternate technique that overcomes this limitation is proposed.

The techniques proposed to directly account for the uncertainty of input variables in pavement reliability analysis are provided in Chapter 4. The study is focused on the development of efficient techniques to incorporate Hot Mix Asphalt (HMA) material variability into reliability analyses. These procedures, however, are general enough to incorporate uncertainties in other input variables in the future. Probabilistic characteristics of the material input variables are obtained from Long Term Pavement Performance (LTPP) literature. Methods that reduce the extensive computational time involved in reliability simulation analysis are identified. Design reliabilities obtained from the current MEPDG method are compared to the proposed methodology.

The efficiency of the proposed procedure is compared with past studies in Chapter 5. This chapter also discusses the relative merits of the simulation techniques, Monte Carlo, Latin Hypercube, and Rosenblueth's Point Estimate in terms of their efficiency, accuracy and computational feasibility in practice. Robust methods to conduct sensitivity and extreme tail analyses with simulation data are presented. The implications of these analyses to practice are discussed.

A summary of the study findings and recommendation for future research are provided in Chapter 6.

CHAPTER 2

BASICS OF MEPDG AND RELIABILITY ANALYSIS

2.1 Introduction

The basic principles of MEPDG are described first followed by a discussion of the salient features of some modern reliability analysis techniques. Since the MEPDG design manual (NCHRP, 2004) is readily accessible, the review is confined to only sections that are used in this study. The chapter concludes with a discussion of some notable simulation techniques of reliability analysis.

2.2 Mechanistic Empirical Pavement Design Guide

The MEPDG is a software that is used to predict the various pavement distresses for given material, traffic and climatic conditions. The designer selects a trial design project and executes the software to compute the distresses to ensure that an established performance criterion is met. The main steps involved in the procedure for the design of flexible (HMA) pavements are illustrated in Figure 2.1. They are briefly described as follows:

1. First, the guide requires as input, the details of pavement structure, material properties and expected site-specific data such as traffic and climate.

2. For the given conditions, the Enhanced Integrated Climatic Model (EICM) and Global aging models which are integral within the software, develop moisture and temperature profile, and calculate the material and climatic input parameters

needed for the distress models. The traffic data is processed to obtain the number of load repetitions for each axle load increment and type.

3. For each incremental design period, structural responses at critical locations corresponding to the distresses are computed using a layered elastic analysis program.

4. Nationally calibrated distress model coefficients in the design guide are modified for local conditions based on available long term performance data.

5. The structural responses, material and traffic data are used by the distress models to compute the accumulated damage at the end of each month of the design period.

6. The reliability of the predicted distress is determined based on predetermined the standard deviation values.

7. Adequacy of the trial design is verified by comparing the distress prediction at the given reliability level with the expected performance values.

The MEPDG evaluates the adequacy of the trial design based on key pavement distresses and profile smoothness for the chosen period. The structural distresses evaluated by the design guide for flexible pavements include:

- Fatigue Bottom-up (or alligator) cracking
- Fatigue Surface-down (or longitudinal) cracking
- Permanent deformation (or rutting)
- Thermal cracking, and
- Fatigue of chemically stabilized layers (for Semi-rigid pavements only)

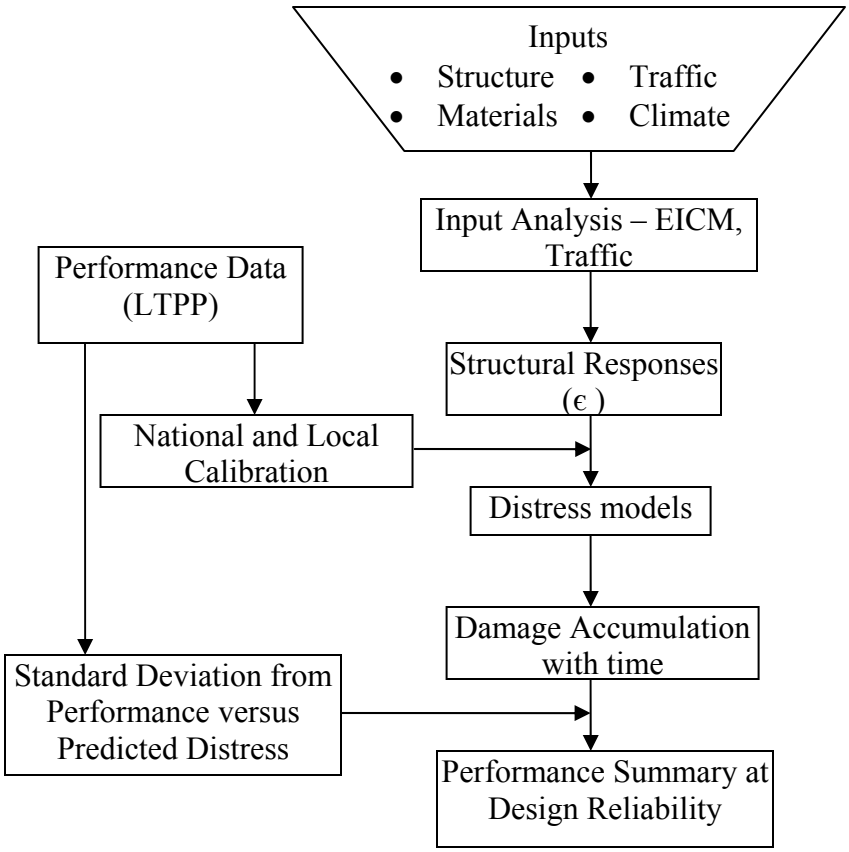

Figure 2.1 Flowchart for MEPDG Design Procedure

The structural response models built within the MEPDG form the core of the mechanistic-based design methodology. The models for the design of flexible pavements in the guide are based on the response computed from the multi-layer elastic program JULEA (Jacob Uzan Linear Elastic Analysis) or on the 2-D finite element program, Disturbed State Concept DSC2D (for non linear analysis). The DSC2D program is used only when the designer chooses to use the Level 1 input to characterize the non-linear response of unbound layer materials (such as bases, sub-bases and/or sub-grades).

The computational procedure for flexible pavements can be summarized as follows:

The trial design (thickness) is analyzed by dividing the target design life into smaller increments (usually monthly). Linear or nonlinear models are used as chosen to compute the stress and/or strain values at specific critical locations for each distress type at each increment period. Note that within each increment, factors such as traffic levels, modulus of asphalt concrete, base, subbase and subgrade that affect the flexible pavement responses are kept constant. The critical stress and/or strain values are converted to incremental distresses, either in absolute terms (incremental rut depth) or in terms of a damage index (fatigue cracking) using appropriate performance models. Incremental distresses and/or damage are summed over all increments. The output of the MEPDG software is usually provided in the form of plots of accumulated damage at the end of each analysis period.

Figure 2.2 shows a typical variation of International Roughness Index (IRI) with time obtained from the MEPDG software. The input parameters of the trial section are modified and the procedure is repeated until a satisfactory design with the required reliability is achieved.

2.3 Uncertainty of MEPDG Input Variables

Pavement deterioration is the result of a combination of different types of distress. They include, fatigue cracking due to repeated loads or environmental cycles, shear deformation of the pavement structure, and disintegration of materials due to breakage of mechanical or chemical bonds as a result of weathering, infiltration, or loading. Thus, an accurate prediction of the pavement deterioration characteristics over the whole life-cycle analysis period of the pavement design is important for pavement management. Pavement maintenance and rehabilitation programs depend on this prediction.

Consequently, the pavement performance prediction model forms an integral part of a pavement management system.

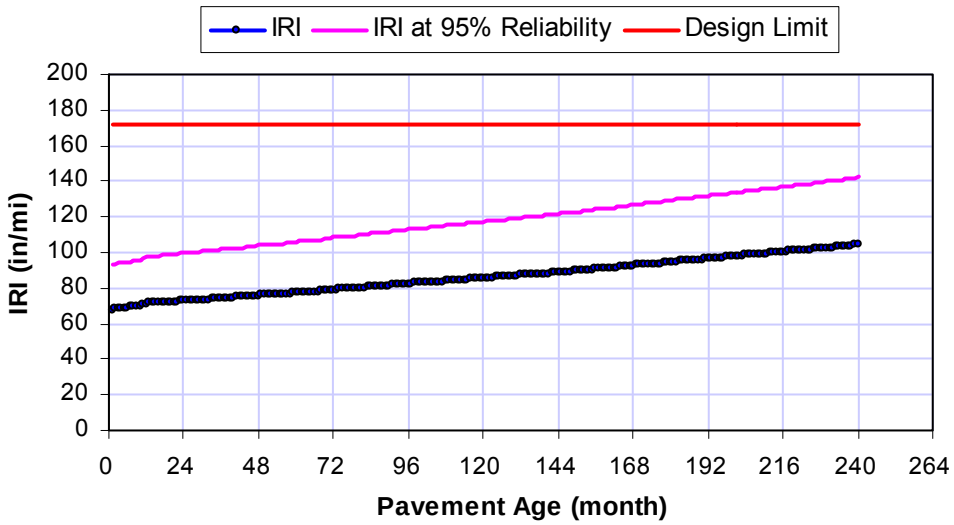

Figure 2.2 Variation of International Roughness Index (IRI) with Design Period (after NCHRP, 2004)

Pavement distress prediction models used in MEPDG are a function of different input variables. These variables have a certain level of uncertainty associated with them. Thus, for a comprehensive reliability analysis, uncertainties associated with input parameters and the prediction models need to be quantified. These include estimation of variance and uncertainties associated with design inputs such as traffic loadings, climate, material properties, layer thickness, and errors in the models themselves.

The incremental distress analysis of the MEPDG requires inputs for each incremental period of the design period. The inputs for the structural response model include:

- Traffic loading
- Pavement cross-section
- Poisson's ratio for each layer
- Elastic modulus for each layer
- Thickness of each layer
- Layer to layer friction
- Coefficient of thermal contraction and expansion for HMA and PCC, respectively.
- Temperature and its gradient in HMA materials
- Moisture gradient in PCC slab.

The effect of input uncertainty on the pavement distress prediction has been studied in the past by several investigators. The effect of uncertainty in material strength and traffic growth on the performance of rigid and flexible pavements was studied using Monte Carlo simulation by Lemer and Moavenzadeh (1971). By treating the uncertainty in material strength with different coefficients of variation, the authors studied the variation between probability of failure and axle loads (in terms of Equivalent Single Axle Load, ESAL) as shown in Figure 2.3. It can be seen that for a given axle load, an increase in the coefficient of variation of material strength increases the probability of failure. These authors have also quantified the effect of traffic growth rate on possible failure age.

The inherent relationship between the probabilistic and deterministic prediction models was analyzed by Li et al. (1997). The pavement distress in terms of Pavement Condition Index (PCI) was evaluated using two deterministic flexible pavement

deterioration models given by Ontario Pavement Analysis of Costs and AASHTO guide. The deterministic equations were converted to probabilistic ones by considering each design variable to be normally distributed. The probability of the pavement at a certain level of deterioration in terms of PCI was tabulated for its design period. Both deterministic and probabilistic designs were found to have similar deterioration during the early stages of the pavements but were found to diverge at later years.

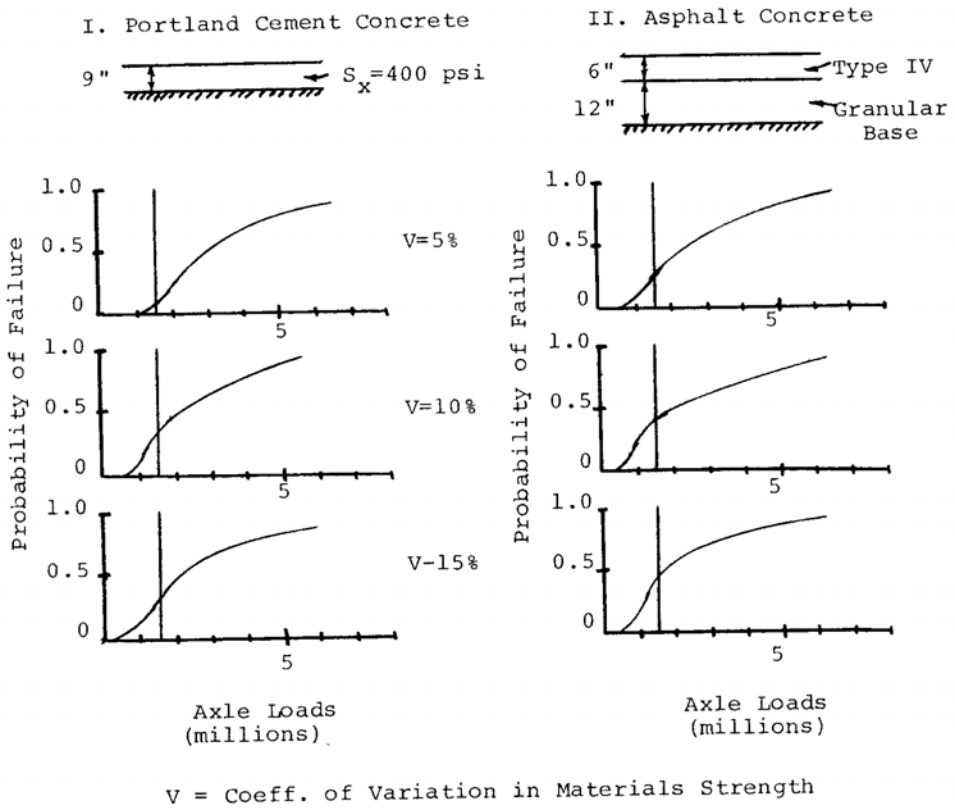

Figure 2.3 Effect of Material Uncertainty on Probability of Failure in Rigid and Flexible Pavements (after Lemer and Moavenzadeh, 1971)

Kim and Buch (2003) categorized uncertainties affecting pavement performance into two groups. The first group termed 'Uncertainties of design parameters' represented the spatial variability and inconsistent estimates of inputs. The second group termed

'Systematic errors' represented model bias and statistical errors. Uncertainties of design parameters led to variations of the shape of probabilistic distribution of the performance function. Systematic errors were found to cause a shift in the location of the probabilistic distribution of the performance function resulting in consistent deviations (Figure 2.4). The representative ratio of the measured to predicted a pavement performance value was used to quantify 'Systematic errors'. This ratio, termed professional factor, reflected uncertainties of the assumption and simplifications used in design models.

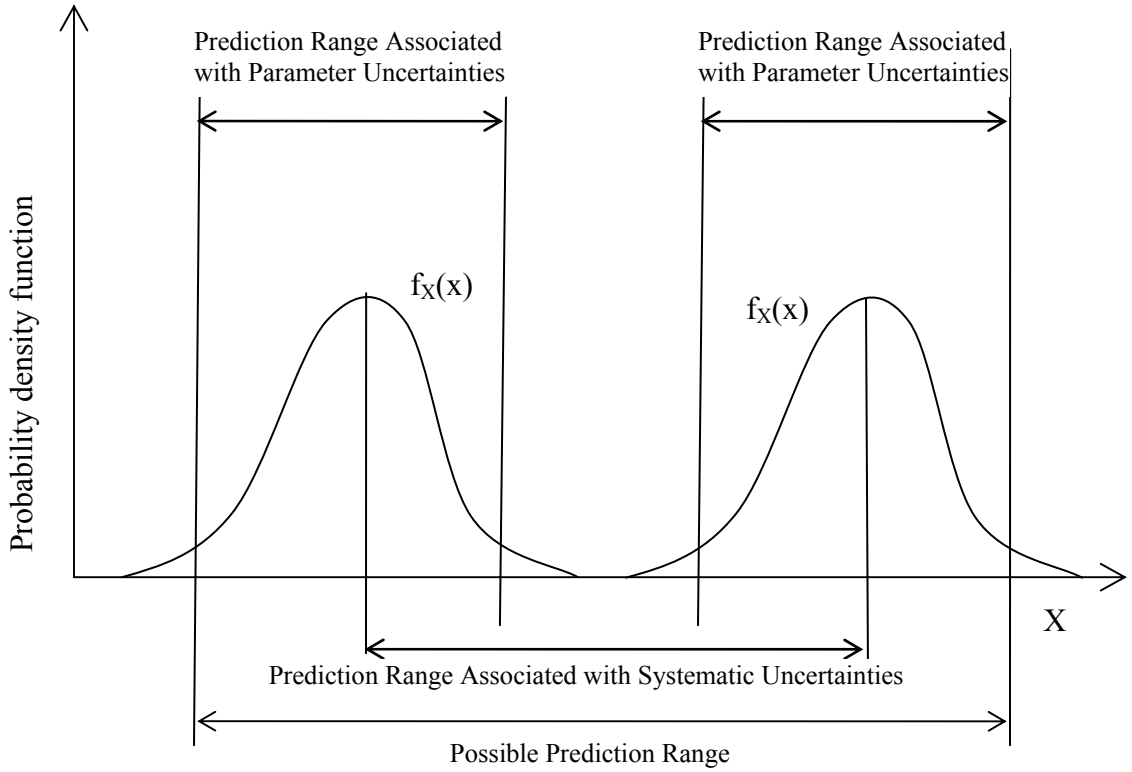

Figure 2.4 Integrated Presentation of Types of Uncertainties Associated with M-E Flexible Pavement Design (after Kim and Buch. 2003)

2.3.1 Probabilistic characteristics of variables

The technique of deriving probabilistic information from observational data makes use of statistical inference. Information obtained from the sample data of the

population is used to make generalizations about population characteristics. It should be noted, however, that the parameters obtained from these samples are only estimates and can only predict the occurrence of an event with an associated probability (Ang and Tang, 1975). The underlying uncertainty may occur as the result of either variability (inherent or natural) or prediction error.

Estimation of probabilistic parameters is divided into Point or Interval estimates. Point estimates calculate a single number, from a set of observational data, to represent the probabilistic parameter of the underlying population. Interval estimates establish a confidence range for the quantity. The point estimate method is used in this study.

The most common point estimate methods are the method of moments and the method of maximum likelihood. The method of moments estimates mean and variance from which other parameters of the probabilistic distribution can be determined. Table 2.1 is a summary of the common probabilistic distributions. The table also highlights the characteristic parameters of these distributions.

The mean and variance estimates of a sample size n, namely x_1, x_2,…, x_n are given respectively by:

$$\text{Sample Mean} = E(X) = \bar{x} = \frac{1}{n}\sum_{i=1}^{n} x_i$$

and (2.1)

$$\text{Variance} = \text{Var}(X) = \frac{1}{n-1}\sum_{i=1}^{n} (x_i - \bar{x})^2$$

where X is the population and x_1, x_2,…, x_n are its values

Table 2. 1 Common Distribution Type and their Parameters (after Ang and Tang, 1975)

Distribution	Probability Density Function (PDF) or mass function (PMF)	Parameters	Relation to Mean and Variance
Normal (Gaussian)	$f_x(x) = \frac{1}{\sqrt{2\pi}\sigma}\exp\left[-\frac{1}{2}\left(\frac{x-\mu}{\sigma}\right)^2\right]$ $-\infty < x < \infty$	μ, σ	$E(X) = \mu$ $Var(X) = \sigma^2$
Lognormal	$f_x(x) = \frac{1}{\sqrt{2\pi}\zeta_x}\exp\left[-\frac{1}{2}\left(\frac{\ln x - \lambda}{\zeta}\right)^2\right]$ $x \geq 0$	λ, ζ	$E(X) = \exp(\lambda + \frac{1}{2}\zeta^2)$ $Var(X) = E^2(X)[e^{\zeta^2} - 1]$
Uniform	$f_x(x) = \frac{1}{b-a}$ $a < x < b$	a, b	$E(X) = (a+b)/2$ $Var(X) = \frac{1}{12}(b-a)^2$

The method of maximum likelihood derives the point estimate of the parameter directly depending on the type of distribution. The likelihood function of n independent observations $x_1, x_2, \ldots, x_n$ is given by (Ang and Tang 1975):

$$L(x_1, x_2, \ldots, x_n; \mu_1, \mu_2) = \prod_{i=1}^{n} f(x_i; \theta_1, \theta_2) \qquad (2.2)$$

where μ_1, μ_2 are the parameters of the underlying distribution function f(X). The maximum likelihood estimator is the value of the parameter μ that maximizes the likelihood function $L(x_1, x_2, \ldots, x_n; \mu_1, \mu_2)$. It can be obtained from the solution of the following differential equation (Ang and Tang 1975):

$$\frac{\partial L(x_1, x_2, \ldots, x_n; \mu_1, \mu_2)}{\partial \theta_j} = 0 \qquad (2.3)$$

The probability density function (PDF) of the random variable is required in most reliability analyses. The underlying distribution of the significant variable can be obtained through goodness-of-fit test such as Test of Skewness and Kurtosis, Chi-Square test or Kolmogorov- Smirnov (K-S) Test.

Limited availability of data in the past had constrained the development of suitable probabilistic distribution functions of the input variables for pavement design. Thus, researchers had usually proposed typical values for the coefficient of variation from their own experience. For example, Alsherri and George (1988) developed a reliability analysis of the 1985 AASHTO design guide using the Monte Carlo simulation technique. The variables were assumed to follow a normal distribution with coefficients of variation as summarized in Table 2.2 and Table 2.3, respectively for flexible and rigid pavements.

Table 2. 2 Typical Variability in Input Data for Flexible Pavements (after Alsherri and George 1988)

Material Characteristic	Mean Value	Coefficient of Variation (%)
Annual Traffic, 18kip ESAL application	600,000	30
Subgrade Resilient Modulus (M_r)	34.4 MPa (5000 psi)	20
Drainage Coefficient Base Sub-Base	 1 1	 10 10
Model Error (σ_{ME})	0.46	NA
Initial serviceability index	4.5	6.7
Terminal serviceability index	2.5	16

Table 2. 3 Typical Variability in Input Data for Rigid Pavements (after Alsherri and George 1988)

Material Characteristic	Mean Value	Coefficient of Variation (%)
Modulus of rupture	4.5 MPa (650 psi)	10
Modulus of Elasticity	34,500 MPa (5E6 psi)	3.8
Load transfer coefficient, J	3.2 (JCP) 2.56 (CRC)	0.32
Modulus of subgrade reaction (k)	0.095 N/mm^3 (350pci)	35
Drainage Coefficient, (C_d)	1	10
Annual precipitation	130cm	15
Freezing index	0	20
Initial serviceability index	4.5	6.7
Terminal serviceability index	2.5	16

With the availability of additional data (e.g. Long Term Pavement Performance (LTPP) database), refined estimates of the probabilistic characteristics for key input variables used in pavement models are reported in the literature. The values are obtained from various design projects and hence a range of possible probabilistic characteristic values for each variable is reported. Table 2.4 summarizes some published probabilistic characteristics values of the input variables used in flexible pavement structural response models.

Variability associated with pavement thickness was analyzed by Jiang et al. (2003) from more than 4000 pavement layers including both flexible and rigid sections in the LTPP database. The study included characterization of the spatial variation in layer thickness at different locations (distribution); comparisons within section layer thickness

measurements from elevation and core thickness measurements; and the extent of differences in layer thickness data between as-designed and mean as-compacted thicknesses.

Table 2. 4 Summary of Variability in Design Input Parameters (After Kim and Buch 2003)

Property	Coefficient of variance, range %	Type of Distribution
AC Thickness	3-12	Normal
	3-12	Normal
AC modulus	10-40	Lognormal
	10-20	Normal
Base Modulus	10-30	Normal
	5-60	Lognormal
Subbase Modulus	10-30	Normal
	5-60	Lognormal
Subgrade Modulus	10-30	Normal
	20-45	Lognormal
Traffic	42	Lognormal

Jiang et al. (2003) performed the goodness of fit test between the assumed theoretical distribution and the distribution of the observed data through Skewness and Kurtosis tests. At 1% level of significance about 86% of all layer thickness frequency distributions were not rejected for being considered as normally distributed. The variances of the layer thickness measured by elevation and core thickness methods were

statistically analyzed through F-test at 99% confidence level. For more than 82% of the sections, the differences in variances were not statistically significant. However, the mean layer thickness computed from these two methods show uniformity only in 56% of all layers analyzed through statistical t-test at 95% confidence level. The differences were reported within 12.7 mm for 74% of the layers and within 25.4mm for 92% of the layers. A summary of statistical deviation of design thickness and as-compacted thickness were presented for different pavement material types. Also it was reported that for the same layer and material type, the mean constructed layer thickness tend to be above the designed value for the thinner layers and below the design value for the thicker layers. The mean constructed layer thicknesses for PCC layers and LC base layers were reported as generally above the designed thickness values.

A report (FHWA-RD-02-001) summarizing the probabilistic characteristics of most variables involved in pavement design was published by Office of Infrastructure of Federal Highway administration (FHWA) at Turner-Fairbank Highway Research Center (TFHRC). It was based on parameters available in LTPP database. The variables were found to be normally distributed with probabilistic characteristics as given in Table 2.5. The current study utilizes only the probabilistic characteristics of the HMA mix variables.

2.4 Hierarchical Input Levels in MEPDG

The MEPDG provides the designer with flexibility to choose the level of inputs for a project, based on its criticality, sensitivity of the pavement performance to a given input, and the availability of resources. This is done using a hierarchical approach with

regard to inputs relating to traffic, materials, and environment. In general, three levels of inputs are provided (NCHRP, 2004).

Table 2. 5 Typical Variability in Pavement Design Inputs (Report No. FHWA-RD-02-001)

Variable	Standard Deviation	COV
Thickness		
HMA – Overlay	27 mm	49.4 %
HMA – Original Surface	51 mm	74.6 %
Base	66 mm	46.4 %
Sub-Base	10 mm	10 %
Air Void	1 to 2 %	
Bulk Specific Gravity		Max 2%
Maximum Specific Gravity		Max 1%
Asphalt content of HMA	Max 0.5 %	Max. 10%
Aggregate Gradation		
Coarse (4.75 to 12 mm)	1.7 to 4.9 %	
Fine (75 μ to 2 mm)	0.4 to 2.8 %	
Subgrade Unconfined Compressive Strength		
Fine Graded	1.5 – 10 kPa	1.6 - 26.1 %
Coarse Graded	1.7 – 49.2 kPa	2.6 – 26.8 %

Level 1 input provides for the highest level of accuracy and, thus, would have the lowest level of uncertainty or error. Level 1 input are typically used for designing heavily used pavements or wherever there is dire safety or economic consequences of early failure. Level 1 material input requires laboratory or field testing. These include dynamic

modulus of hot-mix asphalt concrete, collection of site-specific axle load spectra data, and nondestructive deflection testing of existing pavement. It is evident that Level 1 inputs require more resources and time than for other levels.

Level 2 input is used when resources or testing equipment are not available as in Level 1. These inputs typically could be user-selected, possibly from an agency database, derived from a limited testing program, or estimated from correlations. Examples of level 2 input include, the estimation of asphalt concrete dynamic modulus from binder, aggregate, and mix properties, estimation of Portland cement concrete elastic moduli from compressive strength tests, and use of site-specific traffic volume and traffic classification data in conjunction with agency-specific axle load spectra. Level 2 inputs thus provide an intermediate level of accuracy.

Level 3 inputs provide the lowest level of accuracy. This level is used for cases when there is minimal consequence of early failure as in low volume roads. These inputs are typically user-selected based on averages for the region. Examples include, default unbound materials resilient modulus values or default Portland cement concrete coefficient of thermal expansion for a given mix classes and aggregates used by an agency.

For a given design project, inputs may be obtained using a mix of the three levels, such as concrete modulus of rupture from Level 1, traffic load spectra from Level 2, and subgrade resilient modulus from Level 3. It is important to note regardless of the level of input used, the computational algorithms in the MEPDG perform the same distress calculations.

2.5 Flexible Pavement Materials

Flexible pavement consists of a Hot Mix Asphalt material (HMA) layer followed by unbound layers. The properties required for each of this material layer are summarized in Table 2.6. The procedures outlined by the MEPDG to obtain the material properties at different hierarchal input levels are subsequently discussed.

Table 2. 6 Material Inputs Required in MEPDG (NCHRP, 2004)

Materials Category	**Required Materials Inputs**		
	Materials inputs required for critical response computations	**Additional materials inputs required for distress/transfer functions**	**Additional materials inputs required for climatic modeling**
Hot-Mix Asphalt Materials (surface, binder, base, and sub-base courses)	• Time-temperature dependent dynamic modulus (E*) of HMA mixture. • Poisson's ratio.	• Tensile strength, creep compliance, coefficient of thermal expansion.	• Surface shortwave absorptivity (only required for surface course), thermal conductivity, and heat capacity of HMA. • Asphalt binder viscosity (stiffness)
Unbound Base/ Sub-base and Subgrade Materials	• Seasonally adjusted resilient modulus (M_r). • Poisson's ratio. • Unit weight. • Coefficient of lateral pressure.	None	• Plasticity index, gradation parameters, effective grain sizes, specific gravity, saturated hydraulic conductivity, optimum moisture contents, parameters to define the soil water characteristic curve.
Bedrock	• Elastic modulus (E). • Poisson's ratio. • Unit weight.	None.	None.

2.5.1 Hot mix asphalt materials

The layered elastic analysis program (JULEA) requires the asphalt binder viscosity, dynamic modulus of the mix and Poisson's ratio to compute the structural response for a given load. Asphalt binder stiffness (G*) is used to obtain the relation between the asphalt viscosity and temperature. The Global aging models apply the effect of aging, loading frequency and layer depth on viscosity. The aged viscosity value is used to calculate the shift factors and then the dynamic modulus in each sub-layer. These properties and procedures are explained below.

Asphalt Binder Viscosity (η)

For Level 1 and 2 inputs, the binder viscosity (η) is calculated from the binder stiffness data obtained from Dynamic Shear Rheometer test (AASHTO T315). The relation between the viscosity and the temperature is used to compute regression parameters A and VTS as (NCHRP, 2004):

$$\log\log\eta = A + VTS * \log T_R \qquad (2.4)$$

where, T_R is the temperature in Rankine, the parameters, A and VTS depend on the binder PG grade.

For Level 3 input, values for A and VTS are obtained based on the PG grade used.

Dynamic modulus (E*) Master Curve and Shift Factors

Dynamic modulus (E^*) is the primary stiffness property of interest in asphalt materials. The dynamic modulus of asphalt concrete is a function of temperature, rate of loading, age, and mixture characteristics such as binder stiffness, aggregate gradation,

binder content, and air voids. For input Level 1, dynamic modulus values for a given mixture are determined from tests conducted at different temperatures and frequencies. For Level 2 and 3 inputs the dynamic modulus is calculated from the mixture characteristics, temperature and frequency inputs through a predictive equation presented later (Eq. 2.7). The derived dynamic moduli are transformed to a sigmoid function (termed master curve) at a reference temperature (usually 70^0 *F*). The modulus of the asphalt concrete at all analysis levels is determined from the master curve using appropriate shift factors, to account for effect of temperature, rate of loading, and depth of the layer.

Dynamic Modulus Estimation for different loading frequency and temperature conditions

The time of loading varies along the depth of the pavement as shown in Figure 2.5. Since the loading frequency (inverse of load pulse time) decreases with depth, the dynamic modulus reduces with depth. The Global aging model considers the variation of the frequency with depth and the aging that occurs in the asphalt under field condition and calculates the shift factor. The shift factor computed for each season over the design period is used to get the corresponding asphalt dynamic modulus from the master curve. The procedure is as follows:

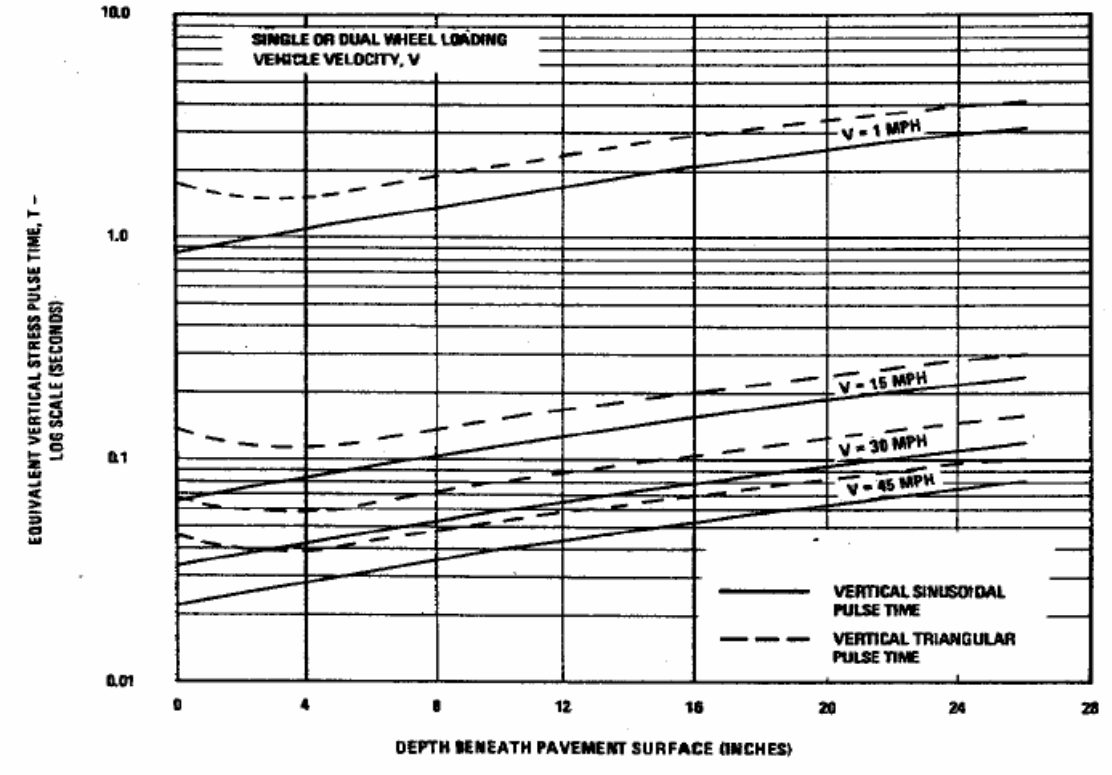

Figure 2. 5 Variation of Equivalent Vertical Stress Pulse Time with Vehicle Velocity and Depth

Step 1: Development of Master Curve and Shift Factors at 70 °F for original condition.

Master curves are constructed using the principle of time-temperature superposition. First, a standard reference temperature is selected (in most cases, 70 °*F*). The data at various temperatures are shifted with respect to time (load frequency) until the curves merge into a single smooth function. The master curve of modulus as a function of time formed in this manner describes the load time dependency of the material. The amount of shifting at each temperature required to form the master curve describes the temperature dependency of the material. Thus, both the master curve and the shift factors are needed for a complete description of the load rate and temperature effects.

Master curve can be represented by a sigmoidal function described by (NCHRP, 2004):

$$\log(E^*) = \delta + \frac{\alpha}{1 + e^{\beta + \gamma \log t_r}} \tag{2.5}$$

where

E^* = Dynamic modulus (psi)

t_r = Time of loading at the reference temperature (shift factor)

δ = Minimum value of E*

$\delta + \alpha$ = Maximum value of E*

β, γ = Parameters describing the shape of the sigmoidal function

The parameter δ is a function of aggregate gradation, and effective binder and air void contents. The parameter α is dependent only on aggregate gradation. Thus, the minimum (δ) and maximum ($\delta + \alpha$) dynamic modulus values are independent of the binder stiffness. This is quite rational since binders tend toward similar high stiffness at very low temperatures. At very high temperatures, internal friction dominates and the influence of the binder stiffness is small. The rate at which the modulus changes from the maximum to the minimum depends on the characteristics of the binder.

The shift factor at the reference temperature can be obtained by:

$$\log(t_r) = \log(t) - c(\log(\eta) - \log(\eta_{Tr})) \tag{2.6}$$

where

t = time of loading at given temperature of interest.

c – material property

η = aged viscosity at evaluation depth and temperature,

η_{Tr} = viscosity at reference temperature and RTFO aging. (used for generating master curve)

Level 1**:** Master curves and the corresponding shift factors are developed experimentally by shifting laboratory frequency sweep data from either dynamic modulus tests, NCHRP 1-28A, or shear tests, AASHTO T320, "Determining Shear Strain and Stiffness of Asphalt Mixtures Using the Superpave Shear Test (SST)". The parameters δ, α, β, γ in Equation 2.5 and c in Equation 2.6 are obtained by nonlinear optimization of the master curve developed from the lab data.

Level 2 or 3**:** Master curves are developed directly from the dynamic modulus predictive equation below (Witczak and Fonseca for NCHRP, 2004):

$$\log E^* = 3.750063 + 0.02932\rho_{200} - 0.001767(\rho_{200})^2 - 0.002841\rho_4 - 0.058097V_a$$
$$- 0.802208\left(\frac{V_{beff}}{V_{beff} + V_a}\right) + \frac{3.871977 - 0.0021\rho_4 + 0.003958\rho_{38} - 0.000017(\rho_{38})^2 + 0.005470\rho_{34}}{1 + e^{(-0.603313 - 0.313351\log(f) - 0.393532\log(\eta))}} \quad (2.7)$$

where:

E^* = dynamic modulus, psi.

η = bitumen viscosity, 10^6 Poise.

f = loading frequency, Hz.

V_a = air void content, %.

V_{beff} = effective bitumen content, % by volume.

ρ_{34} = cumulative percentage retained on the ¾ in sieve.

ρ_{38} = cumulative percentage retained on the 3/8 in sieve.

ρ_4 = cumulative percentage retained on the No. 4 sieve.

ρ_{200} = percentage passing the No. 200 sieve.

The parameters δ, α, β, γ in Equation 2.5 and c in Equation 2.6 are obtained by comparing the master curve and the sigmoidal function. The relations are given by

$$\begin{aligned}
\partial &= 3.750063 + 0.02932\rho_{200} - 0.001767(\rho_{200})^2 - 0.002841\rho_4 - 0.058097V_a - 0.802208\left[\frac{V_{beff}}{V_{beff} + V_a}\right] \\
\alpha &= 3.871977 - 0.0021\rho_4 + 0.003958\rho_{38} - 0.000017\rho_{38}^2 + 0.005470\rho_{34} \\
\beta &= -0.603313 - 0.393532 * \log(\eta_{Tr}) \\
\log(t_r) &= \log(t) - c(\log(\eta) - \log(\eta_{Tr})) \\
\gamma &= 0.313351 \\
c &= 1.255882
\end{aligned} \tag{2.8}$$

Step 2: Accounting for Asphalt Aging:

The effect of aging is incorporated into dynamic modulus using the Global Aging System (NCHRP, 2004). This system provides models that describe the change in viscosity that occurs during mixing and compaction, as well as long-term in-situ aging. The Global Aging System includes four models:

- Original to mix/lay-down model.
- Surface aging model.
- Air void adjustment.
- Viscosity-depth model.

The original to mix/lay-down model accounts for the short-term aging that occurs during mixing and compaction. The surface aging model then predicts the viscosity of the binder at the surface of the pavement after any period of time using the viscosity at mix/lay-down. If warranted, the surface viscosity from the surface aging model can be

adjusted for different air void contents using the air void adjustment model. Finally, the viscosity as a function of depth is determined using the viscosity from the surface aging model or the air void adjusted model, along with the viscosity-depth model. The output of the Global Aging System is a prediction of the binder viscosity at any time and any depth in the pavement system.

Step 3: Calculation of Shift factors using appropriate Viscosity

The shift factors (t_r) are obtained at every evaluation depth for each season. The term t_r acts as a combined shift factor to include the effect of age and temperature and is as given in Equation 2.6. In which the viscosity, η is the aged viscosity at evaluation depth and temperature obtained from Global Ageing Model

Step 4: Calculation of Dynamic Modulus

For each sub-layer, the shift factors are used in Equation 2.5 to calculate the dynamic modulus at the corresponding season. The parameters δ, α, β, γ and c are constant for the given binder.

2.5.2 Unbound and subgrade materials

AASHTO and unified soil classification system (USCS) are used in the design guide to describe the different unbound granular and subgrade materials. The material properties required for unbound granular materials, subgrade and bedrock are summarized in the Table 2.6. The resilient modulus and Poisson's ratio are used to quantify the stress related stiffness of these materials. These two inputs are explained in detail below.

Resilient Modulus

The suggested methods by MEPDG to obtain resilient modulus at different level of inputs are:

Level 1: Laboratory Testing

Level 2: Correlation with other material property

Level 3: Typical values (based on calibration)

Each Level is explained in detail below.

Level 1: Laboratory Testing

Level 1 resilient modulus values are determined by AASHTO T307 procedure for cyclic tri-axial test. The lab resilient modulus values are fitted by the following equation:

$$M_r = k_1 p_a \left(\frac{\theta}{P_a}\right)^{k_2} \left(\frac{\tau_{oct}}{P_a} + 1\right)^{k_3} \tag{2.9}$$

where

M_r = resilient modulus, psi

θ = bulk stress = $\sigma_1 + \sigma_2 + \sigma_3$

σ_1 = major principal stress.

σ_2 = intermediate principal stress = σ_3 ,for M_r test on cylindrical specimen.

σ_3 = minor principal stress/confining pressure

τ_{oct} = octahedral shear stress $= \frac{1}{3}\sqrt{(\sigma_1 - \sigma_2)^2 + (\sigma_1 - \sigma_3)^2 + (\sigma_2 - \sigma_3)^2}$

P_a = normalizing stress (atmospheric pressure)

k_1, k_2, k_3 = regression constants

The three regression coefficients (k_1, k_2 and k_3) are the required inputs in design guide at input Level 1, therefore should be determined outside the design guide.

Note: Level 1 input for unbound materials is not recommended in the current design guide as it utilizes a stress dependent FEM computation through DSC2D which has not been calibrated as yet for distress calculations.

Level 2 – Correlations with other material properties

Direct or indirect correlations between soil index, strength properties, and resilient modulus are used to estimate resilient modulus M_r. The estimated temperature and the moisture profiles from the EICM is used to modify the representative M_r to account for the effects of climate on unbound materials.

Level 3 – *Typical Values (Based on Calibration)*

For Level 3 input M_r values recommended by the design guide at optimum moisture content are used. EICM can be used to modify the representative M_r values for the seasonal effect.

2.5.3 Poisson's ratio

As with other parameters, Poisson's ratio is obtained for the three input levels as shown below.

Level 1 – Laboratory Tests

Poisson's ratio is determined directly from the resilient modulus test data.

Level 2 – Correlation with other Material Properties

Poisson's ratio is estimated from appropriate models and correlations based on local knowledge and experience.

Level 3 – Typical Values

Poisson' ratio values are recommended by the guide based on type of soil.

Note that Poisson's ratio has been found to have less significant effects on computed pavement responses. As such a value of 0.35 is assumed in the design analyses.

2.6 TRAFFIC

Traffic data is one of the key input elements required for structural design/analysis of pavement structures. It is required for estimating the loads and their frequency as applied to a pavement structure throughout its design life. Agencies typically use three methods to collect traffic data; weigh-in-motion (WIM), automatic vehicle classification (AVC), and vehicle counts. These data are analyzed to obtain the required input for the design guide. Four basic types of traffic data are required by MEPDG for the structural design of pavements (NCHRP, 2004). They are:

- Traffic volume - base year information.
- Traffic volume adjustment factors.
- Axle load distribution factors.
- General traffic inputs.

The information required in each basic traffic type is summarized in Table 2.7. They can be obtained through the different hierarchal levels as identified along with the

input variable. Recommended values for Level 3 input are provided in the design software.

Table 2. 7 Traffic Inputs Required for Design Guide (NCHPR, 2004)

Data Elements	Variables
Traffic volume—base year information.	AADT or AADTT for base year*
	Number of lanes in the design direction#
	Percent trucks in design direction (DDF)*
	Percent Trucks in design lane (LDF)*
	Vehicle operational speed#
Traffic volume adjustment factors.	Truck monthly distribution factors (MDF)*
	Truck hourly distribution factors*
	Truck distribution/spectra by truck class for base year (NTP)*
	Truck traffic growth function#
Axle load distribution factors.	Axle load distribution/spectra by truck class and axle type (NA)*
General traffic inputs.	Tire pressure or hot inflation pressure#
	Number of axles by axle type per truck class (*NAT)**
	Axle configuration#
	Truck lateral distribution factor(Wander)#
	Dual Tire Spacing#

* - Input values obtained from site specific, regional and national WIM or AVC data for Hierarchal input Level 1, 2 and 3 respectively
# - Hierarchical levels not applicable for this input

Traffic Volume -Base year information

These inputs are used to compute the number of trucks in the design lane in a given base year. The vehicle operational speed is used to find the load frequency at different AC depth. Shift factors are obtained from frequency values (Figure 2.5), and are used to compute the dynamic modulus from the master curve.

Traffic Volume Adjustment Factors

The hourly truck distribution factors are not used in flexible pavement design procedure, though the input is required by the design software. The truck class and monthly distribution factors are used to compute number of trucks in each class in given incremental period. The growth factor gives the overall traffic growth from the base year information. The growth can be described as linear or compound.

The traffic characteristic over the design period is assumed constant year to year. A proportionate increase in traffic is computed based on traffic growth percentage. The design guide does not account directly for all potential changes in traffic characterization over the design period from the base year input values

Axle Load Distribution Factors

The axle load distribution factors simply represent the percentage of the total axle applications within each load interval for a specific axle type (single, tandem, tridem, and quad) and vehicle class (classes 4 through 13). A definition of load intervals for each axle type is provided below:

- Single axles – 3,000 lb to 41,000 lb at 1,000-lb intervals.
- Tandem axles – 6,000 lb to 82,000 lb at 2,000-lb intervals.

• Tridem and quad axles – 12,000 lb to 102,000 lb at 3,000-lb intervals.

General traffic inputs

The number of axles based on axle type per truck class type (NAT) is used to compute the number of load repetition within each load increment. Tire pressure, dual tire spacing and the axle configuration are used to compute the evaluation points for pavement response in the layered elastic analysis (detailed in section 2.8.3). Tire pressure and dual tire spacing determine the contact area and distance between the two loads respectively in layered elastic analysis. The traffic wander reduces the load repetition or the distress by spreading the traffic over a wide region.

2.6.1 Processing of traffic input data

The various traffic inputs discussed above are processed to obtain the number of axle loads within each load increment group for each axle type in the given incremental period. This number is used in the distress computation as the number of repetition of the load. The steps in computing the number of axle load repetition in each load increment from the traffic inputs are as follows:

1. The average annual daily number of trucks, $AADTT_1$ is calculated for the given year based on a selected growth function. The total number of trucks ($TT_{l,j,i}$) in the design lane at a given incremental period i of month j of year l is calculated using the base year information (Table 2.7).

$$= (\text{AADTT}_l)(\text{MDF}_j)(\text{DDF})(\text{LDF})(\text{No. of Days}_j) \quad (2.10)$$

2. The total number of trucks ($TT_{l,j,i}$) is multiplied by the normalized truck class distribution percentage for a particular truck class k (NTP_k) to obtain the total number of trucks for each truck class, $T_{l,j,I,k}$.

$$T_{l,j,I,k} = (TT_{l,j,I})(NTP_k) \tag{2.11}$$

3. The average number of axles based on axle type for each truck class $NAT_{k,a}$, is multiplied by the total number of trucks within each truck class ($T_{l,j,I,k}$) to obtain the total number of axles for each axle type, a (single, tandem, tridem, and quad) for that truck class, $NA_{l,j,I,k,a}$.

$$NA_{l,j,I,k,a} = (T_{l,j,I,k})(NAT_{k,a})$$

4. The total number of axles in each axle type for a specific truck class ($NA_{l,j,I,k,a}$) are multiplied by the normalized axle load distribution percentage of a specific load group to obtain the number of axles (by axle type) within each load group for a specific axle type under a specific truck class, $AL_{l,j,I,k,a,w}$.

$$AL_{l,j,I,k,a,w} = (NWP_{a,w})(NA_{l,j,I,k,a})$$

5. The axle applications for each axle type (AL) are then summed for all truck classifications to obtain the total number of axle applications within each load group by axle type for that increment analysis period. The total number of axle applications is used within the incremental damage module along with strain predicted by JULEA to predict the load related distresses at the incremental analysis period.

2.7 Climate

Environmental conditions have a significant effect on the long term performance of both flexible and rigid pavements. The material variables required for climatic modeling in flexible pavement were summarized above in Table 2.6. These are the inherent variables that determine the susceptibility of the pavement materials to moisture and freeze-thaw damage, drainability of the paving layers and infiltration potential of the pavement. On the other hand, precipitation, temperature, freeze-thaw cycles, and depth to water table are external factors that determine how much the pavement is subjected to deterioration due to environment.

Enhanced Integrated Climatic Model

The Enhanced Integrated Climatic Model (EICM) is essentially a one dimensional coupled heat and moisture flow program that simulates changes in pavement's material characteristics in conjunction with climatic conditions over the design period. The temperature and moisture profiles in the pavement structure over the design period are calculated in the design guide through EICM. These profiles are used to compute the material property of the pavement structure as well in the distress computations. EICM consists of three major components:

- Climatic-Materials-Structural Model
- Frost Heave and Thaw Settlement Model
- Infiltration and Drainage Model

The inputs required by the climatic model fall under the following category:

- General

- Pavement structure and materials.
- Weather
- Ground water
- Drainage and surface properties

General information includes type of pavement and project time frame details such as construction completion month, traffic opening month. Pavement structure and material category includes details about layer thickness, and material properties as summarized in the last column of Table 2.6.

Weather category contains information about the following parameters on an hourly basis for a minimum of 24 months:

- Hourly air temperature
- Hourly precipitation
- Hourly wind speed
- Hourly percentage sunshine
- Hourly relative humidity

Ground water table depth plays a significant role in the overall accuracy of the pavement moisture contents. Drainage and surface properties category includes information about the infiltration potential of the pavement, drainage path length and pavement cross-slope.

The EICM uses these inputs and generates temperature values at 0.1 hours intervals over the analysis period along the depth of the pavement structure. Since the asphalt material properties are very sensitive the temperature variation, using one

temperature value for the distress prediction will lead to erroneous predictions. To account for extreme temperature variations, the temperatures over a given incremental period are divided into five different sub-seasons defined as 'Quintile'. In a given analysis incremental period (either monthly or 15 days) the temperature values at every 0.1hours are represented by normal distribution. For each sub-season the sub-layer temperature is defined by the mean temperature that represents 20% of the frequency distribution for pavement temperature. Since hourly distribution of the traffic is not used in the design procedure, this sub-season also represents those conditions when 20% of the monthly traffic will occur. This temperature is used to compute the variation of modulus with season along the depth of the AC layer. The moisture variation is used to compute the variation in unbound layer modulus over the analysis incremental period. The temperatures at the surface and 0.5 inch are used to estimate the thermal tensile strain. The tensile strains at these two depths are superimposed with the strains developed at top layer due to traffic loading to estimate top-down cracking.

2.8 Distress

The trial pavement structure is analyzed for adequacy by dividing the target design life into shorter design analysis periods or increments (usually months) beginning with the traffic opening month. Within each increment (each analysis period), all factors that affect pavement responses and damage are held constant. These include material properties, climate and traffic levels. Hourly distribution of the traffic is not included in the current MEPDG flexible design analysis.

Critical stress and/or strain values for each distress type are determined for each analysis increment. These critical stress and/or strain values are converted to incremental distresses, either in absolute terms (e.g., incremental rut depth) or in terms of a damage index (e.g., fatigue cracking). Incremental distresses and/or damage are summed over all increments and the guide summarizes the distress at the end of each analysis period in a excel format.

The distresses analyzed in the design guide for the new flexible pavements are:

- Total Rut Depth and HMA, unbound layer rutting
- Load Related Alligator Fatigue Cracking, Bottom Initiated Cracks (Bottom-up)
- Load Related Longitudinal Fatigue Cracking, Surface Initiated Cracks (Top-down)
- Non-Load Related Transverse Cracking (Thermal cracking)

For the overlay/rehabilitated flexible pavements, in addition to above distresses the guide computes:

- Reflection Cracking in HMA overlays of cracks and joints in existing flexible, semi-rigid, composite, or rigid pavements

The occurrence of surface distress will result in increased roughness, or in other words, a reduction in smoothness. Thus, pavement smoothness in terms of International Roughness Index (IRI) is predicted based on these primary distresses over the design period. IRI is the overall indicator of the given pavement structure performance.

The two major distresses; permanent deformation (rutting) and load related alligator fatigue cracking are discussed in detail below. The rutting distress is predicted in absolute terms. However, the fatigue alligator cracking is computed in terms of damage index and converted to cracking distress using calibrated transfer function.

2.8.1 Permanent deformation

Permanent deformation is one of the most important types of load-associated distresses occurring in flexible pavement systems. It is the depression (rutting) along the wheel path, which develops gradually with the number of load repetitions. These plastic deformations are typically the result of the pavement materials (HMA, aggregate base, and subgrade soils) subjected to (1) densification or one-dimensional compression and consolidation and (2) lateral movements or plastic flow

Rut depths are predicted for each layer/sub-layer as a function of time. The rutting damage is estimated for each sub-season at the mid-depth of each sub-layer of asphalt bound and unbound layers within the pavement system. It is not calculated for chemically stabilized materials. The software examines the type of layer, applies the model corresponding to the material type of the sub-layer, and then computes the plastic strain accumulated at the end of each sub-season. The overall permanent deformation at a given season is the sum of permanent deformation for each individual layer/sub-layer and is mathematically expressed as:

$$RD = \sum_{i=1}^{nSublayers} \varepsilon_p^i h^i \qquad (2.14)$$

where:

RD = Rut Depth

$nSublayers$ = Number of sub-layers

$\varepsilon_p^{\,i}$ = Total plastic strain in sub-layer i

h^i = Thickness of sub-layer i

The process is repeated for each load level, axle type, sub-season, and incremental analysis period of the design period.

Permanent Deformation in Asphalt Mixtures

The asphalt rutting equation implemented in the design guide is:

$$\frac{\varepsilon_{p(HMA)}}{\varepsilon_{r(HMA)}} = \beta_{1r} k_z 10^{k_{1r}} N^{k_{2r}\beta_{2r}} T^{k_{3r}\beta_{3r}} \qquad (2.15)$$

where:

ε_p = Accumulated plastic strain after N repetitions of load (in/in)

ε_r = Resilient strain of the asphalt material as a function of mix properties, temperature and time rate of loading obtained from layered elastic analysis program (in /in)

N = Number of load repetitions

T = Temperature (degree Fahrenheit)

k_{1r}, k_{2r}, k_{3r} = Global field calibration parameters (from the NCHRP 1-40D recalibration; k_{1r} = -3.35412, k_{2r} = 0.4791, k_{3r} = 1.5606).

$\beta_{1r}, \beta_{2r}, \beta_{3r}$ = Local or mixture field calibration constants; for the global calibration, these constants were all set to 1.0.

k_z = depth parameter, to correct for the confining pressure at different depths given by

$$k_z = (C_1 + C_2 Depth)0.328196^{Depth} \quad (2.16)$$

$$C_1 = -0.1039(H_{ac})^2 + 2.4868H_{ac} - 17.342$$

$$C_2 = 0.0172(H_{ac})^2 - 1.7331H_{ac} + 27.428$$

Depth = depth to computation point, inch

H_{ac} = asphalt layer thickness, inch

The above model is based on the work of Leahy (1989), Ayres (1997), and Kaloush and Witczak (2000). National calibration factors were obtained through numerical optimization and other comparison methods with the national field data.

Permanent Deformation in Unbound materials

The basic model for prediction of permanent deformation in unbound material layers is:

$$\varepsilon_p = \left(\frac{\varepsilon_0}{\varepsilon_r}\right) e^{-\left(\frac{\rho}{N}\right)^{\beta}} \varepsilon_v \quad (2.17)$$

where,

ε_p = Permanent strain in asphalt layer/sub-layer (in/in).

N = Number of traffic repetitions.

ε_r = Resilient strain imposed in laboratory test to obtain the above listed material properties, ε_o, β, and ρ (in/in).

ε_v = Vertical resilient strain in the layer/sub-layer as obtained from layered elastic analysis program (in /in)

ε_o, β, and ρ = Material properties obtained from the following equations

$$Log\beta = -0.61119 - 0.017638(W_c) \tag{2.18}$$

$$\rho = 10^9 \left(\frac{C_o}{\left(1 - \left(10^9\right)^\beta\right)} \right)^{\frac{1}{\beta}} \tag{2.19}$$

$$C_o = Ln\left(\frac{a_1 E_r^{b_1}}{a_9 E_r^{b_9}} \right) = 0.0075$$

$$\left(\frac{\varepsilon_0}{\varepsilon_r} \right) = \frac{\left(e^{(\rho)^\beta} * a_1 E_r^{b_1}\right) + \left(e^{(\rho/10^9)^\beta} * a_9 E_r^{b_9}\right)}{2} \tag{2.20}$$

$$W_c = 51.712 \left[\left(\frac{E_r}{2555} \right)^{\frac{1}{0.64}} \right]^{-0.3586 * GWT^{0.1192}} \tag{2.21}$$

where:

W_c = Water content (%).

E_r = Resilient modulus of the layer/sub-layer (psi).

GWT = Ground water table depth (ft).

$a_1 = 0.15$; $b_1 = 0.0$; $a_9 = 20.0$; $b_9 = 0.0$

The above model was proposed by Tseng and Lytton (1989)

The model is calibrated for field performance data. Local (β_{s1}) and Global (k_{s1}) calibration constants are attached to the model as follows: (NCHRP, 2004)

$$\varepsilon_p = \beta_{s1} k_{s1} \left(\frac{\varepsilon_0}{\varepsilon_r} \right) e^{-\left(\frac{\rho}{N}\right)^{\beta}} \varepsilon_v \tag{2.22}$$

where:

k_{s1} = Global calibration coefficients; k_{s1}=1.673 for granular materials and 1.35 for fine-grained materials.

β_{s1} = Local calibration constant for the rutting in the unbound layers;

the local calibration constant was set to 1.0 for the global calibration effort.

Permanent Deformation within infinite subgrade layer

A different approach suggested by Ayres (1997) was used to evaluate the plastic deformation in the last infinite subgrade layer. For this, the plastic strains at the top of the subgrade and at a depth of six inches from it are first computed using the Equation 2.17. Subsequently, the total plastic deformation in the infinite layer is calculated from:

$$\delta = \left(\frac{1 - e^{-k * h_{bedrock}}}{k} \right) \varepsilon_{p,z=0} \tag{2.23}$$

where

δ = Total plastic deformation of the semi-infinite subgrade layer, in.

$h_{bedrock}$ = Depth to bedrock, feet (z=0 represents top of subgrade)

$$k = \frac{1}{6} \ln \left(\frac{\varepsilon_{p,z=0}}{\varepsilon_{p,z=6}} \right) \tag{2.24}$$

$\varepsilon_{P,z=0}$ and $\varepsilon_{P,z=6}$ are the plastic strain computed through Equation 2.17 at top of the subgrade and at depth of 6 inches from the top of the subgrade, respectively.

Utilized Permanent Deformation Approach

Rutting or permanent deformation is not a linear function of the number of load repetitions. Hence, the deformation in successive seasons may not be simply cumulative. Therefore, the 'Utilized permanent deformation approach' suggested by Ayres and Witczak (1998) is used to convert the deformation that occurred in previous season in terms of number of load repetition to the current season.

The 'Utilized permanent deformation approach' is illustrated in Figure 2.6. The total plastic strain $\varepsilon_{p,i-1}$ at a given season *i-1* corresponds to a total number of traffic repetitions $N_{t,i-1}$ at $T_4°F$ (Point A). In the next season *i*, the pavement temperature for the layer is $T_1°F$. For the new temperature condition, the pavement structure responds with a resilient strain equal to $\varepsilon_{r,i}$. For this new condition (Point B) there is an equivalent number of traffic repetitions $N_{tequiv,i}$ that is associated with the total deformation at the beginning of season *i* but under conditions (in this case temperature and resilient strain) prevailing in the new season i. By adding the number of repetitions at season *i* (N_i) to the total equivalent number of repetitions $N_{tequiv,i}$, it is possible to estimate Point C, which corresponds to the accumulated plastic strain at the end of season *i*.

In asphalt layers, $N_{tequiv,i}$ is obtained by solving the permanent deformation model for *N* using the resilient strain and temperature of the new season *i* and the permanent strain from the previous season *i-1* using:

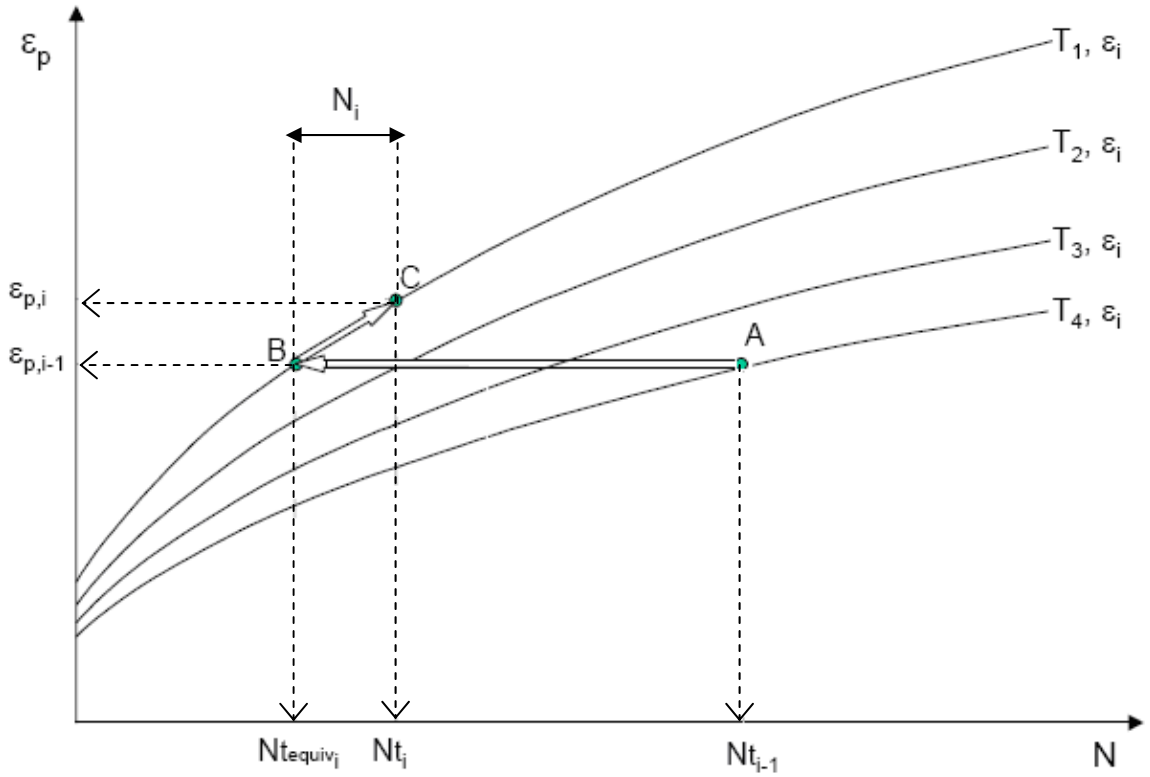

Figure 2. 6 Utilized Permanent Deformation Concept (after Ayres and Witczak, 1998)

$$N = \left(\frac{\varepsilon_{p,i-1}}{\varepsilon_{r,i}} \frac{T_i^{-k_{3r}\beta_{3r}}}{\beta_{1r} k_{z,i} 10^{k_{1r}}} \right)^{1/k_{2r}\beta_{2r}} \qquad \text{(Rewritten from Equation 2.15)} \qquad (2.25)$$

Similarly in unbound layers the material properties $\varepsilon_o/\varepsilon_r$, β, and ρ and resilient strain of new season *i* and permanent strain of the previous season, *i-1* are used to calculate N using:

$$N = \frac{\rho_i}{\left(-\left(\ln\left(\frac{e_p}{e_{v,i} * k_1 * \left(\frac{\varepsilon_0}{\varepsilon_r} \right)_i} \right) \right) \right)^{\left(\frac{1}{\beta_i} \right)}} \qquad \text{(Rewritten from Equation 2.17)} \qquad (2.26)$$

This process is repeated for each sub-season and month over the design period and permanent deformation in each sub-layer is determined. The design guide software summarizes the distress in each layer over the monthly period in an excel format.

2.8.2 Bottom-up fatigue cracking (alligator cracking)

Load-associated fatigue cracking is the other major distress types occurring in flexible pavement systems. This type of fatigue cracking is a result of the repeated bending of the HMA layer under traffic. Basically, the pavement and HMA layer deflects under wheel loads that result in the development of tensile strains and stresses at the bottom of the layer. With continued bending (under repeated load applications), the tensile stresses and strains cause cracks to initiate at the bottom of the layer and then propagate to the surface. This type of fatigue cracking first shows up as short longitudinal cracks in the wheel path that quickly spread and become interconnected to form a chicken wire/alligator cracking pattern.

Bottom-up fatigue cracking is predicted in terms of a damage index, which is a mechanistic parameter representing the load associated damage within the pavement structure. The incremental damage is accumulated for each analysis period using Miner's law as:

$$D = \sum_{i=1}^{T} \frac{n_i}{N_{f,i}} \tag{2.27}$$

where:

D = damage.

T = total number of analysis periods.

n_i = actual number of load repetition for period *i*.

$N_{f,i}$ = Number of load repetition allowed under conditions prevailing in *i*.

The number of load repetition allowed in a given season, $N_{f,i}$ is obtained from Asphalt Institute (1991) fatigue model, which is based on constant stress criterion. The model is nationally calibrated for the field conditions and it is given by

$$N_f = k_{f1}(C)(C_H)\beta_{f1}(\varepsilon_t)^{k_{f2}\beta_{f2}}(E_{HMA})^{k_{f3}\beta_{f3}} \quad (2.28)$$

where,

N_f = number of load repetitions to fatigue cracking.

ε_t = tensile strain at the critical location.

E_{HMA} = stiffness of the material.

k_{f1} ,k_{f2}, k_{f3} = Global field calibration parameters (from the NCHRP 1-40D re-calibration; k_{f1} = 0.007566, k_{f2} = -3.9492, and k_{f3} = -1.281).

β_{f1}, β_{f2}, β_{f3} = Local or mixture specific field calibration constants; for the global calibration effort, these constants were set to 1.0.

C = laboratory to field adjustment factor.

$$C = 10^M$$

$$M = 4.84\left(\frac{V_{be}}{V_a + V_{be}} - 0.69\right)$$

V_{be} = effective binder content (%)

V_a = air voids (%)

C_H = Thickness correction term

$$C_H = \frac{1}{0.000398 + \frac{0.003602}{1 + e^{(11.02 - 3.49 H_{ac})}}}$$

H_{ac} = Total thickness of the asphalt layer, inch

The cumulative damage is converted to physical cracking using calibrated models (transfer functions) that relate the calculated damage to observable distresses. The empirical transfer function to convert fatigue damage computed from Miner's rule to fatigue cracking is given by (NCHRP, 2004):

$$FC_{Bottom} = \left(\frac{1}{60}\right)\left(\frac{C_4}{1 + e^{(C_1 C_1^* + C_2 C_2^* Log(DI_{Bottom} * 100))}}\right) \quad (2.29)$$

where:

FC_{Bottom} = Area of alligator cracking that initiates at the bottom of the HMA layers, percent of total lane area.

DI_{Bottom} = Cumulative damage index at the bottom of the HMA layers.

C_1, C_2, C_4 = Transfer function regression constants; C_4 = 6,000; C_1 =1.00; and C_2 =1.00

$$C_1^* = -2C_2^*$$

$$C_2^* = -2.40874 - 39.748(1 + H_{ac})^{-2.856}$$

H_{ac} = Total thickness of the asphalt layer, inch

2.8.3 Strain computation

For each incremental design analysis period, the linear elastic analysis program JULEA is executed with the corresponding set of layer modulus to compute the critical strain values. These strain values are evaluated at 70 locations (Figure 2.7) in x-y plane, the co-ordinates of which depend on the following:

- Tire pressure and axle load
- Dual tire spacing
- Tandem/tridem/quad Axle spacing

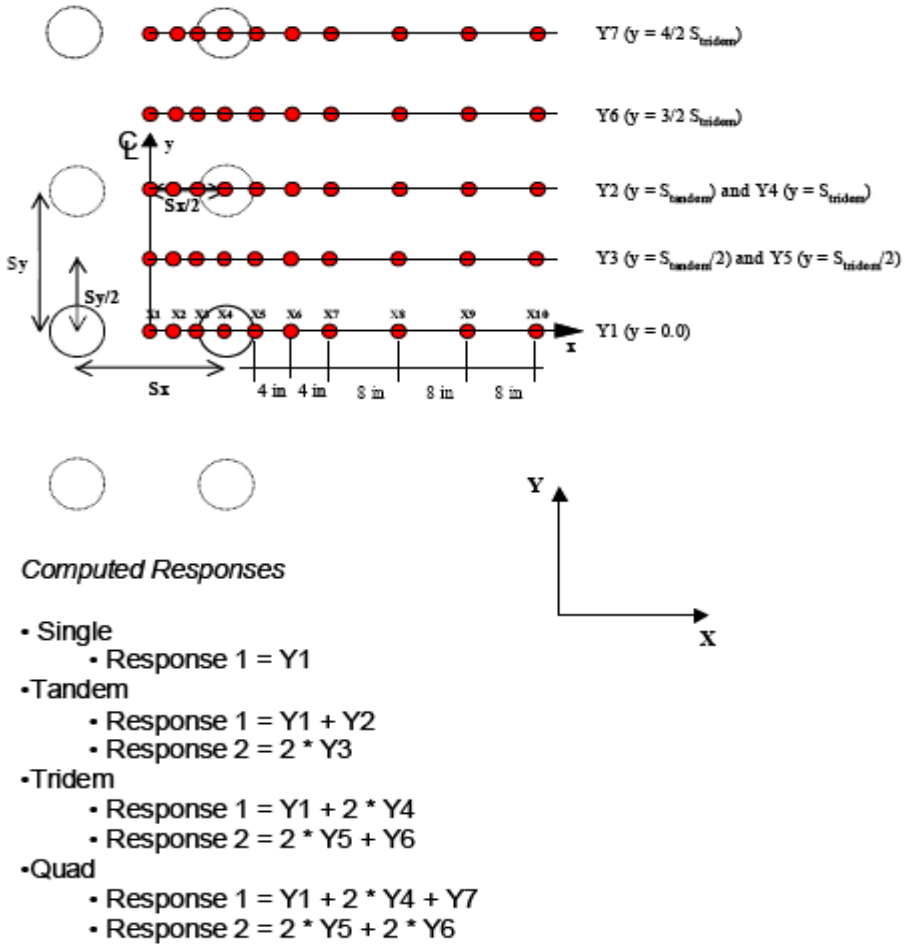

Figure 2. 7 Schematics of Strain Computation Location used in JULEA (after NCHRP, 2004)

The X and Y co-ordinates of the locations are calculated using:

X-Axis Locations: (2.30)

X1 = 0.0 {center of dual tires/tire spacing}

X2 = $((T_{Spacing}/2) - T_{radius})/2$

X3 = $(T_{Spacing}/2) - T_{radius}$

X4 = $T_{Spacing}/2$

X5 = $(T_{Spacing}/2) + T_{radius}$

X6 = $(T_{Spacing}/2) + T_{radius}$ + 4 in

X7 = $(T_{Spacing}/2) + T_{radius}$ + 8 in

X8 = $(T_{Spacing}/2) + T_{radius}$ + 16 in

X9 = $(T_{Spacing}/2) + T_{radius}$ + 24 in

X10 = $(T_{Spacing}/2) + T_{radius}$ + 32 in

where

$T_{Spacing}$ =Dual tire spacing, inch

T_{radius} = tire contact radius calculated from tire pressure and axle load, inch

Y-Axis Locations: (2.31)

Y1: y = 0.0 {center of dual tires/tire spacing}

Y2: y = S_{tandem}

Y3: y = $S_{tandem}/2$

Y4: y = S_{tridem}

Y5: y = $S_{tridem}/2$

Y6: y = $1.5*S_{tridem}$

Y7: y = $2*S_{tridem}$

where

S_{tandem} = tandem axle spacing, inch

S_{tridem} = tridem/quad axle spacing, inch

Evaluation points and the computational procedure differ when the traffic wander is included in fatigue and rutting analysis (NCHRP, 2004). Since Miner's Law used in fatigue analysis is linear with traffic, damage distribution with wander can be computed from the fatigue damage profile obtained with no wander (wander = 0 inch). In rutting analysis, the design guide modifies the actual pavement response (strain values) for the effects of wander and uses this modified response for the calculation of the incremental permanent deformations within each layer.

The depth of evaluation at each x, y co-ordinates is dependent on the type of distress under evaluation. For rutting or permanent deformation, vertical strains are measured at the following critical depths:

1. Mid-depth of each structural layer/sub-layer,
2. Top of the subgrade,
3. Six inch below subgrade surface.

For Fatigue cracking, horizontal tensile strains are measured at the following critical depths:

1. Surface of the pavement (z = 0),
2. 0.5 inches from the surface (z = 0.5),
3. Bottom of each HMA or stabilized layer.

The strain values are computed on a dual tire single axle loaded with 18 kip corresponding to standard axle load. The critical strain for the tandem, tridem and quad axles are computed by superimposing the strain values obtained from single axle as shown in Figure 2.7. The maximum strain value computed on the chosen locations at a given depth for each axle is considered the critical strain for that depth.

The computation of critical strain values at all 39 load increments (discussed in Section 2.6) with the procedure explained above will lead to unpractical computational time. To minimize computing time, the MEPDG makes the assumption that the computed strains are linearly proportional to the applied load and exploits this assumption to extrapolate strains from an 18 kip single axle load and the specified tire pressure to the entire load spectrum in the traffic composition. This load-strain linear proportionality assumption, however, holds true only if the contact area remains the same as load varies, resulting in similar variation in the contact pressure. However, in reality, for truck loads of interest, the contact (tire inflation) pressure remains within a narrow range whereas the contact area changes with axle load. This reality is violated in the load-strain linear proportionality assumption made in the current MEPDG procedure.

Park et al. (2005) studied the relation between axle tire load, tire inflation pressure and tire contact area for different types of tires. Figure 2.8 shows the general decrease in contact area with increase in tire inflation pressure for different tire loads and types. As expected, for each tire type at same tire pressure, the contact area increases with tire load (shown by arrow). The traffic load spectrum input used in MEPDG analysis includes a much wider load levels than that used by Park et al. (2005), varying from 750 lbs to 10,250 lbs per tire load, hence a much larger variation in tire contact area is expected.

Al-Qadi (2007) also studied the variation in contact area with axle load. Figure 2.9 shows the dual tire imprint of an 8,500 lbf axle load over an imprint of a 17,000 lbf axle load. It is evident that an increase in axle load results in an increase in tire imprint (contact area).

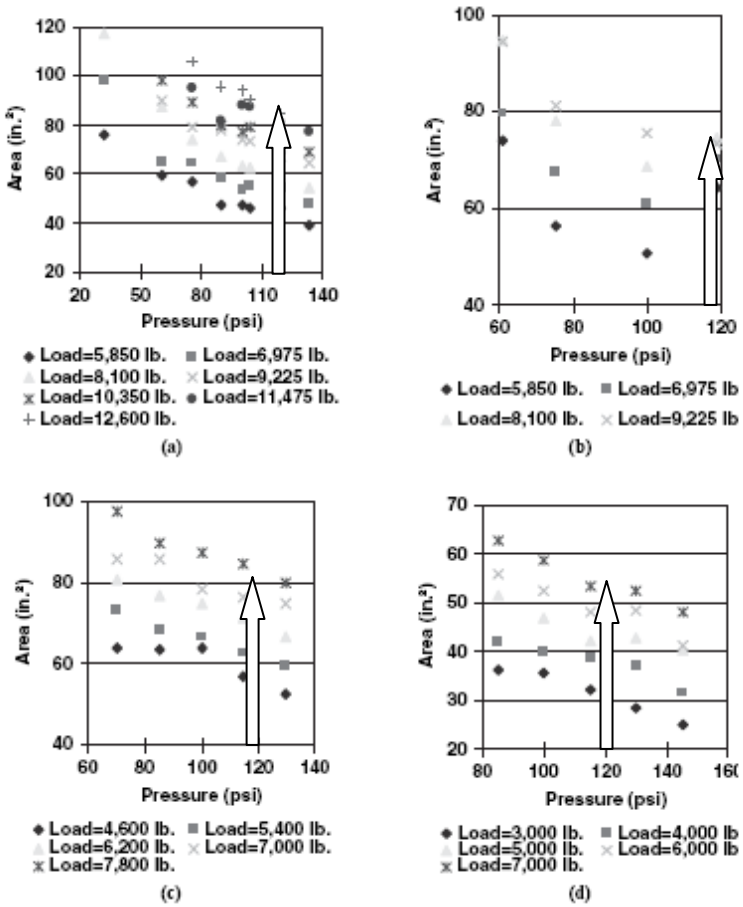

Figure 2. 8 Relationships between Tire Load, Tire Inflation Pressure, and Tire Contact Area for (a) 11R22.5, (b) 295/75R22.5, (c) 11R24.5, and (d) 215/75R17.5 Tire Types (Park et al. 2005)

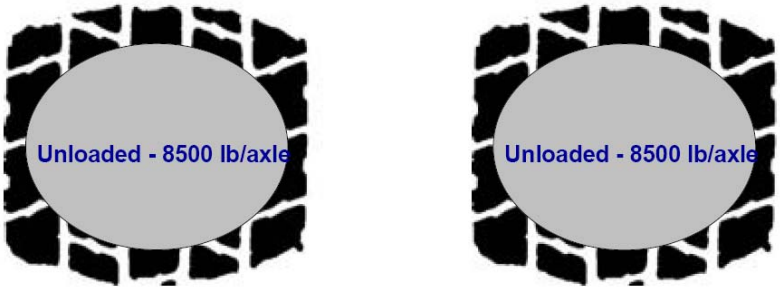

Figure 2. 9 Dual Tire Imprint of 8.5 kip Axle on 17 kip Axle (Al-Qadi, 2007)

The study analyzes the effect of this assumption on MEPDG rutting predictions in Chapter 3. It quantifies the effect of the load-strain linearity assumption and the expected deviation in MEPDG rutting predictions in flexible pavements.

2.9 Reliability Analysis in MEPDG

The reliability analysis of current MEPDG is simplified and is based on a predicted versus measured error-based approach. The predicted output distress is increased from its mean value based on the reliability level required. The reliability analysis carried out in MEPDG was summarized below with an illustration of reliability design for rutting in flexible pavement.

Step 1: Group data points by the level of predicted rutting

A database with record to past performance of similar pavement structure is developed. All data points in the calibration database were divided into subgroups based on the level of predicted permanent deformation.

Step 2: Compute descriptive statistics for each group of data.

For each group HMA rutting data calculate the mean predicted, mean measured and standard deviation of measured value.

Step 3: Determine relationship between standard deviation of the measured cracking and predicted cracking.

Step 4: Reliability analysis:

Adjust the mean value of the predicted distress ($Value_{@mean}$) to calculate the distress level at the desired reliability level (P) using the following relationship

$$Value_{@P} = Value_{@mean} + STD_{meas} * Z_p \quad (2.32)$$

where Z_p was the standard normal deviate corresponding to reliability level P.

The standard deviation (STD_{meas}) computed in Step 3 includes the following sources of variation:

- Errors in estimating traffic loadings.
- Fluctuations in climate over many years.
- Variations in layer thicknesses, materials properties, and subgrade characteristics along the project.
- Differences between as-designed and as-built materials and other layer properties.
- Errors in the measurement of the distress and IRI quantities.
- Prediction model limitations and errors.

Thus the standard deviation calculated in Step 3 is a function of the error associated with the 'past' predicted rutting and the data used to calibrate the permanent deformation models. An improved procedure should make it possible to consider all of the key components of variability and uncertainty involved in the input of given pavement design instead of past status. This would make it possible for the designer to input the mean, variance, and distribution of many key inputs and also incorporate the errors associated with the prediction models providing for much more accurate design reliability. The designer would then be able to determine the sensitivity of the outputs (cracking, rutting, faulting, IRI, etc.) to variations in the inputs providing designers with improved knowledge of the most critical inputs that should be estimated with greater accuracy.

The current study develops a reliability based pavement design procedure capable of including material variability and ways to perform it in a reasonable and practical

manner. Some widely used simulation techniques are incorporated in the reliability approach developed here. The following section gives a summary of the simulation techniques used in the study.

2.10 Simulation Techniques

A number of simulation techniques have been developed to establish the distribution of the response variable according to the probabilistic characteristics of the input random variable. Considering each realization of all the random variables in the problem produces a set of numbers that indicates one realization of the problem itself. Solving problem deterministically for each realization is known as a simulation cycle, trial, or run. Using many simulation cycles gives the overall probabilistic characteristics of the problem, particularly when the number of cycles, N, tends to infinity. The following sections summarize the procedure for Monte Carlo simulation technique. Also, the procedure of computationally efficient simulation techniques such as Latin Hypercube and Rosenblueth's 2K+1 point estimate method are subsequently discussed.

2.10.1 Monte Carlo simulation technique

Monte Carlo simulation is one of the widely used techniques in reliability analysis. The Monte Carlo method is often applied in the following three situations (Nowak and Collins 2000):

a. To solve complex problems for which closed-form solutions are either not possible or extremely difficult to obtain. For example, probabilistic problems involving complicated nonlinear finite element models can be solved by Monte

Carlo simulation provided that the necessary computing power is available and the required input information is known.

b. To solve complex problems that can be solved (at least approximately) in closed form only if many simplifying assumptions are made. Use of Monte Carlo simulation enables the "original" problem to be solved without these assumptions resulting in more realistic results.

c. To check the results of other solution techniques.

The Monte Carlo simulation technique consists of six essential elements:

Step 1: Formulation of the problem in terms of all the random variables.

This first step in simulation is on identifying the variables having uncertainty or the variability. The given problem is defined in terms of identified random variables. The deterministic variables are substituted into the explicit or implicit relations available to reduce the problem in terms of only response and random variables.

Step 2: Quantification of the probabilistic characteristics of all the random variables in terms of their probability density functions and the corresponding parameters.

The underlying distribution of the random variable can be obtained in different ways, the common methods are (Nowak and Collins 2000, Haldar and Mahadevan 2000) (a) drawing a histogram or a frequency diagram, (b) plotting the data on probability paper, and (c) conducting some statistical tests known as goodness-of-fit tests for distribution.

Step 3: Generation of the values of these random variables.

Random numbers are generated according to a specific distribution. In general, all modern computers have the capability to generate uniformly distributed random numbers between 0 and 1. Corresponding to an arbitrary seed value, the generators will produce the required number (N) of uniform random numbers between 0 and 1. By changing the seed value, different sets of random numbers can be generated. Depending on the size of the computer, the random numbers may be repeated after generating large quantity.

Step 4: Evaluation of the problem deterministically for each set of realizations of all the random variables.

The generated uniformly random variables (u) between 0 and 1 are to be converted to required distribution of the corresponding random variable X. The process requires transformation of uniform random variable to standard normal variable and then to random numbers with the appropriate characteristics. This process is commonly known as the inverse transformation technique or inverse cumulative density function (CDF) method and is illustrated in Figure 2-10. For uniformly distributed random variable this transformation is not required. This transformation process is used to convert the generated uniform random variable to normal, lognormal or other commonly used distribution. As shown in the figure, the generated random number, u (Figure 2-10a) between 0 and 1 is transformed in to its corresponding cumulative density function (CDF), $F_U(u)$ (Figure 2-10b). Since u_i is uniformly distributed its CDF will be a linear function. The CDF of both u ($F_U(u)$) and x ($F_X(x)$) are equated and the corresponding

sample value x_i is obtained as in Figure 2-10c. Figure 2-10d shows the probability density function corresponding to the generated value, x_i.

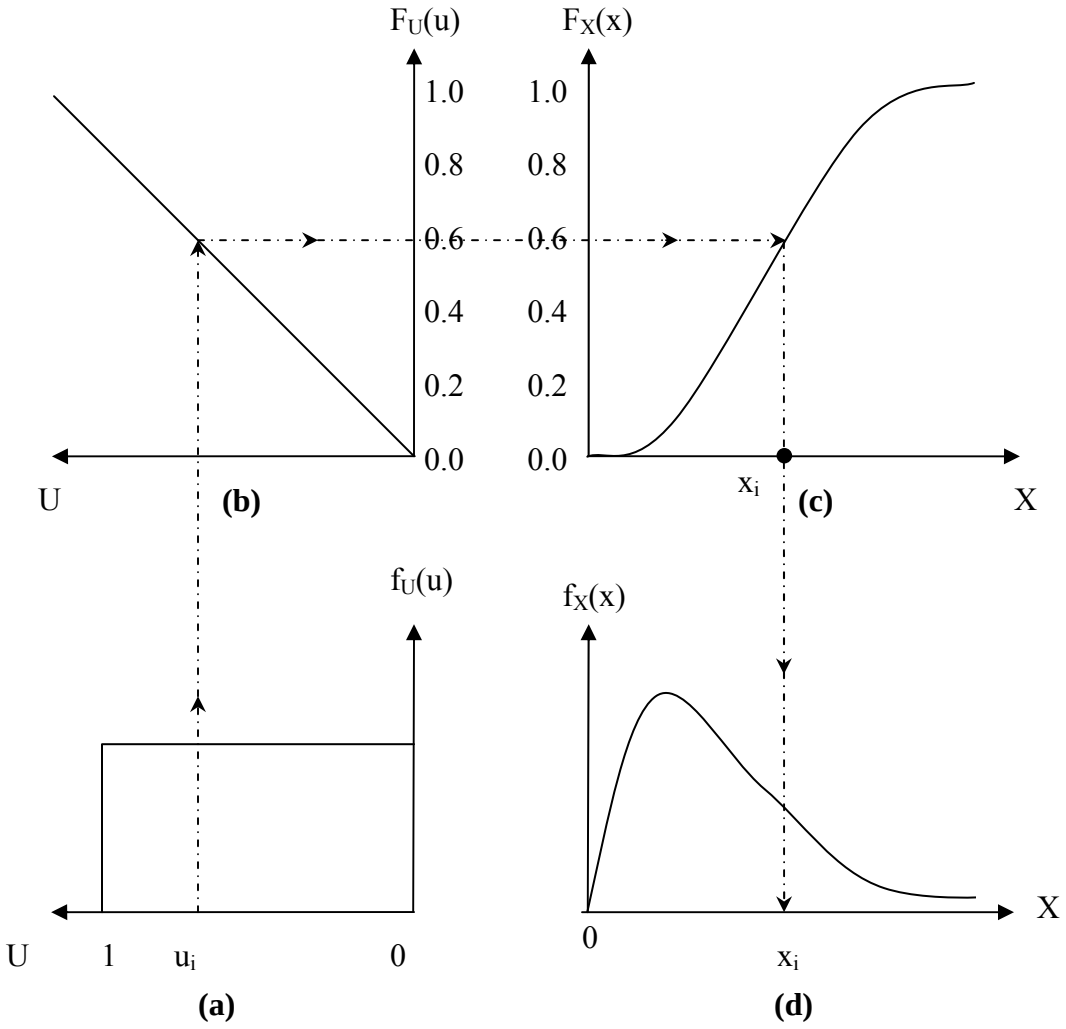

Figure 2. 10 Depiction of Random Variable Generation Process (after Haldar and Mahadevan, 2000)

In the case of *uniformly distributed random variable*, X between two values *a* and *b* $(a \le x \le b)$, the distribution is obtained from the uniform random variables (u) generated using the following formulae

$$x = a + (b - a)u \tag{2-33}$$

Thus the N generated random number in previous step is converted in to N realizations of uniformly distributed random variable X.

A set of *standard normal random numbers* $z_1, z_2, \ldots, z_n$, is generated from a set of uniformly distributed random variables $u_1, u_2, \ldots, u_n$ using the relation

$$z_i = \Phi^{-1}(u_i) \tag{2-34}$$

where Φ^{-1} is the inverse of the standard normal cumulative distribution function.

If z is the standard normal variable the relation with 'u' can be given by (Nowak and Collins 2000)

If $u \leq 0.5$

$$z = \Phi^{-1}(u) = -t + \frac{c_0 + c_1 t + c_2 t^2}{1 + d_1 t + d_2 t^2 + d_3 t^3} \ldots\ldots\ldots\ldots \tag{2-35}$$

where

$$t = \sqrt{-\ln(u^2)}$$

$c_0 =$ 2.515517; $c_1 =$ 0.802853; $c_2 =$ 0.010328

$d_1 =$ 1.432788; $d_2 =$ 0.189269; $d_3 =$ 0.001308

If $u > 0.5$

Φ^{-1} is calculated for $u' = 1\text{-}u$ and use $z = \Phi^{-1}(u) = -\Phi^{-1}(u')$ (2-36)

The method of converting the random number 'u' to the standard normal variate is illustrated for a sample of 10 random numbers and presented in Table 2-8.

Table 2. 8 Conversion of Random Number to Standard Normal Variate

Random Number between 0-1, U	Random Number corrected if u>0.5, $u' = 1-u$; else $u' = u$	$t = \sqrt{-\ln(u^2)}$	Z, calculated from the Equation 2-35	Z, corrected if u > 0.5 Equation 2-36
0.050203	0.050203	2.446091	-1.64325	-1.64325
0.619129	0.380871	1.389456	-0.30276	0.302758
0.872402	0.127598	2.029222	-1.1379	1.137896
0.376568	0.376568	1.39761	-0.31407	-0.31407
0.139927	0.139927	1.983247	-1.08068	-1.08068
0.318491	0.318491	1.51272	-0.4715	-0.4715
0.987671	0.012329	2.965064	-2.24716	2.247161
0.033265	0.033265	2.608927	-1.83525	-1.83525
0.234626	0.234626	1.702799	-0.72343	-0.72343
0.623157	0.376843	1.397087	-0.31334	0.313344
0.957884	0.042116	2.516874	-1.72703	1.727026
0.518906	0.481094	1.209705	-0.04728	0.047281

In the case of normally distributed random variable X with mean μ_X and standard deviation σ_X, the basic relationship between X and the standard normal variable Z is

$$Z = \frac{X - \mu_X}{\sigma_X} \tag{2-37}$$

from which

$$X = \mu_X + Z\sigma_X \tag{2-38}$$

So, given a sample standard normal random value z_i, the corresponding x_i value can be calculated using:

$$x_i = \mu_x + z_i\sigma_x \tag{2-39}$$

Step 5: Extraction of the probabilistic information from N such realizations

N corresponding realizations of random numbers (X_i) were obtained from N uniform random numbers generated for each of the random variables (X_i) in the problem. Thus, solving the problem using these N realizations deterministically will give N response variables. The N response variables can then be used to calculate all the required sample statistics, the histogram, the frequency diagram, the PDF or PMF and the corresponding CDF, and the probability of failure considering various performance criteria. The accuracy of the technique increases as the number of simulation N increases.

Step 6: Determination of the accuracy and efficiency of the simulation.

The relation between the estimated probability of failure, p_f and the number of simulations (N) is given by the ratio (Melchers, 2002)

$$p_f = \frac{\text{number of times } g(X_i) < 0 \text{ (n)}}{\text{total number of simulated } g(X_i) \text{ values (N)}} \tag{2-40}$$

where n is the number of times(out of N simulations) that a particular criterion was achieved (mostly the limit state function, $g(X_i)$ less than zero). The estimated probability p_f is a sample estimate and it may vary unless N is large. Therefore, the estimated

probability itself can be treated as a random variable with its own mean, standard deviation, and coefficient of variation.

Let P_{true} be the theoretically correct probability to be estimated by calculating p_f. Then

$$E[p_f] = P_{true} \tag{2-41}$$

with following probabilistic characteristics

$$\sigma^2_{P_f} = \frac{1}{N}[P_{true}(1 - P_{true})]$$
$$V_{P_f} = \sqrt{\frac{(1 - P_{true})}{N(P_{true})}} \tag{2-42}$$

The uncertainty in the estimate of the probability decreases as the total number of simulations, N, increases. The number of simulations (N) required to estimate true probability (P_{True}) under a given variance (V_P) can be calculated using the Equation 2-42

2.10.2 Latin Hypercube sampling

The time required for running *N* Monte Carlo simulation makes much complex analysis unfeasible. Alternate methods were developed to overcome this limitation. The Latin hypercube method is one such technique for reducing the number of simulations needed to obtain a reasonable accurate result. The technique works on the principle of partitioning the range of possible values of each random input variable into *N* 'Groups' or 'Strata'. A representative value from each 'Strata' is randomly selected for each input variable. These representative values of each input variable is randomly combined with representative random values of other input variables and used to calculate the response

variable. Each representative values is considered once and only once in the simulation process. Hence in this way, all possible values of the random variables are represented in the response variable simulation. Thus *N* response variable are generated involving different combination of input variables.

The procedure is explained in detailed step by step procedure below (Nowak and Collins 2000):

To simulate some values of function *Y* described by

$$Y = f(X_1, X_2, \ldots\ldots, X_k) \tag{2-43}$$

where f( ) is some deterministic function (but possible not known in closed form) and the X_i (i = 1,2,….,K) are the random input variables. The basic steps in Latin hypercube sampling are as follows:

1. The range of each random variable X_i is partitioned in to *N* intervals based on its distribution. The partitioning should be done so that the probability of a value of X_i occurring in each interval is *1/N*.

2. Randomly select a representative value for each X_i variable and each of its *N* intervals. If the number of intervals is large the center point (i.e., the middle values) of each interval can be used for practical simplicity. Now there will be *N* representative values for each of the *K* random variables.

3. The objective of Latin hypercube sampling is to select *N* combinations out of N^k possible combinations such that each representative value appears once and only once in the *N* combinations. To obtain the first combination, randomly select one

of the representative values for each of the *K* input random variables. To obtain the second combination, randomly select one of the *N-1* remaining representative values of each random variable. The process is continued till all the representative values of each random variable are used to generate *N* combinations of values for the input random variables.

4. Evaluate the value of the function *Y* for each of the *N* combinations of input variables. This will lead to *N* values of the function. From the simulated Y values statistical characteristics can be calculated.

2.10.3 Rosenblueth's 2K+1 point estimate method

Another successful technique developed to complement Monte Carlo simulation technique is the Rosenblueth's 2K+1 Point Estimate Method. Problems involving complex analysis which will take long time if done by Monte Carlo simulation technique can be done using this point estimate method proposed by Rosenblueth (1975). This method is thought as a simulation technique in which the number of simulations is *N=2K+1*, where *K* is the number of input random variables. The basic idea is to evaluate a function of random variables at *2K+1* key points and then to use this information to estimate the mean and coefficient of variation of the function. However, the drawback of this method will be that the Cumulative Distribution Function (CDF) of the response function cannot be obtained.

The steps in Rosenblueth's 2K+1 method is explained with a function Y described by

$$Y=f(X_1, X_2, \ldots, X_K) \quad (2\text{-}44)$$

where $f(X_1, X_2, \ldots, X_K)$ is some deterministic function (but possibly not known in closed form) of random input variables X_i ($i = 1, 2, \ldots, K$).

1. The mean (μ_{Xi}) and standard deviation (σ_{Xi}) for each of the K input random variables are determined with the corresponding data available.

2. Define y_0 as the value of the function Y (Equation 2-44) when all input variables are equal to their mean values, that is,

$$y_0 = f(\mu_{X1}, \mu_{X2}, \ldots, \mu_{XK}) \tag{2-45}$$

3. The value of the function Y is evaluated at 2K additional points as follows. For each random variable X_i, evaluate the function at two values of X_i which are shifted from the mean μ_{Xi} by $\pm\sigma_{Xi}$ while all other variables are assumed to be equal to their mean values. These values of the function will be referred to as y_i^+ and y_i^-. The subscript denotes the variable which is shifted, and the superscript indicates the direction of the shift. In mathematical notation,

$$y_i^+ = f(\mu_{X1}, \mu_{X2}, \ldots, \mu_{Xi} + \sigma_{Xi,..}, \mu_{XK})$$

$$y_i^- = f(\mu_{X1}, \mu_{X2}, \ldots, \mu_{Xi} - \sigma_{Xi,..}, \mu_{XK}) \tag{2-46}$$

4. For each random variable, calculate the following two quantities based on y_i^+ and y_i^-

$$\bar{y}_i = \frac{y_i^+ + y_i^-}{2} \tag{2-47}$$

$$V_{y_i} = \frac{y_i^+ - y_i^-}{y_i^+ + y_i^-} \tag{2-48}$$

5. Calculate the estimated mean and co-efficient of variation of Y as follows

$$\bar{Y} = y_0 \prod_{i=1}^{K} \left(\frac{\bar{y}_i}{y_0} \right) \tag{2-49}$$

$$V_Y = \sqrt{\left\{ \prod_{i=1}^{K} \left(1 + V_{yi}^2\right) \right\} - 1} \tag{2-50}$$

There are two distinct advantages to this method. First, it is not necessary to know the distributions of the input random variables; only the first two moments are needed. Second, the number of function evaluations (i.e., "simulations") is relatively small compared to Latin hypercube sampling or general Monte Carlo simulation.

2.11 Reliability Based Pavement Design

The reliability based pavement design has been studied in the past. Both simulation techniques and analytical methods have been explored. However, there is a constant need of improvement in reliability analysis with the advancement in pavement design procedures.

The importance and benefit of using reliability analysis over safety factor in the pavement design was discussed by Lemer and Moavenzadeh (1971). They used Monte Carlo simulation with Markov models to predict pavement performance. The special feature of Markov process was predictions of the probability that the process will be in any particular state at some future time, was based on observations of the current state. A Markov model was used by first describing the service behavior of the facility in terms of

state and possibly interstate transitions, and then values of probabilities were estimated. Using Monte Carlo simulations the distribution of probability of normal failure as a function of axle load repetitions and construction quality was found. The probability matrices were postulated for a 6-month computation period and this 'subprocess' was computed for 30 transitions to find failure distributions for a 15 year design.

A simulation model to calculate the reliability of pavements was developed by Alsherri and George (1988). A computer program using Monte Carlo simulation technique called Reliability Analysis and Performance of Pavements (RAPP –I) was used to solve the design equations. The design models from AASHTO design guide 1985 were used. The scheme of computing the reliability involved comparison of Present Serviceability Index (PSI) at a specified time and Terminal Serviceability Index. Errors due to idealization of the model were included in the PSI calculation through standard deviation of model prediction values. The program calculated the PSI and the corresponding reliability at the end of each year through 500 simulation data, from which the expected life of the pavement was calculated.

Chou (1989) used Rosenblueth's point estimate method to estimate the mean and variance of allowable repetition strain in flexible pavements, based on the input variability of four independent parameters namely load, layer thicknesses and moduli of subgrade and asphalt concrete layers. A computer program called RELIBISA was used to compute the reliabilities and allowable strain repetitions for given subgrade and asphalt concrete. Figure 2.11 show the number of strain repetitions to achieve the desired reliability under different pavement layer thickness (The coefficient of variance and the values for other input variables were assumed).

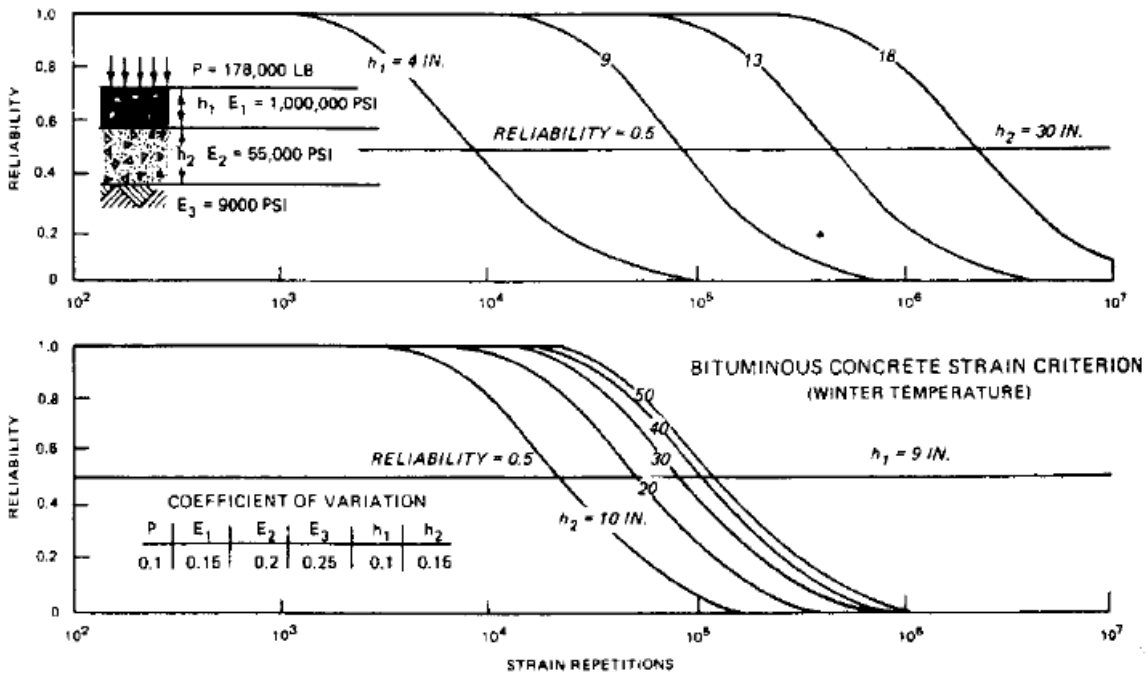

Figure 2. 11 Relationships between Reliability and Allowable Strain Repetitions (after Chou, 1989)

Monte Carlo simulation technique was also used by Montano et al (1989) to make an economical concrete pavement design with consideration for uncertainty in input parameters to evaluate the service life of the pavement. Service life was considered to be influenced by variations in traffic, thermal effects and flexural fatigue of concrete. Simulation was carried out for one year since thermal effect has a return period of one year. 200 simulations were carried out with daily traffic volume. The results showed that the standard deviation and the coefficient of variation were not influenced by the number of operation repetitions. However, stable distribution (Skewness and kurtosis) were achieved after 150 operation repetitions. Right-skewed Beta distribution was fitted to the simulated service life data and the reliability of concrete pavement was calculated for the design period.

Stochastic finite element analysis was used by Phoon et al (1990) to compute the reliability index for pile settlement. A random variable was assigned as the spatial average of the soil modulus across the i^{th} element in the finite element mesh. The soil was assumed to be an isotropic linear elastic medium and the soil modulus was assumed to be axisymmetric. The mean and coefficient of variation of the pile head settlement for single piles were evaluated using advanced first-order second moment (AFOSM) method using first-order Taylor series expansion about the mean. The reliability index was calculated through Hasofer and Lind (1974) method through minimum distance from the origin to the limit state surface. The search algorithm by Rackwitz and Fiessler was used in the study to determine the nearest point to the origin. The relationship of reliability index with slenderness ratio of the pile, stiffness matrix of the soil, lateral and vertical scale of fluctuation and co-efficient of variance of soil modulus was found. To avoid time consuming stochastic finite element analysis 'reliability index charts' were developed using the above relationships.

A reliability based procedure to include the uncertainties in the analysis of existing and new airfield pavements was made by Sues et al (1993). Multi-nested Monte Carlo Simulation (MCS) technique was developed to handle the nonlinear complex damage models. An outer loop using direct simulation of the entire pavement life and inner loop using stratified sampling of load variation was selected. This able to incorporate large number of random variables in to the simulation and to obtain accurate results involving multiple failure modes. Computer code called PROJULEA capable of computing stress and strain incorporating variation in pavement properties and loading was used. A balanced design attaining similar probability of failure for both asphalt and

subgrade layer was targeted and achieved. A reliability curve with service life was generated at design thickness obtained through simulation technique.

Val and Melchers (1997) studied the reliability of RC slab bridges with reinforcement corrosion. A nonlinear finite element model was used to describe the structural behavior of the bridge. The structural reliability was estimated using FORM. A two-dimensional model to study longitudinal flexural failure modes were used to reduce the computational effort. The reliability index was developed for both brittle and ductile failure modes.

As discussed previously, a mechanistic pavement model, WESLEA and empirical transfer functions were used to assess the effect of input variability on fatigue and rutting failure models by Timm et al., (2000). Monte Carlo simulation technique was used to study the uncertainty through a computer program called ROADENT. The results of the simulations were analyzed to reach a constant model output distribution. The distribution was monitored by recording the percentile values of the output distributions as a function of the number of cycles. By including the seasonal variations 5000 cycles was reported to be adequate to achieve a fair precision. The model outputs were reported to follow the Extreme value Type I distribution. The probabilistic properties of the input parameters were used from the existing literatures. The reliability computed through ROADENT was reported lesser than that computed through AASHTO 1993 design guide.

The advantage of reliability based design over old AASHTO 1993 procedure was discussed by Kim and Buch (2003). They characterized the reliability of the performance function through Hasofer-Lind reliability index. A Load and Resistance Factor Design (LRFD) format was used for practical reliability-based M-E flexible pavement design

procedure. A safety factor reflecting specified target reliability was used; it depends on the partial safety factor of each random variable for reduction or amplification of its amount. Thirteen pavement sections were designed using both AASHTO 1993 procedure and the newly suggested 'Reliability Based Design' procedure. The thickness suggested by both methods were different, and the reliability index determined by the FORM method showed that it was successful in yielding cross sections whose reliability indices were close to the target reliability indices, whereas AASHTO 1993 method did not generally produce designs of uniform reliability for actual mechanistic failure criterion.

The result from U.S. Crops of Engineers equation for pavement thickness equation was analyzed by Huang (2004) through Taylor's expansion (FOSM) and Rosenblueth's 2K+1 method. The design equation contained four uncertain variables. The coefficient of variation for each variable was taken as 0.1. The results showed close agreement between two methods, even though Rosenblueth's method does not require computation of derivatives as in FOSM.

The advancement in reliability analysis from AASHTO 1993 pavement design procedure to MEPDG was discussed in Darter et al. (2005). The authors suggested improving the current "Predicted versus measured error-based approach" (MEPDG) by accounting the effect of design input variability on the design reliability through Monte Carlo Simulation. The authors applied the Monte Carlo technique to the JPCP transverse cracking model. Instead of incremental design procedure adopted in AASHTO 1993, Neural Networks (NNs) have been developed based on the ISLAB2000 finite element (FE) structural model to compute critical stresses and deflections virtually instantaneously. The principles of dimensional analysis and equivalent pavement system

were used extensively in the development and implementation of the neural network. About 25 input pavement parameters for the model were included into pavement responses through the use of three composite parameters: equivalent slab thickness, radius of relative stiffness and Korenev's non-dimensional temperature gradient. The distributions of these parameters were obtained first before neural network was used to significantly improve computational speed. For acceptable execution time the authors suggested the use of Monte Carlo based analysis to be propagated throughout the distress prediction process.

2.12 Summary

This chapter presented details of the basic MEPDG methodology as applied to flexible pavements. It also presented details of the basic reliability procedures. To facilitate the computations, the distress models in the MEPDG are coded in FORTRAN with the required inputs about traffic, material properties and climatic data. It is used in subsequent chapters. The layered elastic analysis program JULEA is used to compute the stress-strain response. JULEA code has been modified to compute only required structural responses.

CHAPTER 3

EFFECTS OF NONLINEAR LOAD-STRAIN BEHAVIOR ON DISTRESS PREDICTION[1]

3.1 Introduction

The structural response computation (Chapter 2.8.3) in the MEPDG design procedure assumes that the load-strain relationship is linearly proportional (NCHRP, 2004). For example, the strain due to a 9,000 lbf load is assumed to be twice as that of 4,500 lbf load. This assumption is exploited to significantly reduce the computation time. For each time increment, the layered elastic analysis procedure JULEA is executed to compute strains for a 9,000 lbf dual tire load (representing a 18 kip single axle) and strain responses for the remaining load spectrum, ranging in dual-tire loads of 1,500 lbf to 20,500 lbf are obtained from the load-strain linear proportionality assumption.

The load-strain linearity assumption, however, holds true only if the contact area remains the same while load varies resulting in a similar variation in the contact pressure. For example, assuming a 120 psi tire inflation pressure for the 9,000 lbf dual tire load the contact area for a dual tire will be 75 sq. inches. For the load-strain linear proportionality to be valid, the contact area must remain 75 sq. inches for all load levels. Thus the tire inflation pressure has to vary from 20 psi (1500 lbf/ 75 sq. inch) for 1,500 lbf dual tire load to 273 psi (20,500 lbf/ 75 sq. inch) for 20,500 lbf dual tire load. However, for truck loadings of interest, classes 4 through 13, the contact (tire inflation) pressure remains within a narrow range; thus the contact area changes with axle load. For commonly used

[1] - part of this chapter has been accepted for presentation and publication in 84th annual meeting of Association of Asphalt Paving Technologies

tires, the cold tire inflation pressure ranges from 96 psi to 120 psi (NCHRP, 2004). Under normal operating conditions, tires are inflated to these manufacturers' recommended inflation pressures and are not adjusted to the instantaneous load being carried by the vehicle. Instead, the contact area changes as the vehicle is operated at loads ranging from fully loaded to empty, as reflected in the traffic load spectrum. The change in contact area may not necessarily be proportional to the change in load and is a function of tire characteristics and vehicle dynamics. However, under the simplifying assumptions used in the MEPDG LEA procedure JULEA, the loaded area is assumed to be circular with uniform contact pressure. Under this assumption, the change in contact area will be linearly proportional to the change in load.

The MEPDG only accepts one tire pressure value for the entire load spectrum. Tire inflation pressures for the composition of trucks represented in the traffic load spectrum would mostly likely vary as a result of tire type and tires not being maintained always at the recommended inflation pressures. However, as discussed in the previous paragraph, the recommended cold tire inflation pressures for commonly used truck tires falls within a narrow range (96 psi to 120 psi) and the use of single tire pressure in MEPDG analysis is not considered to be a significant limitation. This tire inflation pressure variation is smaller and different than the systematic and much wider range (20 psi to 273 psi) investigated in this study.

The load-strain linear proportionality assumption was reached by looking at the strains at some depth (NCHRP, 2004) where the effect of constant contact pressure versus the constant contact area vanishes and incorrectly concluded that the load-strain relationship is linearly proportional. Further discussion on this assumption was included

in a response to NCHRP (Highway Community EXchange, 2005) that referenced analyses done on typical tire loads, pressure and axle load configurations for the study where it was found that the as the axle load increased, tire pressure also increased while the tire contact area remained fairly constant. However, this appears to contradict the physics of the problem and published experimental data reviewed in the next section.

This study analyzes the deviation in MEPDG distress predictions due to the load-strain linear proportionality assumption exploited in computing strains from one reference axle load to the full traffic load spectrum.

3.2 Test Pavement Structure

The effect of load-strain linear proportionality assumption on performance prediction was evaluated using a test pavement structure with climatic conditions corresponding to Dulles International Airport, Washington DC. The pavement section, material properties and traffic data used in the analysis are summarized below.

The pavement section

- HMA Layer: Thickness 10 inch
- Base Layer: Thickness 6 inch Crushed stone
- Sub-Base Layer: Thickness 10 inch A-2-4 material
- Subgrade Layer: Semi-infinite A-6 material
- Poisson's ratio is assumed to be 0.35 for all the layers.

Material Properties

- Asphalt binder: PG 70-34
- Mix properties: Effective binder content 11 % (by volume), Air Void 7.0 % (by volume), Total Unit weight 148 pcf.
- Aggregate gradation: Cumulative percentage retained in 3/4 inch, 3/8 inch and #4 sieves are 0, 21, and 60% respectively. And 3% passing the #200 sieve.
- Asphalt thermal conductivity and heat capacity are assumed with default Level 3 input values.
- Modulus and gradation for the unbound materials are taken as Level 3 input values.

Traffic

- AADTT: 2000, with 4% compound traffic growth.
- Traffic wander is assumed zero.
- Tire pressure: 120 psi.
- Dual tire spacing: 12 inch.
- Vehicle Class Distribution: Predominant single-unit Trucks.
- Traffic volume adjustment factors, axle load distribution factors and other General traffic inputs are assumed with default Level 3 input values.

The MEPDG divides pavement layers into sub layers to better model the temperature and moisture variations as well as material properties and thereby calculate more accurately the responses throughout the pavement structure. The EICM and Global Aging models calculate the modulus of asphalt concrete and unbound sub-layers at each

time increment by applying adjustment factors for aging and environmental conditions. The thicknesses of the sub-layers utilized by the MEPDG are summarized in Table 3.1.

The effect of load-strain linear proportionality assumption was evaluated both in terms of strain values computed using the layered elastic analysis program JULEA and rutting computed using calibrated distress prediction models.

Table 3. 1 Test Pavement Section

Material	Layer Thickness, inch	MEPDG Sub-layer Thickness, inch
Asphalt Concrete	10	0.5
		0.5
		1.0
		1.0
		1.0
		4.0
		2.0
Base	6	2.0
		4.0
Sub-Base	10	4.0
		6.0
Subgrade	Semi-infinite	24.3
		24.3
		24.3
		252.0

3.3 Vertical Strain

For permanent deformation or rutting prediction, the MEPDG distress models require vertical strain at mid-depth of each sub-layer. Vertical strains were calculated for an 18 kip single axle load using JULEA and the principle of superposition is used to compute strains for other axle groups and load-strain linear proportionality assumption is used to compute strains for other axle load levels. The principle of superposition is valid for layered elastic analysis and in this section the vertical strains for a single axle load are considered for evaluating the load-strain linear proportionality assumption on computed vertical strains. The location where the critical strains will occur cannot be predetermined and MEPDG uses a matrix of computation points in JULEA to ensure that the critical strain is captured. For single axle load, MEPDG uses 10 computational points (Section 2.8.3) and the same approach was followed in this analysis to determine maximum vertical strains for each sub-layer.

Figure 3.1 shows the deviation in vertical strains computed using JULEA at 3, 18 and 36 kip single axle loads corresponding to the following two criteria:

- Constant contact area – as assumed in the MEPDG design software. The strain values at 3 and 36 kip single axle loads are computed with load-strain linear proportionality assumption from values computed at 18 kip single axle load.

- Constant tire pressure – strains are computed using JULEA for all three load levels with a constant tire pressure of 120 psi. The contact area varies depending on the axle load. The JULEA responses computed assuming constant tire pressure are

referred to as “actual values” in subsequent sections for brevity as this represents the field conditions more closely.

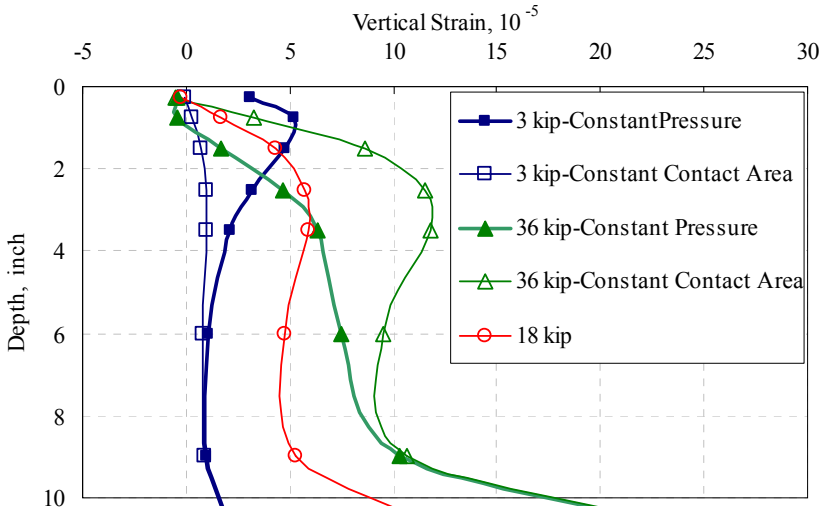

Figure 3. 1 Vertical Strain with Depth for Different Axle Loads with and without the Load-Strain Linear Proportionality Assumption

It can be seen that the strains at 3 kip single axle load, computed from the 18 kip single axle load with the load-strain linear proportionality assumption (constant contact area condition) are much lower than the actual values (Figure 3.1). Similar trends were observed for tandem, tridem and quad axle configurations. The opposite is true for 36 kip single axle load - the strains computed from the 18 kip single axle load with the load-strain linear proportionality assumption are much higher than the actual values.

The ratio between the strains computed with constant contact area to the actual values is used illustrate the effect of the constant contact area assumption. The variation of this strain ratio with depth is shown in Figure 3.2 for 3 and 36 kip single axle load. Note that strain ratio of unity indicates that the strains computed by both criteria are equal. It can be seen that the strains computed with constant contact area are less than

actual values for axle loads less than 18 kip but higher for loads greater than 18 kip. The strains computed under both criteria converge as the evaluation depth increases.

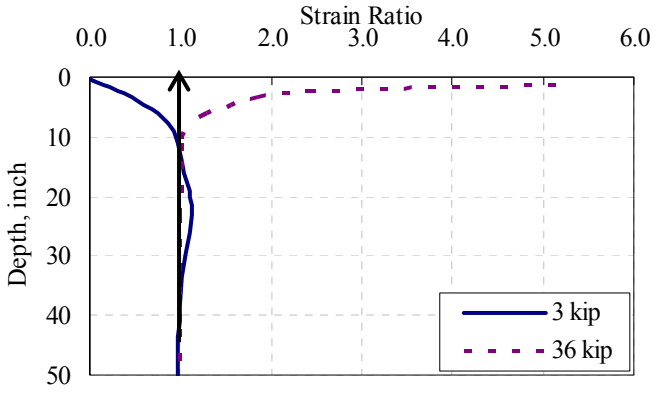

Figure 3. 2 Effect of Load-Strain Linear Proportionality Assumption on Vertical Strain with Depth

The load-strain response for the pavement structure at a number of evaluation depths is as shown in Figure 3.3. It is seen that the load-strain response becomes linearly proportional only at a depth of 9 inches. This implies that the strains used in the MEPDG distress models for the top several sub-layers of the pavement structure would deviate significantly from the actual values. In the top few inches of the pavement structure, the strain decreases (in some cases, tensile strain) with increasing axle loads probably due to the confining effect of wider contact areas.

3.4 Horizontal Strain

The MEPDG uses the tensile strain at bottom of HMA layer to compute the fatigue damage caused by load repetitions. Since the effect of load-strain linear proportionality assumption is more pronounced at the top few inches of the pavement

structure (Figure 3.2), it will have a significant bearing on fatigue prediction of thin overlays used in pavement rehabilitation.

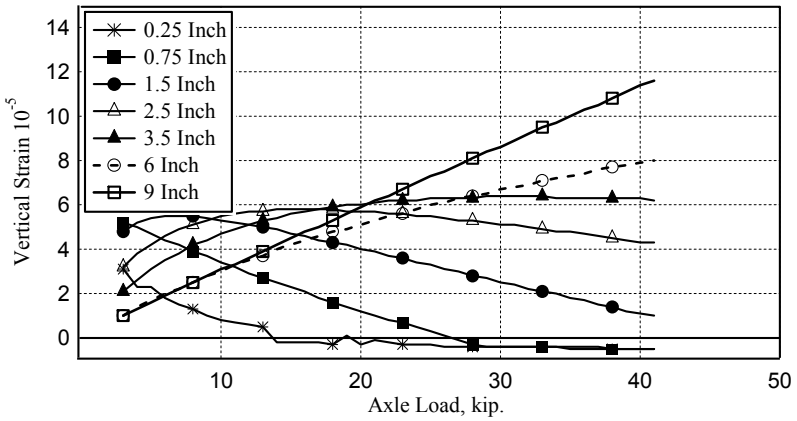

Figure 3.3 Load-Strain Relationship at Mid-Depth of the HMA Sub-Layers

A 2 inch overlay, having the same HMA material properties as the HMA layer of the test pavement structure previously described, was considered. For the test pavement structure with overlay, the horizontal tensile strains at various axle load increments were calculated using JULEA at the bottom of the overlay and also at the bottom of the existing HMA layer, at depths of 2 inches and 12 inches, respectively.

Figure 3.4 shows the load-strain response for the overlaid test pavement structure. At a depth of 2 inches, the load-strain response deviates significantly from the linear proportionality assumption and the assumption could introduce significant error in the fatigue damage prediction of the overlay. However, at a depth of 12 inches, the load-strain response is very close to being linearly proportional and the fatigue damage prediction at the bottom of existing HMA will not be significantly affected by this assumption.

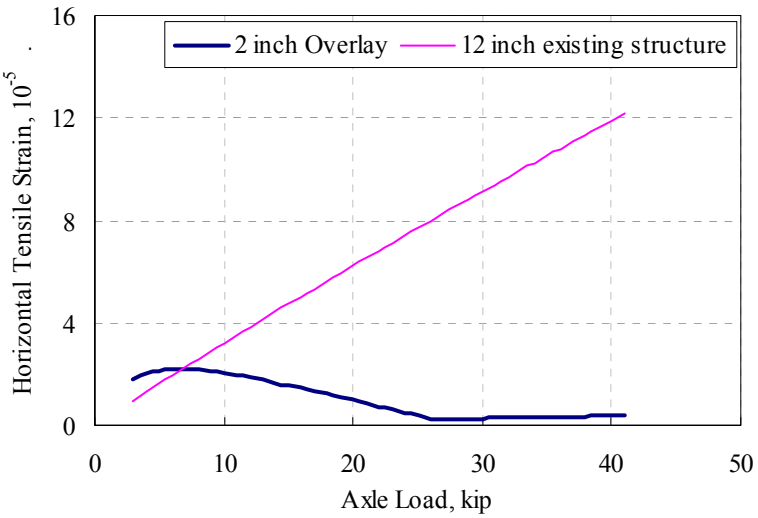

Figure 3. 4 Load-Strain Relationship at the Bottom of HMA Layer

3.5 Traffic Spectrum

The default traffic spectrum included in the MEPDG for "Principal Arterials and Interstates" is used to quantify the effect of the load-strain linear proportionality assumption on rutting predictions.

In the MEPDG, traffic data inputs are processed to determine the number of axle load repetitions within each load increment group for each axle type. The load increments used in MEPDG for the four axle types are as follows:

- Single axles – 3,000 lbf to 40,000 lbf at 1,000 lbf intervals.
- Tandem axles – 6,000 lbf to 80,000 lbf at 2,000 lbf intervals.
- Tridem and quad axles – 12,000 lbf to 102,000 lbf at 3,000 lbf intervals.

The number of load repetitions by axle type and load group for each time increment are then used within the incremental damage module to predict and accumulate the load related distresses with time.

Figure 3.5 shows the cumulative percentage of axle load repetitions as a function of load group for single axle type. The chart was developed using level 3 inputs with predominantly single-trailer trucks on Principal Arterials and Interstates and default level 3 axle load distribution factors. The trend is similar for other route categories, including Local Routes and Minor Collectors. The figure shows that most of the traffic (96%) fall below the standard single axle load of 18 kip. As discussed earlier, the MEPDG uses an 18 kip single axle load as the reference load in JULEA and uses load-strain linear proportionality assumption to compute strains for other load levels. Since, as shown in Figure 3.2 and discussed in the previous section, the strains computed assuming load-strain linear proportionality are less than actual values for load levels less than the reference load, the distresses computed by MEPDG for the full traffic load spectrum will be less than that resulting from constant pressure condition.

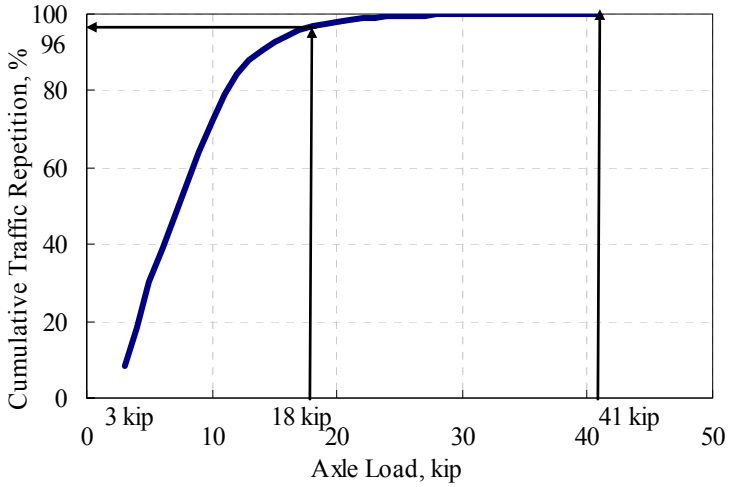

Figure 3. 5Cumulative Load Repetition in Single Axle for a Typical Traffic Spectrum

3.6 Permanent Deformation

The discussion up to now focused on the impact of load-strain proportionality assumption on vertical and horizontal strains. This section discusses the impact of the deviation in vertical strains on rutting prediction. The extent of deviation in distress predictions due to nonlinear load-strain behavior cannot be evaluated using MEPDG. It requires an external analysis that models the MEPDG procedures without the load-strain linear proportionality assumption. For this purpose, the MEPDG rutting models were coded and incorporated along with JULEA into a stand-alone application to conduct independent analysis for comparison with MEPDG predictions. The stand-alone application utilizes the MEPDG computed climatic and material properties.

The MEPDG pre-processes the traffic data to compute the number of load repetitions for each axle load and axle type for each month within the design period. In addition, the MEPDG divides each month within the design period into one or two time increments based on climatic conditions. The time increments are further divided into quintiles based on temperatures. For each quintile, the modulus values for the different sub-layers are calculated from the specified material properties along with the EICM and Global Aging models. The damage computed is then accumulated over the quintiles, time increment within each month and each month within the design period. The quintiles within each time increment will be referred to as incremental period in subsequent sections for brevity. Material modulus, number of load repetitions by load and axle type, and the number of incremental periods per month used in the MEPDG analysis were obtained from the output files generated by the MEPDG software during these steps.

Two sets of analyses were conducted. The first analysis was to compare and validate predictions from the stand-alone application to that from MEPDG. The second analysis was to evaluate the effect of the load-strain linear proportionality assumption on the predicted performance. The stand-alone application was used to analyze the test pavement structure with load-strain linear proportionality assumption and the rutting predictions were compared with MEPDG predictions.

For each incremental period, JULEA was used to calculate critical strains within test pavement structure with the corresponding set of layer moduli for an18 kip single axle load, the same standard axle load used in MEPDG. The strains for other load levels were computed using load-strain linear proportionality assumption and for other axle types were computed using the principle of superposition. The critical vertical strains at the midpoint of sub-layers were obtained as the maximum strains at a matrix of horizontal locations as referenced in the MEPDG documentation (Section 2.8.3).

The rutting predictions from the stand-alone application were compared with the MEPDG predictions at 50% reliability. Figure 3.6 shows the rutting predicted by the stand-alone application and the MEPDG at 50% reliability for the each of the structural layers. The rutting predicted by the stand-alone application agrees within 7% of the MEPDG prediction for all layers for the entire design period. It is hypothesized that the minor deviations are related to inherent differences in the numerical implementation of the distress models and damage accumulation equations in the stand-alone application and MEPDG.

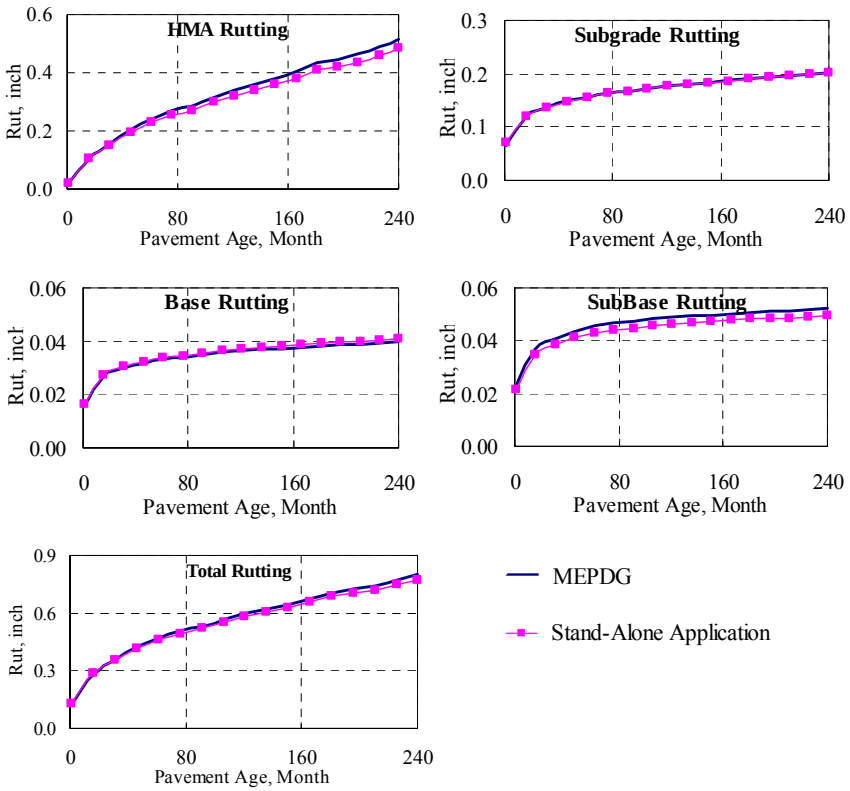

Figure 3.6 Predicted Rutting in Pavement Layers by the MEPDG and the Stand-Alone Application with Load-Strain Linear Proportionality Assumption

Permanent Deformation with Constant Tire Pressure Condition

The effect of load-strain linear proportionality assumption exploited in MEPDG for predicting rutting performance was investigated by comparing the results obtained in the previous analysis with analysis that did not make this assumption. In the latter, for each incremental period, the critical strains were calculated using JULEA for all 39 single axle load levels considered in the MEPDG traffic load spectrum, from 3 kip to 41 kip, in increments of 1 kip. As with the previous analysis, the strains for other axle types were computed using the principle of superposition. The rutting in each sub-layer was computed using the actual strains calculated at the respective load level in contrast to strains computed from the reference 18 kip single axle load using the load-strain linear

proportionality assumption used in MEPDG and in the previous analysis. Figure 3.7 compares the rutting predicted with and without the load-strain linear proportionality assumption used in the MEPDG. As expected from Figure 3.2, the effect of the assumption is significant for the HMA layer but diminishes for the deeper layers. The load-strain linear proportionality assumption significantly under predicts rutting in the HMA layer and for the test structure. The trend is similar for three other pavement structures evaluated with different traffic load spectra.

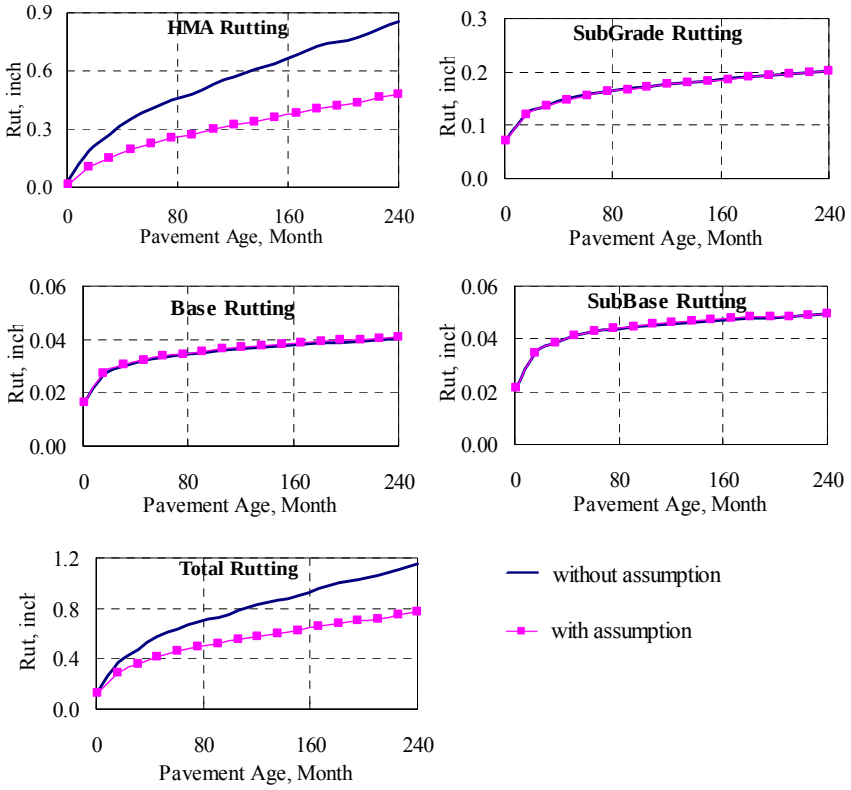

Figure 3. 7 Predicted Rutting in Pavement Layers by Stand-Alone Application with and without Load-Strain Linear Proportionality Assumption

Figure 3.8 shows the deviation in predicted rutting for each sub-layer at the end of the design period with and with out load-strain linear proportionality assumption. The thickness of the each sub-layer is given in the Table 3.1. The effect is again seen to be

more pronounced within top few inches of the pavement structure but to diminish for deeper sub-layers.

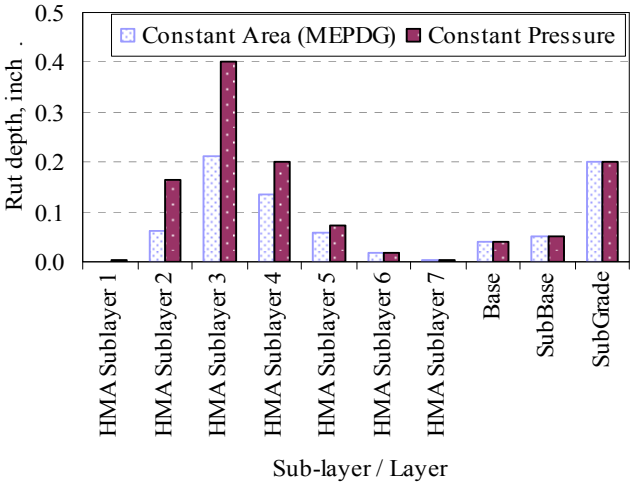

Figure 3. 8 Difference in Rutting Prediction in HMA Sub-Layers and Unbound Layers

Table 3.2 compares the values of total rutting in HMA layer predicted by

- MEPDG
- stand-alone application with the load-strain proportionality assumption
- stand-alone application without the load-strain proportionality assumption

The table shows the deviation in the rutting prediction with time. The load-strain linear proportionality assumption significantly under predicts rutting depths for the traffic spectrum considered, for the test pavement structure by as much as 90% in the HMA layer. Three other pavement structures were analyzed under different traffic and climatic conditions and the load-strain linear proportionality assumption resulted in under prediction of rutting by over 50% in all three cases. The amount of variation will depend on the pavement structure, material properties and traffic and climatic conditions.

Table 3. 2 Summary of HMA Rutting Predicted by (a) MEPDG, (b) Stand-Alone Application Considering Constant Contact Area and (c) Constant Tire Pressure

Month	Rutting in HMA layer, inch			% Deviation $\frac{(b-c)}{b}*100$
	Load-Strain are Linearly Proportional		Load-Strain are not Linearly Proportional	
	MEPDG (a)	Stand-Alone (b)	Stand-Alone (c)	
1	0.016	0.017	0.032	-88.2
2	0.017	0.018	0.034	-90.6
3	0.018	0.019	0.035	-83.7
4	0.018	0.019	0.035	-86.3
5	0.019	0.019	0.036	-91.6
6	0.020	0.021	0.039	-84.8
7	0.024	0.025	0.047	-88.8
8	0.033	0.035	0.065	-85.4
9	0.060	0.059	0.106	-79.4
10	0.086	0.083	0.147	-77.6
11	0.098	0.095	0.168	-76.9
12	0.102	0.099	0.176	-77.6
……				
240	0.484	0.452	0.801	-77.3

3.7 Alternative Approach

For each incremental period in the MEPDG, an analysis that uses the load-strain linear proportionality assumption requires one JULEA evaluation while conducting the same analysis without this assumption requires 39 JULEA evaluations corresponding to each single axle load increment. This has significant computing time implications for routine analysis and is not a practical approach to overcome the error introduced by the load-strain linear proportionality assumption.

A viable alternative to improve the accuracy while minimizing the impact on computing time was investigated. The approach makes use of three appropriately selected reference load levels and interpolates or extrapolates the computed strain values to other load levels. The reference loads were selected as 6, 18 and 24 kip single axle loads. This is referred to as the 3-Point approach in the subsequent discussions.

Figure 3.9 shows the predicted rutting for each layer of the test pavement structure using the 3-Point approach and the analysis described in the previous section, without the load-strain linear proportionality assumption. There is good agreement throughout the design period. The approach was validated with three other pavement structures with similar results. For space consideration, the rutting predicted by 3-Point approach and without the load-strain linearity assumption is illustrated in Figure 3.10 for one additional pavement structures. The analyses show that the 3-Point interpolation to be a promising alternative.

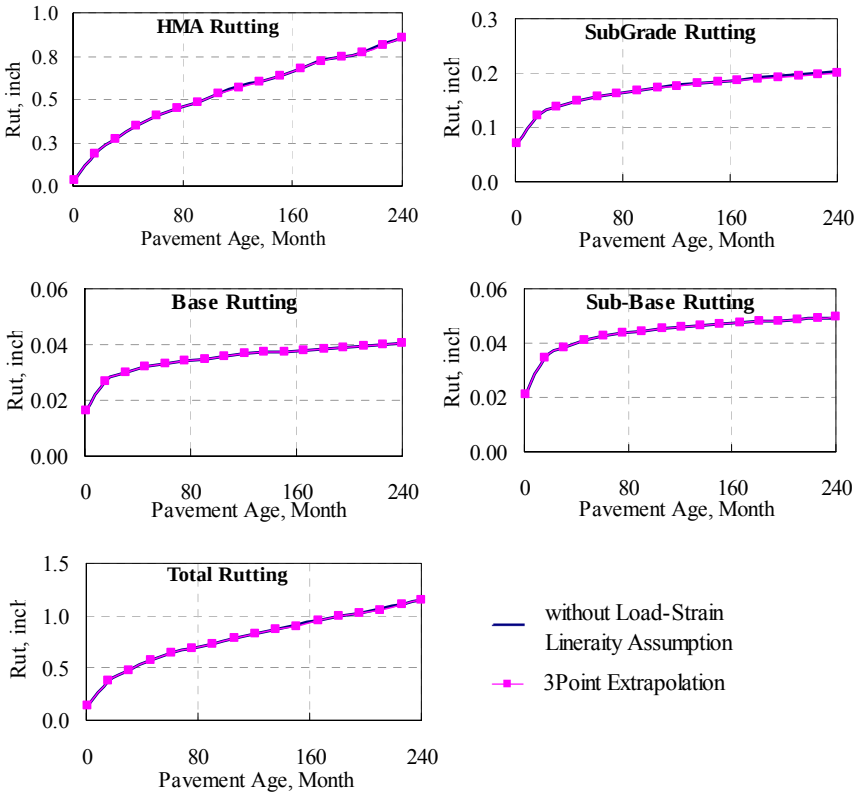

Figure 3. 9 Predicted Rutting in Pavement Layers without Load-Strain Linear Proportionality Assumption and 3-Point Extrapolation

The 3-Point interpolation will results in approximately three times the computation time as that of current MEPDG. However, the accuracy gained can be significant, particularly in the prediction of HMA layer rutting. JULEA computing time increases almost proportionally with number of evaluation depths. Computing efficiency can be achieved by limiting the 3-Point interpolation approach to only the top several inches since, as shown previously, the effect of load-strain linear proportionality assumption vanishes with increase in depth.

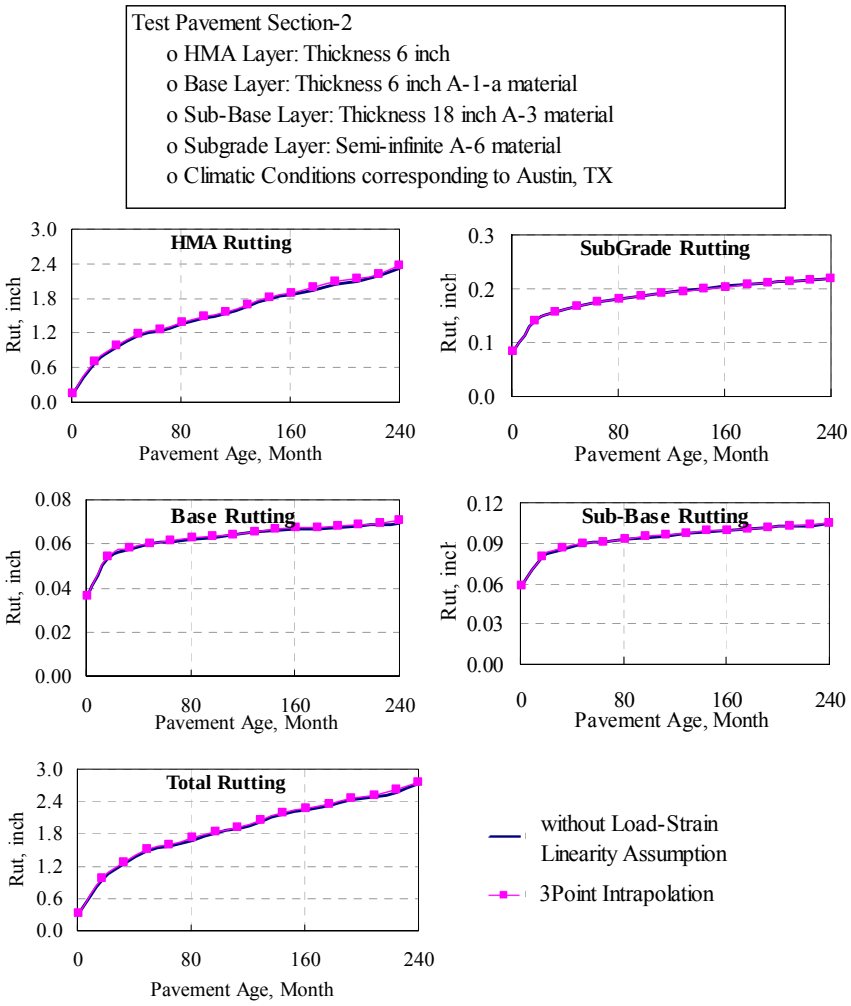

Figure 3. 10 Predicted Rutting in Pavement layers of Test Pavement Section-2 without Load-Strain Linear Proportionality Assumption and 3-Point Extrapolation

CHAPTER 4

PROPOSED RELIABILITY PROCEDURES

4.1 Introduction

The pavement distress prediction models incorporated within the MEPDG are complex functions of many input variables. As discussed before (Section 2.3) these input variables are associated with certain level of uncertainty. Therefore, the effect of the uncertainties in input variables must be incorporated systematically in a reliability based design procedure to predict the probability of failure. However, the current method for incorporating uncertainty into the MEPDG design guide (NCHRP 1-37A) is based only upon the assessment of the overall standard error of the predicted distress as compared to the observed distress. This procedure is inherently incapable of predicting the cumulative effect of the uncertainties in input variables. Reliability techniques that can incorporate their uncertainty in a systematic manner are presented here.

4.2 Proposed Reliability Procedure

The proposed reliability procedure is developed to include uncertainties in HMA material input parameters in the analysis of flexible pavement design. The probabilistic characteristics of the input variables reported in Table 2.5 are used for this purpose. The methodology is demonstrated on the prediction of two classical pavement distresses, the bottom up fatigue cracking and the permanent deformation (rutting). The new procedure is general enough to be extended to other distress computations in the future. The proposed procedure is shown in the form a flow chart in Figure 4.1. It consists of the following five stages:

1) Simulation of the material input variables based on Monte Carlo simulation techniques. Simulations using Latin Hypercube and Rosenblueth 2K+1 Point estimate method were also performed to identify their relative merits (See Chapter 5))

2) Execution of the MEPDG with mean material input values. This is used to extract modulus values for each sub-layer, climate and traffic intermediate data to be used in Stages 3 and 5.

3) Computation of the aged dynamic for each of the simulated set of material input values.

4) Identification of the representative set of layered elastic (LE) structures.

5) This stage consists of the computation of the strain response using layered elastic program JULEA, the prediction of the distress under each set of simulated variables and the computation of the design reliability. Note that the computation using JULEA is only done for the representative LE structure.

Detailed explanation of the techniques used in each of the stages is presented in the sections below.

The developed procedure was analyzed using a test pavement structure with climatic conditions corresponding to a site in Rochester, Minnesota. The pavement section, material properties and traffic data used in the analysis are summarized below:

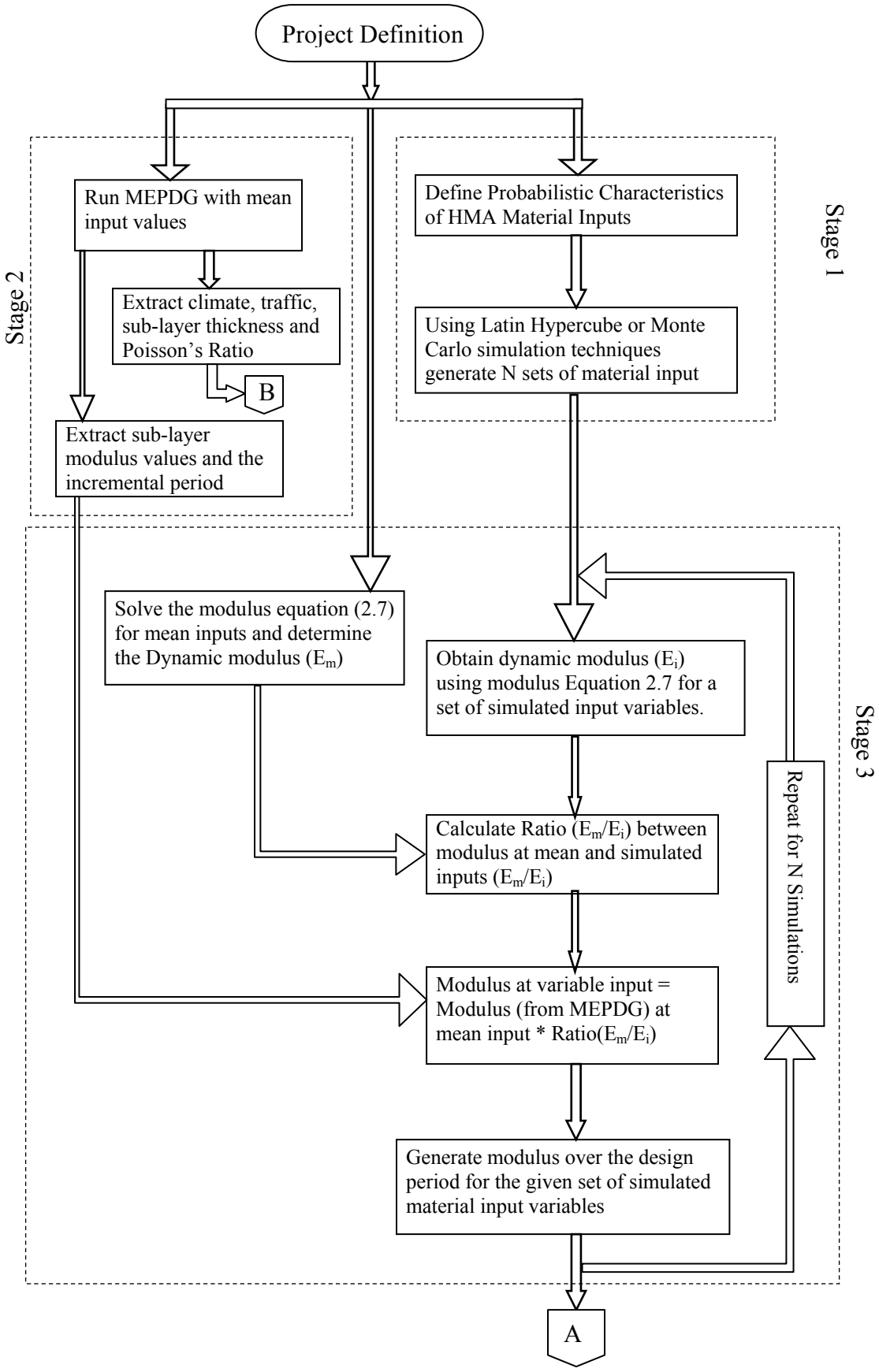
Project Definition
Stage 2
Run MEPDG with mean input values
Extract climate, traffic, sub-layer thickness and Poisson's Ratio
B
Extract sub-layer modulus values and the incremental period
Stage 1
Define Probabilistic Characteristics of HMA Material Inputs
Using Latin Hypercube or Monte Carlo simulation techniques generate N sets of material input
Stage 3
Solve the modulus equation (2.7) for mean inputs and determine the Dynamic modulus (E_m)
Obtain dynamic modulus (E_i) using modulus Equation 2.7 for a set of simulated input variables.
Calculate Ratio (E_m/E_i) between modulus at mean and simulated inputs (E_m/E_i)
Modulus at variable input = Modulus (from MEPDG) at mean input * Ratio(E_m/E_i)
Generate modulus over the design period for the given set of simulated material input variables
Repeat for N Simulations
A

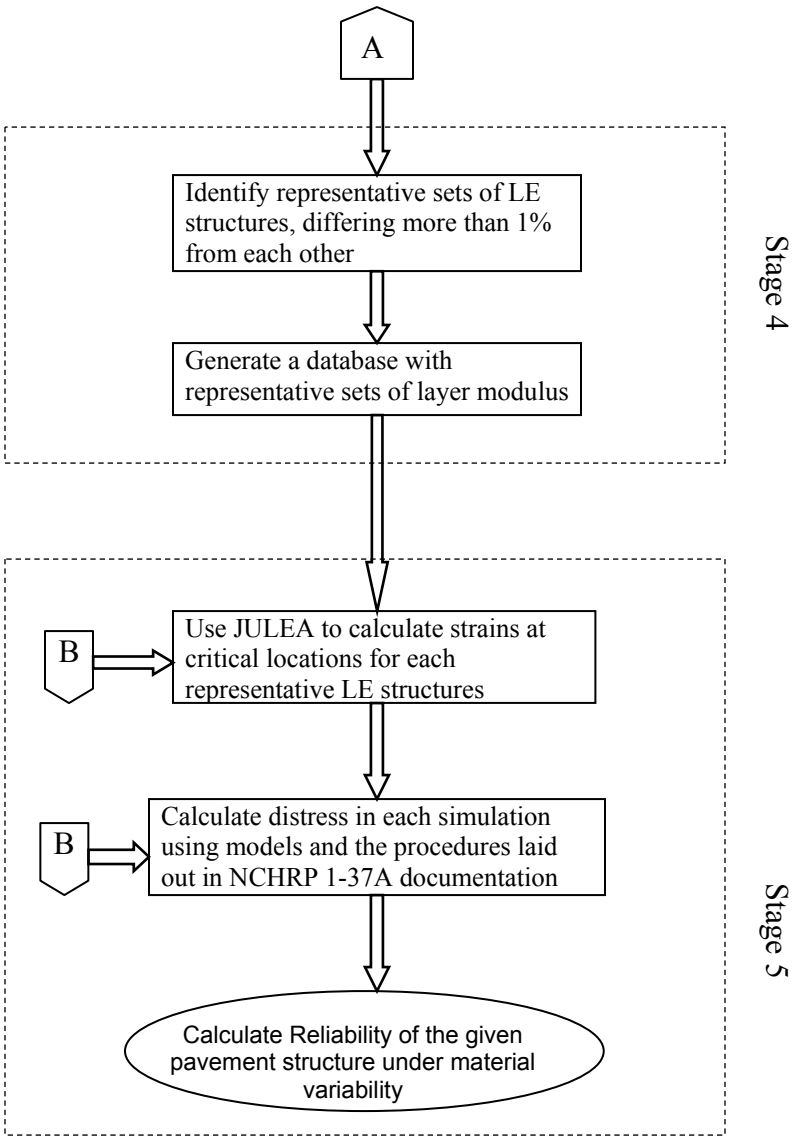

Figure 4. 1 Developed Reliability Procedure for Flexible Pavements

The pavement section

- HMA Layer: Thickness 6 inch
- Base Layer: A-1-a Granular material, Thickness 6 inch
- Sub-Base Layer: A-3 Granular material, Thickness 18 inch
- Subgrade Layer: A-6 material, Semi-infinite.
- Poisson's ratio is assumed to be 0.35 for all the layers.

Material Properties

o Asphalt binder: PG 58-34

o Mix properties: Effective binder content 12.5 % (by volume), air void 6.5 % (by volume), total unit weight 148 pcf.

o Aggregate gradation: Cumulative percentage retained in 3/4 inch, 3/8 inch and #4 sieves are 4, 21, and 60% respectively, and 3% passing the #200 sieve.

o Asphalt thermal conductivity and heat capacity are assumed with default Level 3 input values.

o Modulus and gradation for the unbound materials are taken at default Level 3 input values.

Traffic data

o AADTT: 2000, with 4% compound traffic growth.

o Traffic wander: 10 inch standard deviation.

o Tire pressure: 120 psi.

o Dual tire spacing: 12 inch.

o Vehicle class distribution: Mixed truck traffic with a higher percentage of single-trailer trucks.

o Traffic volume adjustment factors, axle load distribution factors and other general traffic inputs are assumed with default Level 3 input values.

Stage 1: Simulation of HMA Material Input Variables.

The HMA layer is characterized by material dynamic modulus (Section 2.5.1). For Level 3 input Equation 2.7 developed by Matthew Witczak (NCHRP 1-37A final report, 2004) is used to calculate the dynamic modulus. The eight material input parameters needed in modulus predictive equation are: air void content, effective bitumen

content, cumulative percentage aggregate retained on the 3/4 in sieve, cumulative percentage aggregate retained on the 3/8 in sieve, cumulative percentage aggregate retained on the No. 4 sieve, percentage aggregate passing the No. 200 sieve, loading frequency, and binder viscosity. The loading frequency is dependent on the operational speed on the pavement structure. Binder viscosity (η) (Equation 2.1) is dependent on the performance grade (PG) of the binder. These two inputs, loading frequency and binder viscosity, are considered as deterministic and equal to the mean input used in MEPDG.

The probabilistic characteristics of the six remaining parameters simulated based on LTPP data base (Table 2.5) are as shown in Table 4.1 The air void content and effective binder content are assumed as correlated input variables with a correlation coefficient of -0.2. Monte Carlo simulation is first used in developing the proposed reliability analysis. The Monte Carlo simulation technique with high number of simulations is supposed to yield the most accurate distress prediction and hence 4000 iterations are made with Monte Carlo simulation technique.

Stage 2: Running of the MEPDG with mean material input values

The design software is executed with mean material input values along with other relevant pavement design information. The following information is extracted from MEPDG output for use in the reliability analysis:

1) The modulus values generated by the design software are used to compute modulus values with simulated input variables as explained in the next stage.

Table 4. 1 Probabilistic Characteristics of the Inputs used in the Reliability Analysis

Simulated HMA Material Input	Distribution	Mean	Standard Deviation (Target)	Standard Deviation (Obtained)
Cumulative Aggregate Retained in 3/4inch Sieve, %	Normal	4	1.80	1.75
Cumulative Aggregate Retained in 3/8inch Sieve, %	Normal	21	2.50	2.56
Cumulative Aggregate Retained in No.4 Sieve, %	Normal	60	3.50	3.50
Aggregate Passing No.200 Sieve, %	Normal	3	1.00	1.02
Air Void content, %	Normal	6.5	1.50	1.49
Effective Binder Content, %	Normal	12.5	0.50	0.50

2) The number of load repetition per day in each load increment for each axle type from the given mean traffic inputs. Since uncertainty in traffic input is not accounted in the proposed reliability analysis, for each simulation, the load repetitions calculated by design software are used in the distress computation. However, if required, uncertainties in traffic data can be accounted for by using the procedure outlined in Section 2.5.

3) Temperature profile in each HMA sub-layer over the sub-season in each month of the base year. This value is assumed to be the same for each simulation in the reliability analysis.

Stage 3: Computation of Aged Dynamic Modulus for Simulated Material Inputs

The pavement structure with different material layers are further sub-divided internally within MEPDG design software to sub-layers that are characterized by their corresponding material modulus (Section 2.5.1). Distress prediction for each set of simulated material input requires the value of modulus to be determined for each sub-layer over the design period. The HMA dynamic modulus predictive equation 2.7 (in input Level 3) or the laboratory test (in input Level 1) computes the HMA layer modulus corresponding to the initial construction stage. Note that the HMA and unbound layer modulus need to be corrected for temperature and moisture based on the depth of the sub-layer and the environmental conditions. The Enhanced Integrated Climatic Model (EICM) Chapter 2.6) in the design software is used to generate the temperature and moisture profile and the dynamic modulus is adjusted accordingly. Global aging model (Section 2.5.1) corrects the asphalt dynamic modulus for environmental aging effects.

An efficient scheme is developed to incorporate EICM and Global aging models in the reliability analyses. It is used to compute the modulus values for the simulated input variables based on the modulus values extracted from the design software calculations in Stage 2. The simulated modulus values are subsequently corrected for temperature, moisture and other environmental deterioration effects. This process eliminates the need for repeated execution of the global aging model and the EICM (Chapter 2.6) for each iteration.

The scheme to compute the layer modulus for each iteration is detailed as follows:

Step 1: Determination of the un-aged modulus master curve corresponding to mean input values using the prediction equation (Equation 2.7) for Level 3 inputs.

Step 2: Use of the modulus prediction equation (Equation 2.7) and determine the un-aged modulus corresponding to a set of simulated input variables.

Step 3: Calculation of the ratio of the un-aged modulus values computed using mean input variables (Step 1) and simulated variables (Step 2).

Step 4: Multiplication of the asphalt dynamic modulus values obtained from MEPDG in Stage 2 by the ratio obtained in Step 3 to get the material property (dynamic modulus) of each asphalt sub-layer at each quintile (section 2.7) over the design period.

Step 5: Repetition of Step 2 to 4 for N set of sampled input variables and generate a database with asphalt dynamic modulus for different pavement structure over the design period.

Laboratory measurement of HMA dynamic modulus is required in input Level 1. Any uncertainty in its measurement can be handled by a direct simulation of the laboratory measured HMA dynamic modulus with the expected standard deviation without using Steps 1 and 2 in the above scheme. The ratio between simulated and the mean modulus is obtained as in Step 3 for input Level 3 above, as are other remaining steps.

Validation

The efficiency of the above in reproducing modulus value for simulated variables is validated by comparing the dynamic modulus computed by the developed procedure with that computed by the MEPDG. The results are summarized in Table 4.2. The column (a) consists of the modulus values (E_M) as calculated by the MEPDG for the first sub-layer at the first quintile of the first month of the design period. This value (Column a) is obtained by running the MEPDG using mean material input values (Stage 2). The column (b) consists of the dynamic modulus (E_S) values, for the same pavement structure, as calculated by the MEPDG, but with one set of simulated values for the HMA material input variables. The objective of the scheme here is to compute the dynamic modulus values E_S from E_M without executing the MEPDG for each simulated material input.

The dynamic modulus prediction Equation (2.7) is used to calculate the dynamic modulus values in top sub-layer with both mean and simulated input material variables, E_1 and E_2 respectively (column c and d). These modulus values are not adjusted for environmental conditions.

The ratio between E_1 and E_2 are then calculated (Column e). It was found that the ratio remained constant not only throughout the design period but also for the different sub-layers. Dynamic modulus values (E_C ,Column f) for simulated material inputs are calculated by dividing the modulus values obtained from MEPDG at mean material input values (E_M) by the ratio calculated (Column e). Column (g) calculates the deviation between the predicted dynamic modulus values (E_C) from the modulus values calculated

by MEPDG (E_S) both at simulated material input values. It can be seen that the maximum ratio of the deviation of the simulated values is less than 0.5 %.

Table 4. 2 Computation of Dynamic Modulus for Simulated Input Variables

Calculated by MEPDG		Calculated from Equation 2.7				
Mean material inputs, E_M (a)	Simulated material inputs, E_S (b)	Mean material inputs, E_1 (c)	Simulated material inputs, E_2 (d)	Ratio E_1/E_2 (e)	Computed HMA Dynamic Modulus, E_C (f)	Ratio of Deviation from MEDPG values, $\frac{(E_S - E_C)}{E_S}100$ (g)
HMA Dynamic modulus, psi					psi	%
5369250	*4430840*	3453220	2845005	1.2138	*4423565*	0.164
5369170	*4430770*	3047253	2510541	1.2138	*4423499*	0.164
5359560	*4422870*	2538781	2091626	1.2138	*4415581*	0.165
5207210	*4297510*	1938478	1597054	1.2138	*4290065*	0.173
3858750	*3187150*	1436056	1183124	1.2138	*3179109*	0.252
2958400	*2444870*	1097294	904028	1.2138	*2437337*	0.308
2689780	*2223250*	1028756	847561	1.2138	*2216029*	0.325
2766180	*2286290*	1058742	872266	1.2138	*2278973*	0.320
3288220	*2716870*	1331462	1096952	1.2138	*2709066*	0.287
3764270	*3109270*	1913999	1576887	1.2138	*3101270*	0.257
5369500	*4431040*	2725581	2245525	1.2138	*4423771*	0.164
5369330	*4430910*	3478721	2866014	1.2138	*4423631*	0.164

The modulus corresponding to the third HMA sub-layer in the given pavement structure at third quintile is compared to demonstrate the efficiency of the proposed scheme as shown in Figure 4.2. This figure shows the variation of modulus values

calculated by the proposed scheme and that calculated by MEPDG for the same simulated input material variable as a function of time. It can be seen that the two results match very well demonstrating the accuracy of the proposed scheme. The comparison was repeated for all asphalt sub-layers and sub-seasons (Quintiles) and found to hold well.

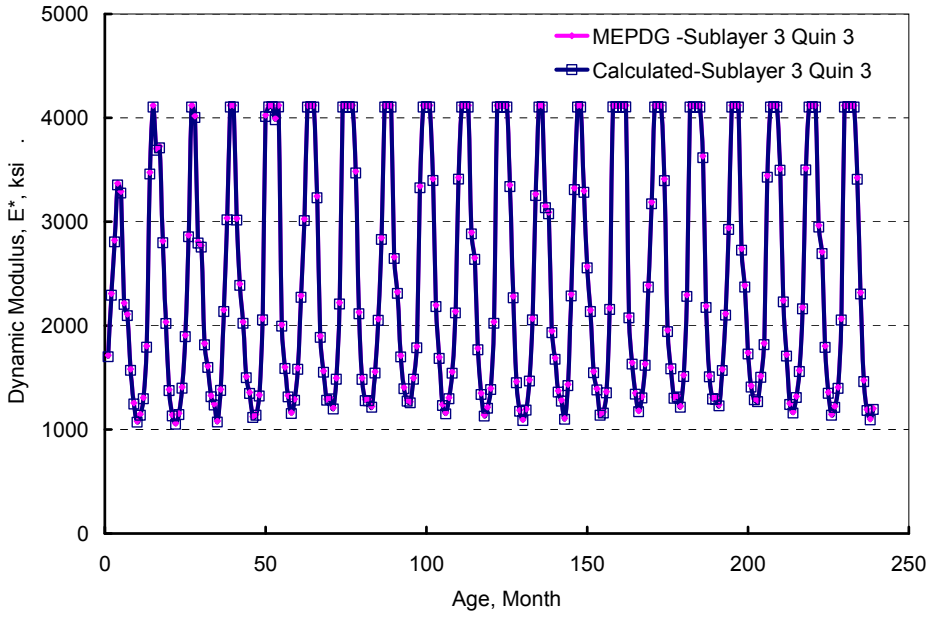

Figure 4. 2 Corrected and MEPDG generated Dynamic Modulus

The difference between modulus determined using this scheme and that directly obtained from MEPDG using simulated values were found to be much less than 1% over the entire design period for different pavement structural conditions. This minimal difference makes the use of the scheme to compute the HMA dynamic modulus applicable to any pavement structure.

The proposed schemes is thus used to generate a database 'DB1' that contains sets of layer modulus (each termed as 'layered elastic structure' or 'LE structure' in the subsequent sections) generated over the design period and 'N' number of simulations.

Stage 4: Identification of Representative Layered Elastic Structures

The MEPDG generates five layered elastic (LE) structures per incremental period (monthly or 15 days) to account for the environmental moisture and temperature variations more accurately. The distress prediction requires the strain response at critical locations of each LE structure. The design guide uses the layered elastic analysis program JULEA for determination of load-structure response. In a typical analysis with 20 year design period about 1400 LE structures are generated for each design iteration i.e. JULEA has to be executed 1400 times. Since reliability computations require several hundreds of iterations, execution of JULEA for each LE structure within database DB1 is the single most time consuming process that requires a significant computational time usually in the order of a few weeks to complete. It was identified as the main limitation to the use of reliability analysis as identified in the design manual (NCHRP Project 1-37A Final Report, 2004).

In order to minimize the number of JULEA executions, a technique was developed to identify a subset of representative layered elastic (LE) structures from the set of simulated LE structures (DB1) that will represent the entire set of LE without significant loss of accuracy. When a reliability analysis is performed involving hundreds of iterations where each iteration involves hundreds of LE structures, a large number of them are bound to constitute near identical modulus values. This fact is exploited here in developing a practical reliability analysis procedure. Execution of JULEA is done only

for LE structures whose sub-layer modulus values are not within 1% of an LE structure that had already been analyzed. This reduces the required number of JULEA executions significantly without compromising the accuracy of the final results. For example, our computations have shown that for 4000 design simulations, such a choice could reduce the JULEA computational time down to about 1% of that for all LE structures.

A database (DB1) is generated with a set of 'n' LE structures over the design period and for required number of simulation (as explained in Stage 3). This stage generates two databases DB2 and DB3. The database DB2 containing 'm' representative LE structures and database DB3 containing all 'n' simulated LE structures along with the identity number (ID) referring to the corresponding closest representative LE structure in DB2. JULEA is executed only for the LE structures in database DB2.

The procedure is explained in detail below and a sample calculation is provided in Appendix A.

Step 1: Write the first LE structure from database DB1 to database DB2 and DB3. Since first LE structure is always the representative one, m=1

Step 2: Calculate the deviation between corresponding sub-layer modulus between LE structure 'i' in DB1 and 'j' in DB2 as

$$Deviation(j,z) = abs\left|\frac{E_{DB}(j,z) - E_n(i,z)}{E_n(i,z)}\right| * 100 \qquad (4.1)$$

where $E_n(i, z)$ - i^{th} LE structure in database DB1. i = 2 to n

$E_{DB}(j, z)$ –j^{th} LE structures in database DB2. j = 1 to m.

z – Sub-layer in the LE structure. z = 1 to total number of sub layers

n – Total number of LE structures in DB1 generated in stage 3.

Step 3: Repeat Step 2 for all sub-layers and obtain the maximum deviation.

Step 4: Repeat Step 2 and 3 for 'm' LE structures in DB2.

Step 5: Obtain minimum of the deviation over 'm' LE structures in DB2. If the minimum deviation is:

(i) More than 1%: identify $E_n(i, z)$ as representative LE structure and append to DB2 (m= m+1). Also, mark the LE structure as m^{th} representative LE structure and append to DB3.

(ii) Less than or equal to 1%: Identify the LE structure $E_n(i, z)$ by the ID of LE structure $E_{DB}(j, z)$ corresponding to minimum deviation and append the LE structure $E_n(i, z)$ to DB3.

Step 6: Repeat Step 2 to Step 5 for n LE structures in database DB1.

Validation

The effect of the choice of representative LE structure on strain response was evaluated before it was used in reliability analyses. For this purpose, one LE structure was taken as representative and the procedure was used to identify 20 similar LE structures from DB1 (whose modulus varied less than 1%). The strain values at the critical locations were computed using JULEA with the actual sub-layer modulus values of 20 LE structures and the representative LE structure. The strain values calculated for representative LE structure and each similar LE structure are compared and the deviation in strain values at each critical location were computed. The maximum deviation in

strain values at any critical point (for the given pavement structure, strain is calculated at 18 critical locations) between representative LE and the 20 actual LE structure is summarized in Table 4.3. The proposed procedure of executing JULEA for the chosen LE structures results in a maximum of 3% deviation in computed strain values with 80% of the deviation less than 1%.

Table 4. 3 Effect of the Efficiency Procedure on Strain Values

Similar Layer Elastic Structure	Maximum Deviation from the reference LE structure, %	
	in Sub-layer Modulus	in Strain Values
1	0.72	1.5
2	0.46	1.62
3	0.99	1.3
4	0.40	1.05
5	0.32	1.03
6	0.32	1.03
7	0.32	1.03
8	0.91	2.86
9	0.72	1.44
10	0.32	1.03
11	0.91	2.93
12	0.47	1.59
13	0.67	1.45
14	0.74	1.38
15	0.18	1.98
16	0.64	1.48
17	0.73	1.45
18	0.35	1.03
19	0.91	2.93
20	0.55	1.52

The choice was also analyzed with respect to computed HMA rutting. The study was to quantify the effect of the deviation observed in strain over the distress predicted. The HMA rutting predicted by the Stand-Alone application (Section 3.6) was compared by running JULEA for

1) All layered elastic (LE) structures generated.
2) Only representative layered elastic (LE) structures (the procedure explained above).

Figure 4.3 compares the HMA rutting predicted over the design period for both cases. The distress computed for both cases were found to be similar at the end of each month over the design period. The results show that the proposed choice has little effect on predicted distress values.

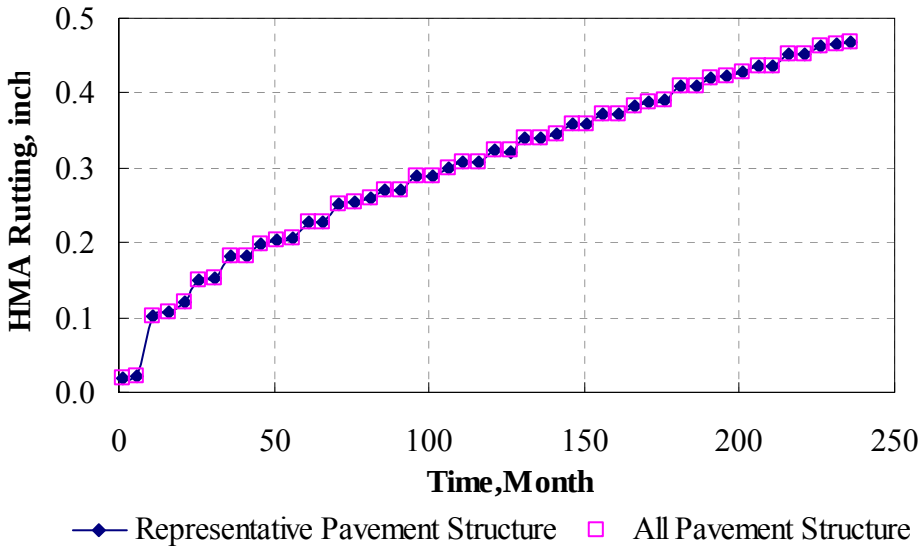

Figure 4. 3 Effect of JULEA Execution only on Representative Layered Elastic Structure

Efficiency

The developed technique leads to a significant reduction in computation time by limiting the required number of JULEA executions. The efficiency increased with increase in the number of iterations. For the pavement under evaluation for 300 simulations, JULEA has to be executed 529,500 times (Total number of LE structures) without this technique. The procedure has identified only 24734 (4.7%) set of LE structures whose moduli varied by more than 1% from other structures that are thus taken as the representative ones. This number reduces to 0.8% when the number of simulation is increased to 4000.

Stage 5: Prediction of Reliability of the Distress

This stage consists of computation of the distress in each simulation and the calculation of the reliability of each predicted distress. The steps involved in this stage are detailed below.

Step 1: Use the representative LE structures from database DB2 and JULEA to calculate strains at critical locations.

Step 2: Calculate pavement distresses (Rutting and Fatigue cracking) at critical locations using the Stand-Alone application (Section 3.6) with the prediction models as given in the MEPDG user documentation. The climate and traffic information obtained in Stage 2 are used.

Step 3: Repeat Step 2 for required number of simulations.

Step 4: Compute the reliability of the given pavement structure.

The database DB3 that contains all simulated LE structures is used in step 2. The ID of each LE structure in the database DB3 is used to trace the strain values from the corresponding LE structure in DB2, for which JULEA has already been executed and strain values are computed at critical locations.

The stand-alone application developed (Section 3.6) has been modified to perform the developed reliability procedure. The procedure stated in MEPDG documentation to compute both rutting and fatigue bottom-up cracking has been incorporated in the stand-alone application. The required number of simulation with Monte Carlo sampling technique has been verified by a convergence test.

4.3 Check for Convergence

The number of iterations required for output distributions to converge is dependent on the model being simulated and the distribution functions included in the model. More complex models with highly skewed distributions will require larger number of iterations than simpler models. It is important to run sufficient number of iterations so that the statistics generated on outputs are representative. However, there comes a point where results converge and the time spent for additional iterations is essentially wasted because the characteristics of the statistics generated do not change much.

In the Monte Carlo simulation, convergence monitoring was deployed to evaluate the stability of the output distributions during simulation. As number of iteration increases, output distributions become more "stable" as the statistics describing each

distress distribution change less with additional iterations. The statistics describing each distress distribution was monitored at the end of every 100 iterations. The number of simulations required for convergence is based on the calculation of the normalized error as defined below at five locations (10^{th}, 25^{th}, 50^{th}, 75^{th} and 90^{th} percentiles) of the statistical distribution:

$$Error = \left| \frac{(DValue@i^{th}\,simulation - DValue@(i-100)^{th}\,simulation)}{S\tan dardDeviation@i^{th}\,simulation} \right| \qquad (4.2)$$

where, DValue - distress value at p^{th} percentile in the distress generated distribution.

In addition, the normalized error in the standard deviation (taken as DValue) of the entire distribution is estimated using the above equation. The required number of simulations is assumed to be attained when the absolute maximum of the above six error measures falls below a specified convergence tolerance.

Figure 4.4 (a) and (b) shows the variation of maximum error calculated after every 100 iterations respectively in HMA rutting and fatigue cracking distribution. It can be seen that the fatigue model converges faster than the rutting model. The maximum error in HMA rutting distribution (Figure 4.4 (a)) converges to a constant value of around 1% after 3000 iterations. In the case of fatigue cracking distribution (Figure 4.4 (b)) the maximum error converges to 2% just after 1800 iterations. Thus for the given problem, if Monte Carlo sampling technique is used, it is necessary to run more than 3000 iterations in order to capture the actual statistical properties of the distress distribution.

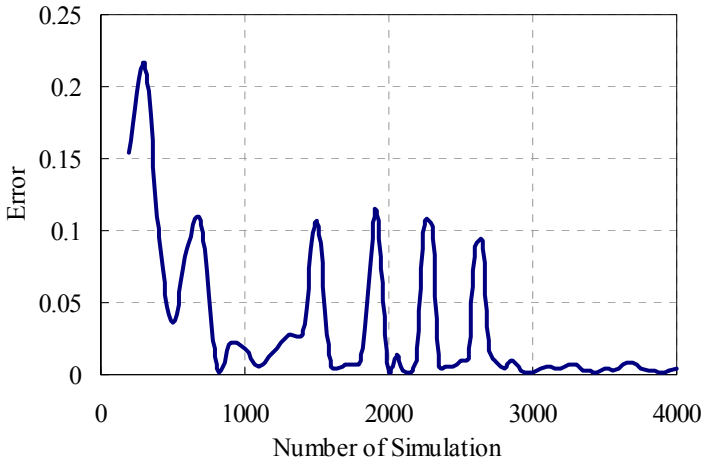

(a) on HMA Rutting Distribution

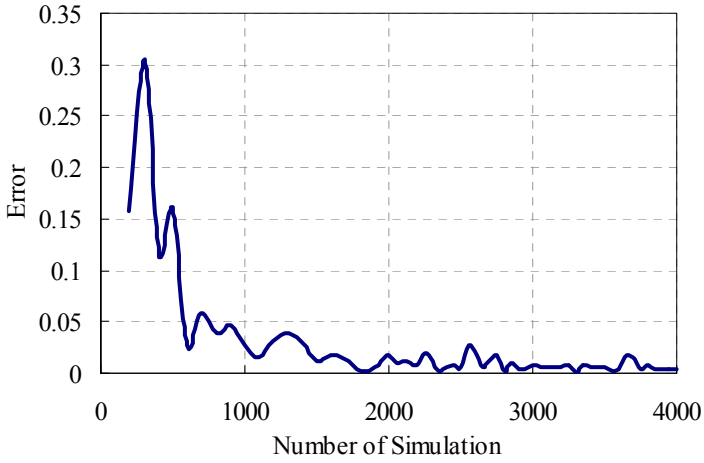

(b) on Fatigue Bottom-Up Cracking Distribution

Figure 4. 4 Convergence Test on Monte Carlo Simulation

4.4 Statistical Properties of Predicted Distress Distribution

Figure 4.5 (a), (b), and (c) show the distribution of predicted pavement distresses, HMA rutting, total rutting, and fatigue bottom-up cracking, respectively for a given level of HMA material uncertainty (Table 4.1) generated using Monte Carlo simulation method. It can be seen that that the predicted distribution for HMA and total rutting

closely resemble normal distribution (Figure 4.5 (a) and (b)). It was also found that the rutting pattern for base, sub-base and subgrade showed a similar distribution. On the other hand, the distribution of fatigue bottom-up cracking closely resembles a log-normal one.

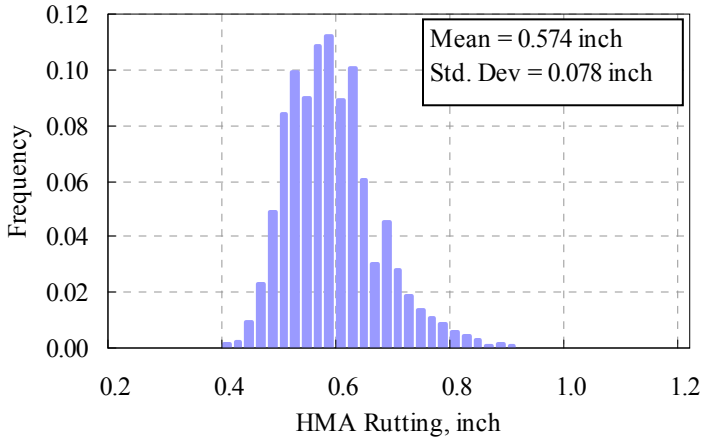

(a) HMA Rutting

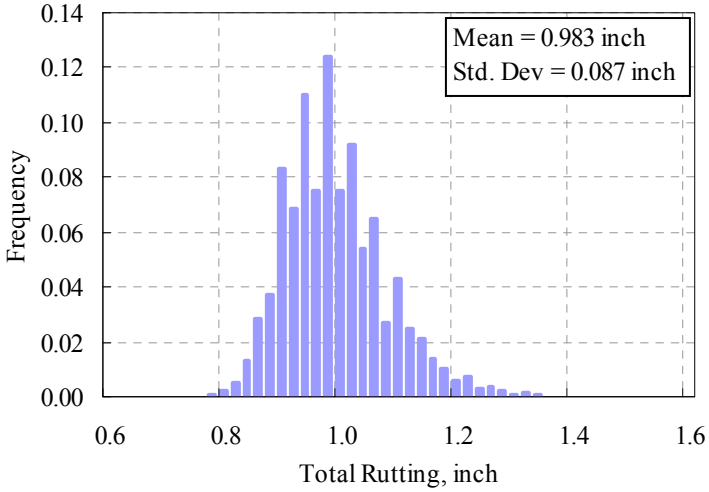

(b) Total Rutting

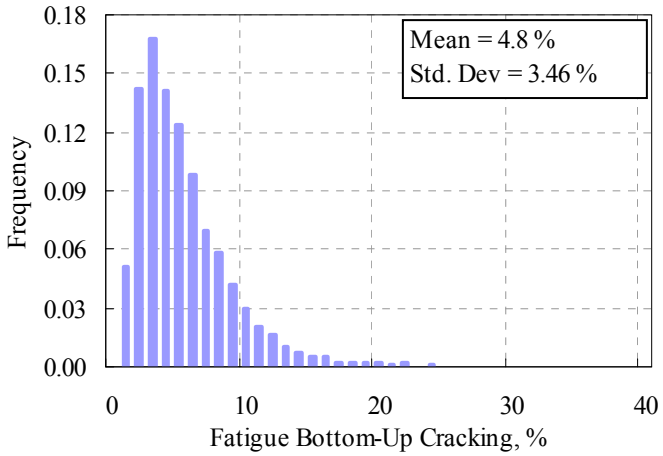

(c) Fatigue Bottom-Up Cracking

Figure 4. 5 Distribution of different Predicted Pavement Distress under HMA Material Variability

Figure 4.6 (a), (b), (c) show the cumulative distribution of HMA rutting, total rutting and fatigue bottom-up cracking predicted, respectively for the given level of HMA material uncertainty. It can be seen that for HMA and total rutting the left tail of the normal distribution is truncated at 0.4 inch and 0.78 inch respectively (Figure 4.6 (a) and (b)) show. The same effect is much pronounced in fatigue performance with log normal distribution (Figure 4.6 (c)), which indicate higher effect of material uncertainty on poor fatigue performance.

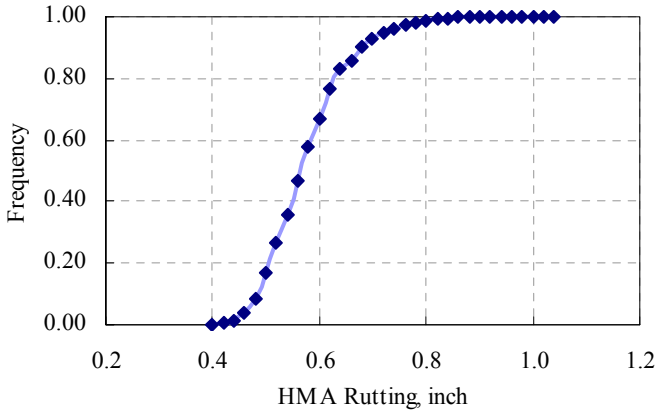

(a) HMA Rutting

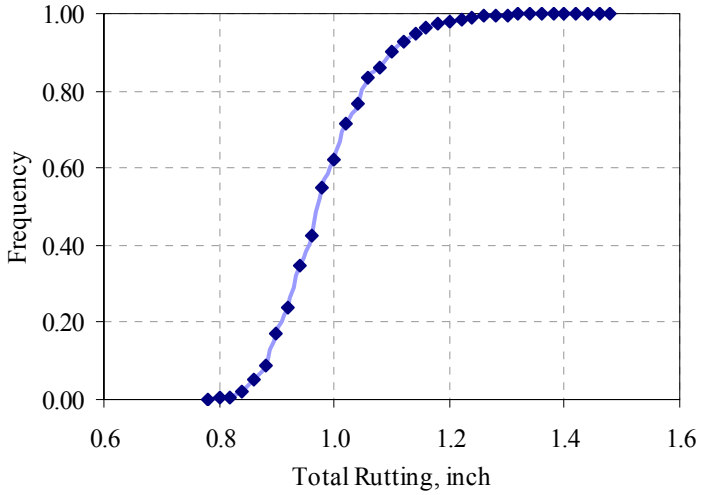

(b) Total Rutting

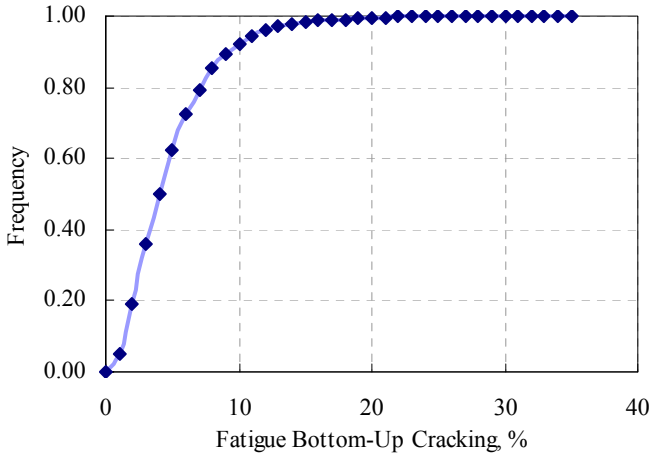

(c) Fatigue Bottom-Up Cracking

Figure 4. 6 Cumulative Distribution of the Predicted Pavement Distress under HMA Material Variability

For the combination of the site conditions, design features, and the binder grade considered in the simulation, Table 4.4 compares the distress predicted by MEPDG and the developed reliability procedure at 90% reliability. It can be seen that distress values (both total rutting and fatigue bottom-up cracking in Table 4.4) predicted by the new procedure is less than that by the MEPDG. This is due to the fact that the MEPDG

calculations at the given reliability level (90%) includes variability in layer thickness, binder type, error due to the model lack-of-fit, measurement error apart from the uncertainty in mix design. However, the proposed procedure includes only the uncertainty in mix design in to the reliability analysis. The potential distribution of distress predicted by the MEPDG and the developed reliability procedure is shown schematically in Figure 4.7. As seen the use of HMA material uncertainty only in the new procedure leads to less variability in the predicted distress as seen in the values predicted by the developed procedure at 90% reliability.

Table 4. 4 Distress Predicted at 90% Reliability

Pavement Distress	MEPDG	Developed Reliability Procedure Monte Carlo Simulation (N=4000)
HMA Rutting, inch	N/A*	0.6736
Base Rutting, inch	N/A*	0.0867
Sub-Base Rutting, inch	N/A*	0.1114
Subgrade Rutting, inch	N/A*	0.2226
Total Rutting, inch	1.1966	1.094
Fatigue Bottom-up Cracking, %	22.15	9.14

*- MEPDG doesn't report the rutting at 90% reliability in individual layers

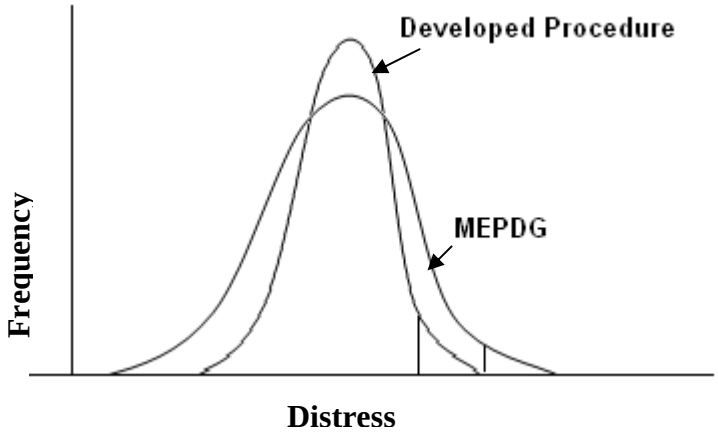

Figure 4. 7 Variability in Predicted Distress Computed by MEPDG and Developed Procedure

The predicted reliability at the target distress by the MEPDG and the proposed technique is compared in Table 4.5. The less variability in distress predicted by the proposed technique (Figure 4.7) translates into lesser reliability at target HMA and total rutting (both of which will be at the left tail of the distribution when predicted reliability is very less) and higher reliability at target fatigue bottom-up cracking (which will be at right tail of the distribution when the predicted reliability is very high).

Table 4. 5 Reliability Predicted at Target Distress

Pavement Distress	Target Distress	Predicted Reliability	
		MEPDG	Developed Reliability Procedure Monte Carlo Simulation (N=4000)
HMA Rutting	0.25 inch	1.84	<0.01
Total Rutting	0.75 inch	8.83	<0.01
Fatigue Bottom-up Cracking	25 %	96.48	99.99999

4.5 Relative Merits of the Proposed Reliability Procedure

The following summarizes the merits of the proposed reliability procedure compared to the existing one in the MEPDG.

1) The procedure makes it possible to consider the variability in key HMA material inputs into pavement reliability analysis.

2) The procedure can be expanded to include the uncertainties in other material inputs, traffic characteristics and also to incorporate the errors associated with the prediction models. Thus, the designer can input the mean, standard deviation and distribution of input variable and obtain much more accurate design reliability values.

3) The sensitivity of the distress to variations in the inputs can be analyzed from the reliability results obtained through the developed procedure (Chapter 5.5). This provides the designer with improved knowledge of the most critical inputs that should be estimated with greater accuracy.

CHAPTER 5

RELIABILITY TECHNIQUES AND SENSITIVITY ANALYSES

5.1 Introduction

The last chapter used the Monte Carlo simulation technique to develop reliability analysis of pavements. While, this technique is one of the most powerful and accurate methods of reliability analysis, it is computationally very intensive for routine applications. Monte Carlo simulation method with less number of iterations is not recommended because of the possibility of failing to replicate the input distribution adequately in the sampled inputs. Therefore, two other methods, namely, the Latin Hypercube and the Rosenblueth's Point Estimate Method, that are computationally less intensive to calculate the reliability of pavements are discussed in this chapter. The results are compared with those from Monte Carlo simulation. Finally, the effectiveness of the three simulation techniques is compared. The methods are also verified with a similar study done in the past but with large computational time. Sensitivity analyses of HMA input variables on computed distress is performed using the data obtained from the Monte Carlo simulation method.

5.2 Latin Hypercube and Rosenblueth's Point Estimate Methods

Inputs were sampled with the probabilistic characteristics in Table 4.1. Latin Hypercube sampling method (Section 2.10.3) is used with 300 simulations. In the case of Rosenblueth's 2K+1 point estimate method the number of simulation is dependent on the number of uncertain variables considered (Section 2.10.3). In this study, uncertainty in

six material variables (K= 6) were considered and hence 13 simulations are required for Rosenblueth's method.

The proposed reliability analysis is performed on simulated set of input variables. Pavement section described in Section 4.2 is used in the analysis. Table 5.1 summarizes the results from reliability analysis from the two simulation methods. They include the values of the mean, co-efficient of variation (COV) and the distress at 90% reliability. For comparison purposes, the results using Monte Carlo simulation are also shown in the same table. Equations 2.49 and 2.50 were used in the calculation of the mean and COV of the distress distribution for the Rosenblueth's point estimate method. The correlation coefficient between air void content and effective binder content is not used in Rosenblueth's point estimate method. Note that the Rosenblueth's point estimate method is not capable of calculating the distress distribution (Section 2.10.3). Thus, the distress reported at 90% reliability for Rosenblueth's point estimate method (Table 5.1) was computed by assuming it to have a normal distribution. Therefore, if the entire distress distribution characteristics (including distribution type) of a variable are required it is necessary to run actual simulation using either Monte Carlo or Latin Hypercube. It can be seen that the mean and COV of the output distribution obtained from both Latin Hypercube and Rosenblueth's 2K+1 point estimate method are quite close to values obtained from Monte Carlo Simulation.

Table 5. 1. Comparison of Simulation Techniques

Distress	Latin Hypercube Simulation (N=300)			Rosenblueth's Point Estimate Method (N=13)			Monte Carlo Simulation (N=4000)		
	Mean	COV	@ 90% reliability	Mean	COV	@ 90% reliability	Mean	COV	@ 90% reliability
HMA Rutting, inch	0.575	14.2	0.692	0.575	13.7	0.676	0.574	13.7	0.674
Base Rutting, inch	0.082	4.68	0.087	0.082	4.6	0.087	0.082	4.46	0.087
Sub-Base Rutting, inch	0.108	2.9	0.112	0.108	2.8	0.112	0.108	2.7	0.111
Subgrade Rutting, inch	0.22	1	0.223	0.22	0.89	0.220	0.22	0.95	0.223
Total Rutting, inch	0.985	9.2	1.115	0.985	8.85	1.097	0.983	8.86	1.094
Fatigue Bottom-up Cracking. %	4.86	73.3	9.01	4.79	62.9	8.65	4.8	72.1	9.14

5.3 Effectiveness of Simulation Techniques

The convergence test on results from Monte Carlo simulations (Chapter 4.3) suggests that 4000 simulation is large enough to predict accurate results for the case study problem. Hence, the results from Monte Carlo simulation are considered accurate and compared with the results from Latin Hypercube and Rosenblueth's method in terms of accuracy and time efficiency.

The reliability of pavement distress prediction for a given level of uncertainty in material input is evaluated using these different simulation techniques. Table 5.2 summarizes the execution time taken for different simulation runs based on computer with 3 GHz Intel processor and 1GB RAM. Execution of 4000 simulations by Monte Carlo method required 4.5 days of computation time. For the number of probabilistic variables involved, the convergence test in Chapter 4.3 suggested a minimum of 3000 Monte Carlo simulations for accurate reliability analysis; which will take 3.5 days (since in the developed procedure JULEA is executed only for representative pavement structures, the number of simulations and computation time are not linearly proportional). For the reliability analysis to be time efficient there is a necessity to determine an alternate sampling method that can predict results at the same level of confidence to Monte Carlo simulation method with fewer number of iteration.

Latin Hypercube sampling method, can compute entire probabilistic characteristics of the output distress distribution with accuracy that is comparable to that of the Monte Carlo Simulation within a reasonable computation time. Also, the data from the Latin Hypercube simulation is required for a robust sensitivity analysis of the input data (Chapter 5.4). Hence, Latin Hypercube is an efficient alternate to the Monte

Carlo simulation technique. With few iteration, Rosenblueth's 2K+1 point estimate method can compute the mean and co-efficient of variation of the distress characteristics to the accuracy close to Monte Carlo simulation method; however the method is not capable to determine the distress distribution type. Hence, Rosenblueth's 2K+1 point estimate method can only be used to get initial approximate distress distribution characteristics or a sensitivity estimate (as in past literatures Chapter 5.4).

Table 5. 2 Execution Time for Reliability Analysis

Simulation Method	Execution Time
Monte Carlo Simulation (N=4000)	4.5 day
Monte Carlo Simulation (N=3000)	3.5 day
Latin Hypercube Simulation (N=300)	25 hour
Rosenblueth's 2K+1 Point Estimate Method (N=13)	3 hour

5.4 Validation of the Reliability Procedures

The proposed reliability procedure is verified on a pavement structure studied by Khazanovich et al (2008) in their reliability analyses. Khazanovich et al (2008) developed a framework to include the variability of HMA materials in pavement design reliability analysis by combining DAKOTA, a software toolkit for performing uncertainty quantification on engineering models, along with the MEPDG. The variables along with their probabilistic characteristics used in the analysis are summarized in Table 5.3. DAKOTA software was used to simulate 300 samples for each uncertain input variable through Latin Hypercube sampling technique. Macros were written in 'Workspace Macro Pad' and 'Excel' to generate MEPDG project files with

corresponding input samples generated by DAKOTA. The MEPDG was executed for 300 iterations which took two computers 4 days of computational time. This included the execution of EICM and the JULEA execution for each L-E structures 300 times. The characteristics of the distress distribution were obtained from the values computed by MEPDG at 50% reliability level. The drawback of the developed technique as reported in Khazanovich et al (2008) attribute to the computation time involved in repeated execution of MEPDG.

Table 5. 3 Probabilistic Characteristics used in Khazanovich et al. 2008

HMA Material Property	Distribution	Distribution Characteristics
Effective Binder Content, %	uniform	between 10 and 15 %
Air voids, %	Uniform	between 5 and 8 %
Cumulative of Aggregate Retained in 3/4 inch sieve, %	Deterministic	0
Cumulative Aggregate Retained in 3/8 inch sieve, %	Normal	Mean 21%, Standard Deviation 0.42%
Cumulative Aggregate Retained in No. 4 sieve, %	Uniform	between 57 and 63 %
Aggregate Passing No.200 sieve, %	Uniform	between 2.85 and 3.15 %

The problem studied by Khazanovich et al (2008) is repeated with the proposed reliability procedures. Default values in the MEPDG were used for inputs that were not included in the paper. Execution of JULEA for only the representative layered-elastic structures in the proposed procedure rather than for the entire layered-elastic structures

and also the avoidance of redundant EICM execution reduced the computational time to 25 hours in one computer. i.e. approximately eight times faster than that reported by Khazanovich et al (2008).

Table 5.4 summarizes the distress predicted by the MEPDG and the developed reliability procedure at 90% reliability. Table 5.5 compares the reliability predicted by the MEPDG and the developed reliability procedure at the target distress mentioned in the design analysis. Note as detailed before (Section 4.2) the proposed reliability procedure is restricted to consideration of the variability corresponding to HMA mix only. Thus, the distribution computed by the proposed procedure is expected to have less uncertainty in the predicted distress compared to the MEPDG values (See also Figure 4.7).

Table 5.4 Distress at 90% Reliability

Distress	Distress @ 90% Reliability	
	MEPDG	Developed Reliability Procedure
HMA Rutting, inch	NA	0.659
Base Rutting, inch	NA	0.086
Sub-Base Rutting, inch	NA	0.111
Subgrade Rutting, inch	NA	0.222
Total Rutting, inch	1.227	1.078
Fatigue Bottom-up Cracking. %	22.39	7.4

NA – Not reported in MEPDG

Table 5. 5 Reliability predicted at Target Distress

Distress	Target Distress used in Design Analysis	Reliability @ Target Distress	
		MEPDG	Developed Reliability Procedure
HMA Rutting	0.25 inch	1.84	<1
Total Rutting	0.75 inch	8.83	<1
Fatigue Bottom-up Cracking	25 %	96.48	99.99999

Table 5.6 summarizes the distress predicted by the MEPDG (both reported in Khazanovich et al (2008) and obtained by re-execution with available data) and the stand-alone application using the mean values for the uncertain input variables (Table 5.3). It is noted that even at 50% reliability, there is discrepancy in the HMA rutting values obtained directly from MEPDG and the values reported in Khazanovich et al (2008). The MEPDG analysis reported here used MEPDG default input values except for those that were explicitly provided in Khazanovich et al. (2008). It is possible that the discrepancy may be due to the difference in some non-default values that were used.

Table 5.7 summarizes the COV of the distress distribution obtained by the developed reliability procedure and those reported in Khazanovich et al. (2008). From the table it can be seen that the COV of the distress distribution of the developed reliability procedure and that by Khazanovich et al. match well. Therefore, even though the mean values were different, the fact that the COV of the distress matches well shows that the proposed reliability procedure captures the effect of uncertainty well.

Table 5. 6 Comparison of Distress Predicted at Mean Input Values (Pavement Structure from Khazanovich et al. 2008)

Distress	Computed by MEPDG		Computed by Stand Alone Application
	Reported in Khazanovich et al. (2008)	Obtained in this Study	
HMA Rutting, Inch	0.326	0.557	0.584
Base Rutting, Inch	N/A*	0.091	0.083
Sub-Base Rutting, Inch	N/A*	0.126	0.108
Subgrade Rutting, Inch	N/A*	0.234	0.220
Total Rutting, Inch	0.955	1.007	0.995
Fatigue Bottom-up Cracking, %	3.63	4.41	4.08

* - information not reported in Khazanovich et al. (2008)

Table 5. 7 Comparison of Reliability Results: Proposed Method Vs Khazanovich et al (2008)

Distress	Co-efficient of Variance, %	
	Developed Reliability Procedure	Khazanovich et al (2008)
HMA Rutting	9.2	9.2
Total Rutting	6	4.1
Fatigue Bottom-up Cracking. %	47.3	52.5

5.5 Sensitivity Analyses

The design guide (MEPDG) recommends performing a sensitivity analysis of any new design project to identify its key variables and to group them according to their significance in affecting the output. The inputs are grouped into Groups 1, 2 or 3 based on whether the input has a significant, moderate, or minor effect on the output,

respectively. Based on such analysis, the designer can invest greater effort towards the accurate determination of inputs that are deemed sensitive.

In the past, sensitivity analyses were primarily carried out by changing a specific variable by some fixed measure (such as the coefficient of variation) while keeping other variables constant. The percent change in distress was taken as a measure of sensitivity of the variable on the predicted distress.

Chou (1990) studied the effect of load, layer thicknesses and moduli of subgrade and asphalt concrete on allowable load (strain) repetition in flexible pavements. The effect of each individual parameter was analyzed by keeping the variance of other five parameters as zero. Figure 5.1 show the sensitivity of each variable on number of load repetition. Based on this, it was found that the sensitivity of the pavement performance was most dependent on concrete thickness followed by load, asphalt concrete modulus, and subgrade modulus.

Sensitivity analyses were also carried out by Sues et al. 1993 to study the importance of certain input variables on the pavement thickness and design reliability of air field pavements. It was found that there was a significant reduction in probability of failure with the removal of heavy loads in the design highlighting the importance of estimating the exact number of heavier traffic loads. Their sensitivity analyses also showed that the load wandering along the width of the pavement significantly increased the life of the pavement compared with that of channelized traffic. The effect of increased construction quality (represented by the coefficient of variation of the mean thickness) on reducing the required pavement layer thickness was also verified by sensitivity analysis.

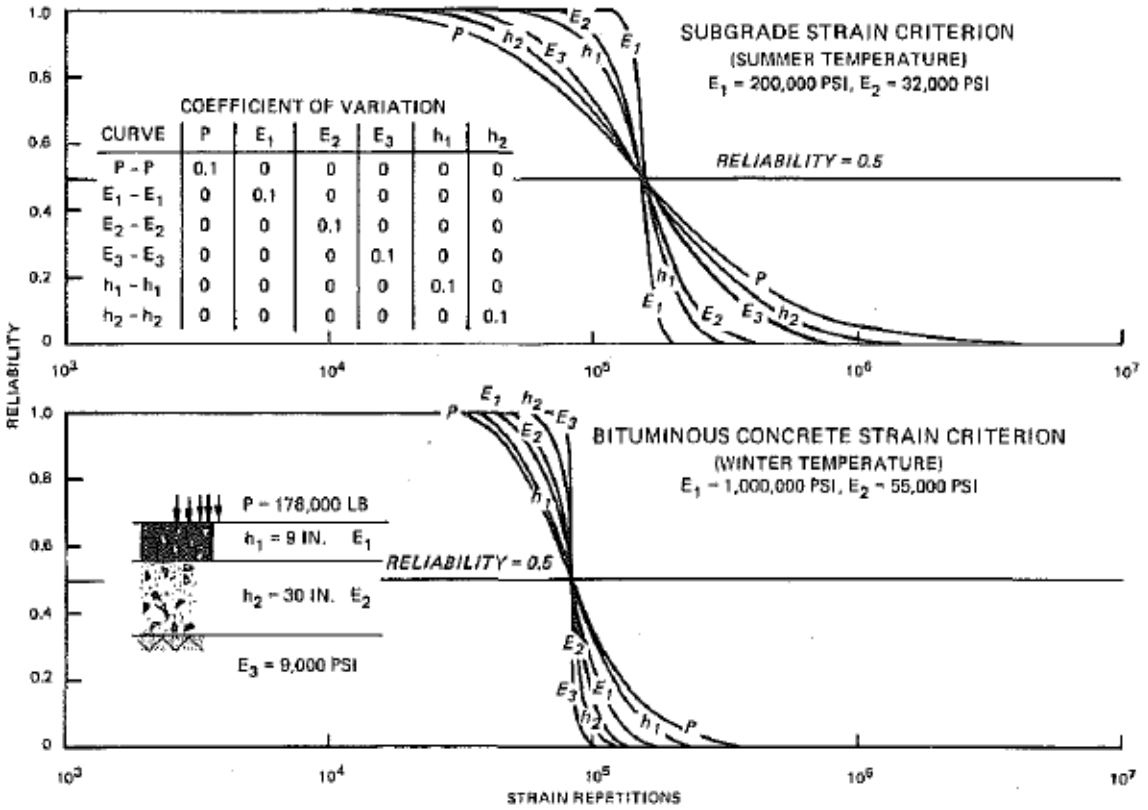

Figure 5. 1Relationships between Input Variability and Strain Repetition (after Chou, 1990)

Sensitivity analyses of input parameters to pavement design were also performed by Killingsworth and Zollinger (1995). The design inputs used in the study were the subgrade strength, the traffic level in ESAL per year, the surface layer modulus, and surface thickness. Both rigid and flexible pavement designs were evaluated under low traffic- weak subgrade and heavy traffic-strong subgrade conditions. The study was conducted by varying the chosen design inputs with an assigned positive or negative coefficient of variation from the mean value of the design inputs. The results of the study are as shown in Figure 5.2 for the case of flexible pavement under low traffic. Similar results were presented for rigid pavements. It can be seen that at low traffic and weak subgrade design conditions, the flexible pavement was found to be moderately sensitive to changes in subgrade modulus, traffic load and surface modulus; however, it was much

less sensitive to changes in surface thickness. On the other hand, for the same conditions, the rigid pavement design was not found to be sensitive to change in subgrade modulus and traffic loads. The flexible pavements were more sensitive to surface thickness at higher traffic loads and stronger subgrade. For rigid pavements, as the allowable traffic increased, the design became more sensitive to changes in subgrade modulus and input traffic but considerably less sensitive to variations in surface thickness.

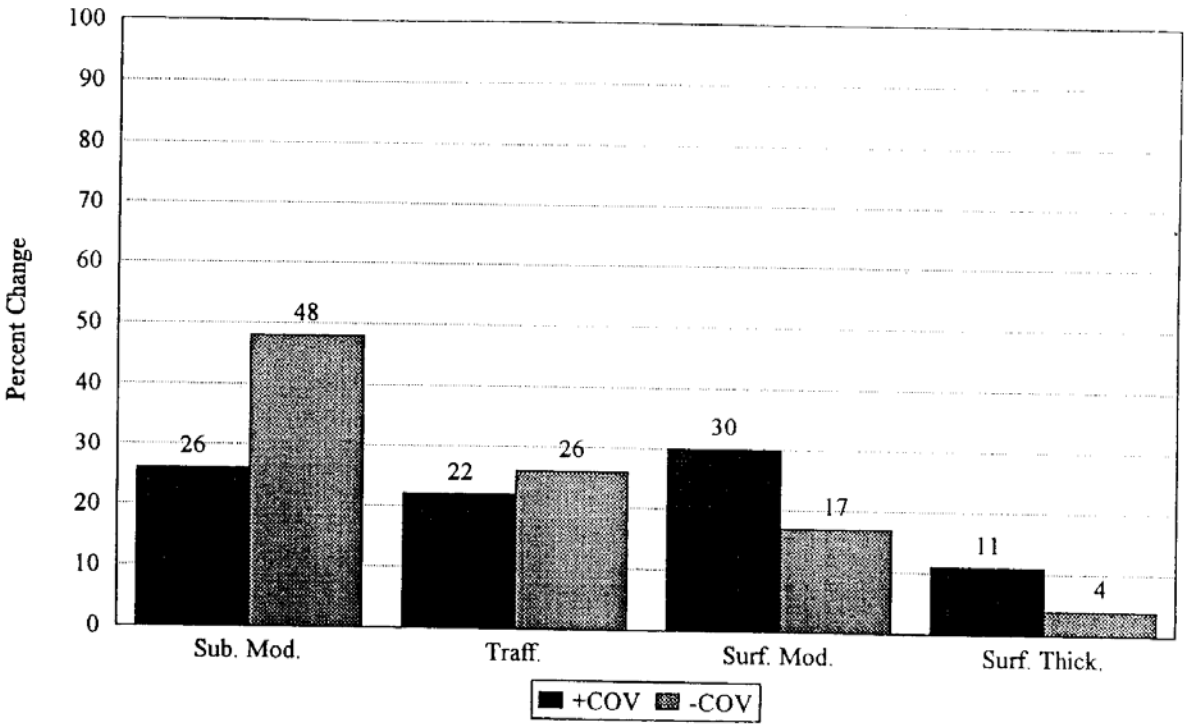

Figure 5. 2 Percent Change in Design Life from Mean Input in Flexible Pavement (after Killingsworth And Zollinger, 1995)

Li et al. (1997) reported the results of a sensitivity analysis of the Ontario flexible pavement deterioration model (developed by Jung et al. 1975) with changes in major input parameters such as ESALs (Equivalent Single Axle Load), subgrade resilient modulus, and total equivalent granular thickness. The effect of each of these input parameters on the pavement condition index (PCI) was studied by keeping the other input

parameters constant. The results showed significant variation in design life (to maintain minimum PCI) with variation in any of these key variables.

A mechanistic pavement model, WESLEA and empirical transfer functions were used to assess the effect of input variability on fatigue and rutting failure models by Timm et al. (2000). The software ROADENT was used to conduct Monte Carlo simulations and study the sensitivity of input parameters in fatigue and rutting failure models keeping traffic load constant. The thickness and stiffness of the AC layer were found to have the most significant effect on the fatigue prediction. In the case of rutting failure, base thickness was also found to be significant. When the traffic load was included in the analysis, the variability of the model doubled. It was thus concluded that traffic load was the single most important input parameter in pavement design.

Haider et al. (2007) identified 23 input variables to be significant in affecting the crack prediction in rigid pavements by MEPDG in the state of Michigan. Based on site characteristics and analysis of input variables this number was reduced to six with two levels (high and low) and the climate with three levels (three different places in Michigan). The levels were selected based on the inputs from Michigan Department of Transportation state of practice for rigid pavements.

A series of frequency histograms were developed by Haider et al (2007) for each input variable for which the data was available in the LTPP Release 19.0 of DataPave. Sensitivity analyses were carried out using the extreme values (taken as mean ± standard deviation) of each input variable in MEPDG (Figure 5.3). Two methods were used to determine the significance of the variable (Figure 5.4): performance threshold and age threshold. In performance threshold method, the period required to reach the particular

distress level was measured (Figure 5.4a). The variable was considered significant if the difference in age of the rigid pavement was more than 5 years from that calculated with mean value. In the age threshold method the performance predicted by the extreme values were analyzed at given design period (Figure 5.4b). Statistical analysis through Analysis of Variance (ANOVA) identified the significant input parameters and their interactions.

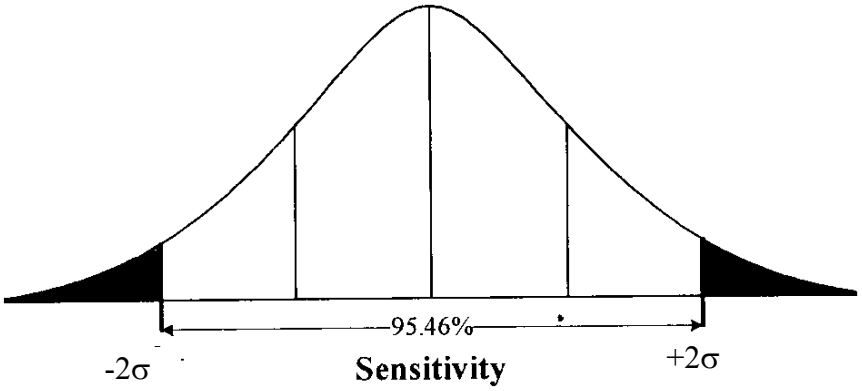

Figure 5. 3 Extreme Values for Sensitivity Analysis of Normal Input Variable (after Haider et al., 2007)

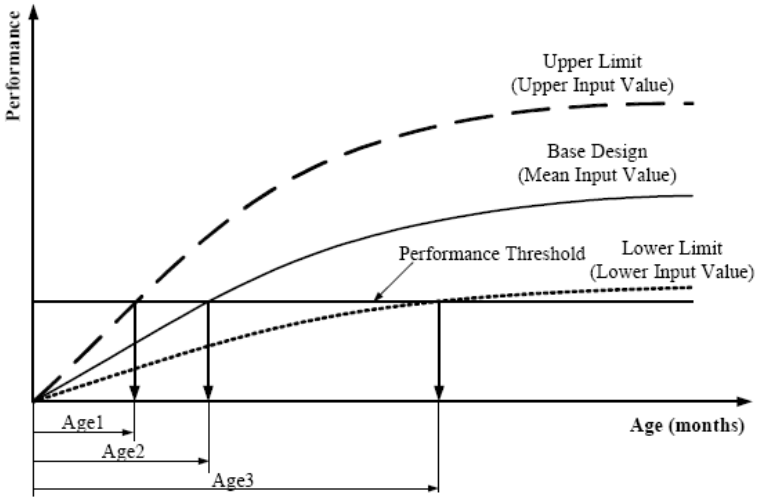

(a) Performance Threshold

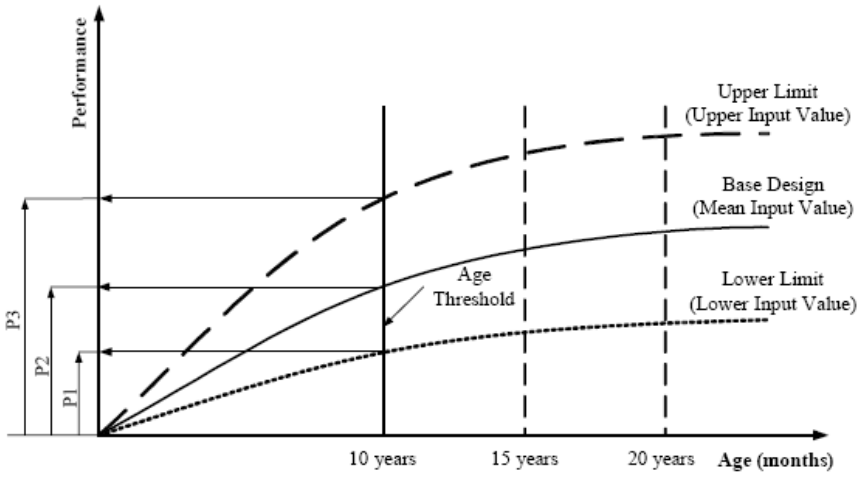

(b) Age Threshold

Figure 5.4 Effects of Input Variables on Pavement Performance (after Haider et al. 2007)

5.5.1 Need for robust sensitivity analyses

A sensitivity analysis which focuses only on one variable at a time in a design may not effectively capture the effects of interplay between variables that occur in the field. For an effective sensitivity analysis, the potential uncertainty of each input variable in the field must be included collectively. Thus, such a sensitivity analysis should include a simulation technique that could sample the input variables collectively based on their potential variability and evaluate their effect on a specific distress of a pavement structure.

The sensitivity of an input on the distress prediction depends on the pavement structure and climatic and traffic conditions of a particular design or analysis. Very often, a sensitive variable under a certain set of pavement conditions may not necessarily be sensitive under a different set of conditions. The sensitivity of an input could vary with changes in design conditions. Therefore, generalization of sensitivity analyses for

different problems may challenge the very purpose of sensitivity analysis. Such generalization may misdirect the effort in the accurate determination of sensitive variable. Therefore, it is necessary to incorporate sensitivity analysis within the design procedure, instead of determining it a priori, so that the sensitive variables are accurately identified for the problem at hand and efforts are spent on the accurate prediction of problem specific sensitive variables.

The reliability procedure developed here makes it possible for performing more robust sensitivity analyses. 'Tornado plots' and 'Extreme tail analyses' are accepted as better methods of analyzing the sensitivity of the variable (Vose, 1997, Eschenbach, 2006). The Tornado plot is used to observe the effect of the input on the distress whereas extreme tail analysis is used to examine the effect of the variability in input on the variability in output. The large number of Monte Carlo simulations in the new reliability method enables us to perform rigorous sensitivity analyses in an efficient manner.

5.5.2 Tornado plots

A sensitivity analysis is conducted to identify key material variables that have the most significant effect on overall pavement performance. The sensitivity analysis of uncertain HMA material input on the predicted distress is studied. The degree of correlation between the distress and material input parameter is calculated using rank order correlation coefficient.

Rank order correlation is a non-parametric technique for quantifying the relationship between two variables. The rank order correlation coefficient is independent of the relationship between the input and output. Thus, it is suited for the study here that

involves non-linear distress models. Rank order correlation uses the positions (rank) of the data point in an ordered list to compute correlation co-efficient. The rank order correlation coefficient known as Karl Spearman's 'r' is calculated between the output and each dependent variable as (Vose, 1997):

$$r = 1 - \left(\frac{6\sum (\Delta R)^2}{n\left(n^2 - 1\right)} \right) \tag{5.1}$$

where

ΔR – difference in the ranks between the input and the output values in the same data pair

n – number of simulations

The magnitude of 'r' identifies the extent of correlation between the input and output. As the absolute value of r is close to one the effect of the variable on predicted distress is maximum and when the value of r is close to zero the effect of the variable on predicted distress is minimal. A positive correlation value indicates low value from the input will lead to low value in output and a negative correlation indicates low value from the input will lead to high value in output. A sample computation of the Karl Spearman's correlation coefficient 'r' is provided in Appendix B.

A 'Tornado plot' is a pictorial illustration of the degree to which the predicted distress is affected by its dependent individual input variable. In this study, rank order correlation coefficient is used to compute the degree of correlation and hence the 'Tornado plot for a distress' is the plot of correlation coefficient of each dependent input variable.

For the case study pavement structure and probabilistic characteristics of the input variable considered (Section 4.2), 'Tornado plots' for the sensitivity of material inputs on HMA, base, sub-base, subgrade and total rutting are shown in Figures 5.5 (a) to (e), respectively. Table 5.8 summarizes the spearman's correlation co-efficient 'r' computed between each simulated material input and rutting of each layer. The variation of each simulated variable in this study has a similar effect on rutting in both HMA and unbound layers (Figure 5.5 (a) to (e)) indicated by near identical correlation coefficients. The design procedure transforms each set of simulated input variables to corresponding HMA layer stiffness (dynamic modulus). The distresses in the unbound layers are dependent on the HMA stiffness. Thus, a weaker HMA layer not only leads to increased rutting in it , but also in unbound layers since the stresses in unbound layers are higher thus resulting in near identical correlation coefficients. However, as can be seen from COV in Table 5.1, the effect of HMA stiffness on rutting performance of unbound layers is not as significant as it is for HMA layer and, as expected, decreases with the depth of unbound layer (with small COV).

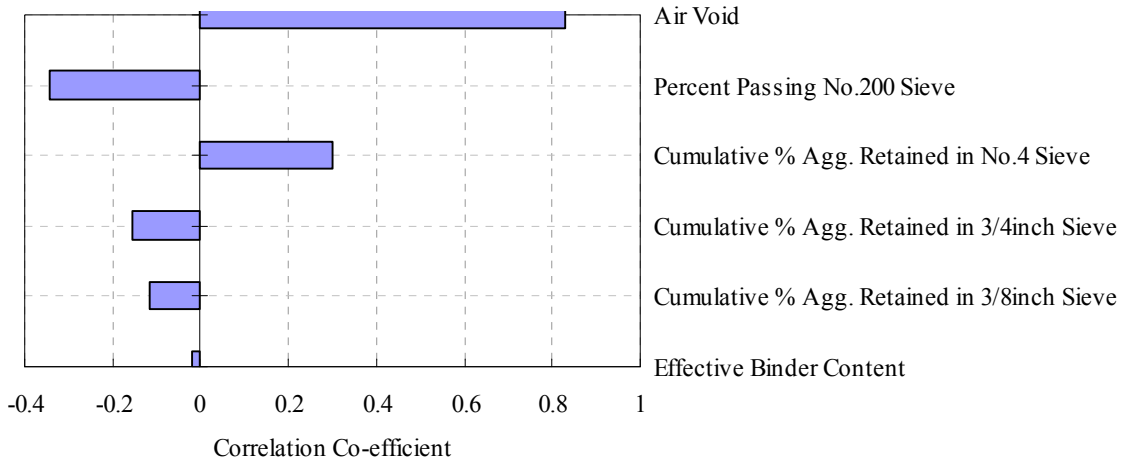

(a) HMA Rutting

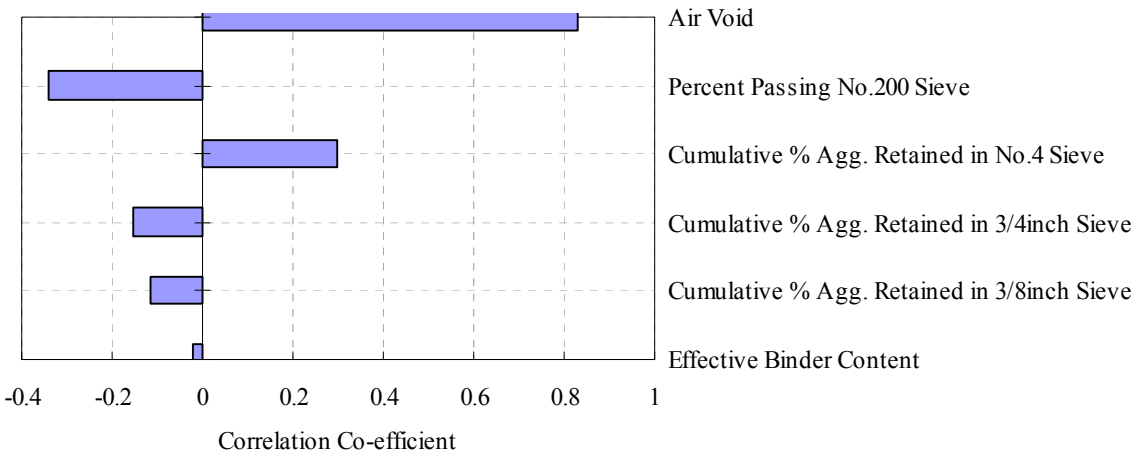

(b) Base Rutting

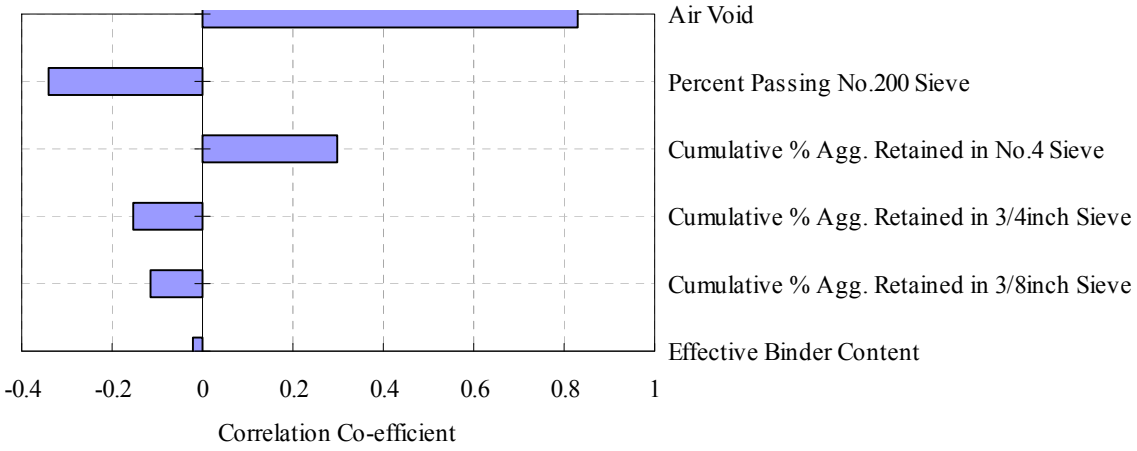

(c) Sub-Base Rutting

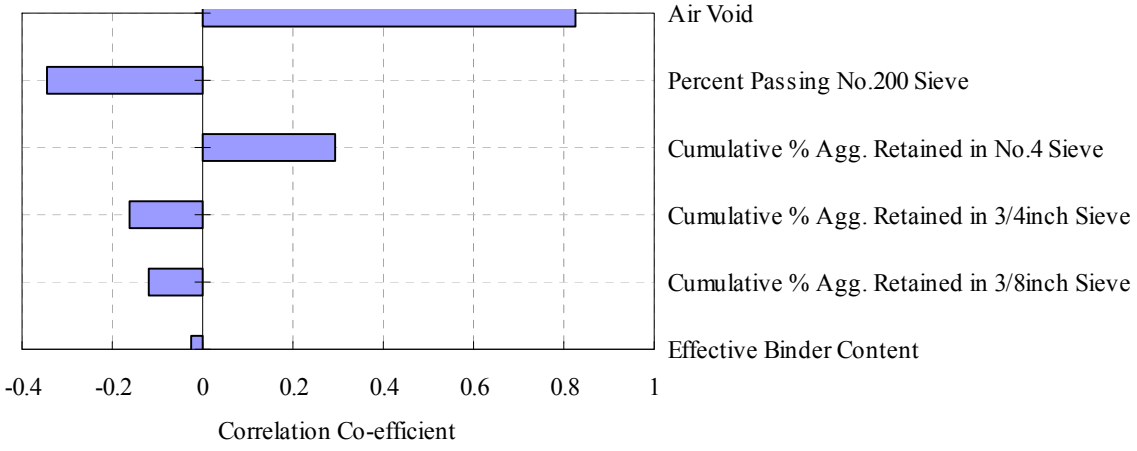

(d) Sub-Grade Rutting

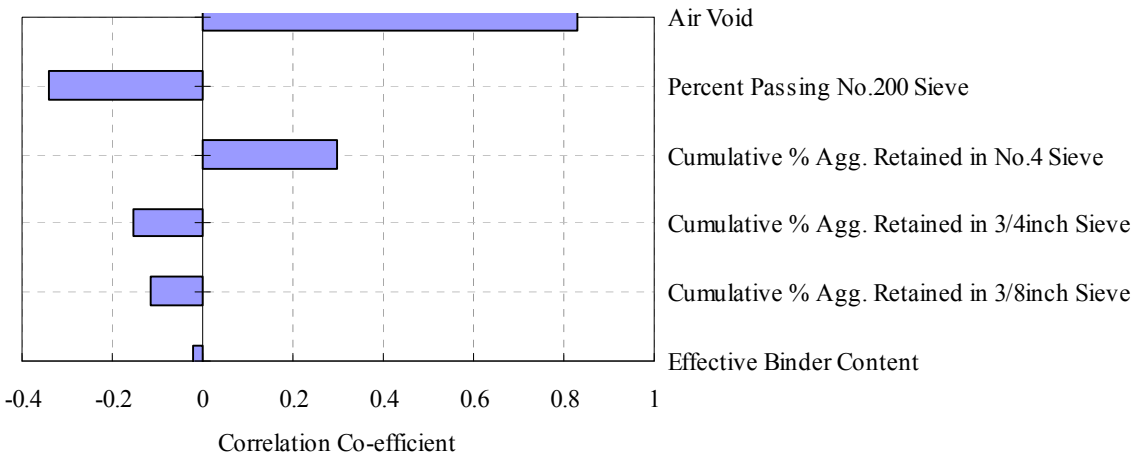

(e) Total Rutting

Figure 5. 5 Sensitivity of HMA Material Inputs on Rutting

Table 5. 8 Sensitivity of HMA Material Properties on Rutting (Permanent Deformation)

HMA Material Input	Spearman Correlation Co-efficient, r (Equation 5.1)				
	HMA	Base	Sub-Base	Sub-Grade	Total
Air Void, %	0.83	0.83	0.83	0.83	0.83
Aggregate Passing No.200 Sieve, %	-0.34	-0.34	-0.34	-0.35	-0.34
Cumulative Aggregate Retained in No.4 Sieve, %	0.30	0.30	0.30	0.29	0.30
Cumulative Aggregate Retained in 3/4inch Sieve, %	-0.15	-0.16	-0.15	-0.16	-0.15
Cumulative Aggregate Retained in 3/8inch Sieve, %	-0.11	-0.11	-0.11	-0.12	-0.11
Effective Binder Content, %	-0.02	-0.02	-0.02	-0.03	-0.02

From Figure 5.5 (a), it can be seen that among the inputs studied, the air void content in HMA layer is the most sensitive in the prediction of HMA rutting. The high positive correlation co-efficient indicates a significant positive relation between air void content and HMA rutting – higher air void content will lead to higher HMA rutting and vice versa.

Aggregates passing No.200 sieve, which indicate percentage particles less than 75 micrometer (μm) in aggregate gradation, is negatively correlated with predicted HMA rutting. Hence, high percentage of fine particles reduces HMA rutting to a relatively significant level. Cumulative aggregate retained in No.4 sieve, which indicate percentage particles larger than 4.75 millimeter (mm), is positively correlated with predicted HMA rutting. However, cumulative aggregate retained in 3/4 inch (19mm) and 3/8 inch (9.5mm) sieves are negatively correlated with predicted HMA rutting though to a lesser extent. Hence, high percentage of coarse particles between ¾ inch (19 mm) and 3/8 inch (9.5 mm) in aggregate gradation will lead to low rutting in the HMA layer. The effective binder content in HMA is practically insensitive to the predicted HMA rutting.

Figure 5.6 is the 'Tornado plot' for the sensitivity of material inputs on HMA fatigue bottom-up cracking. Table 5.9 summarizes the spearman's correlation co-efficient (r) computed between each simulated material input and fatigue bottom-up cracking in HMA layer. The fatigue cracking is most sensitive to the air void content in HMA layer, among the input variable studied. A high correlation co-efficient close to unity indicates an increase in air void content will increase the fatigue cracking almost in every other condition. Effective binder content which is insensitive to rutting is sensitive to the bottom-up fatigue cracking. The negative correlation co-efficient indicates high

effective binder content can possibly reduce the bottom-up fatigue cracking. Also, the aggregate gradation in HMA has little effect on bottom-up fatigue cracking.

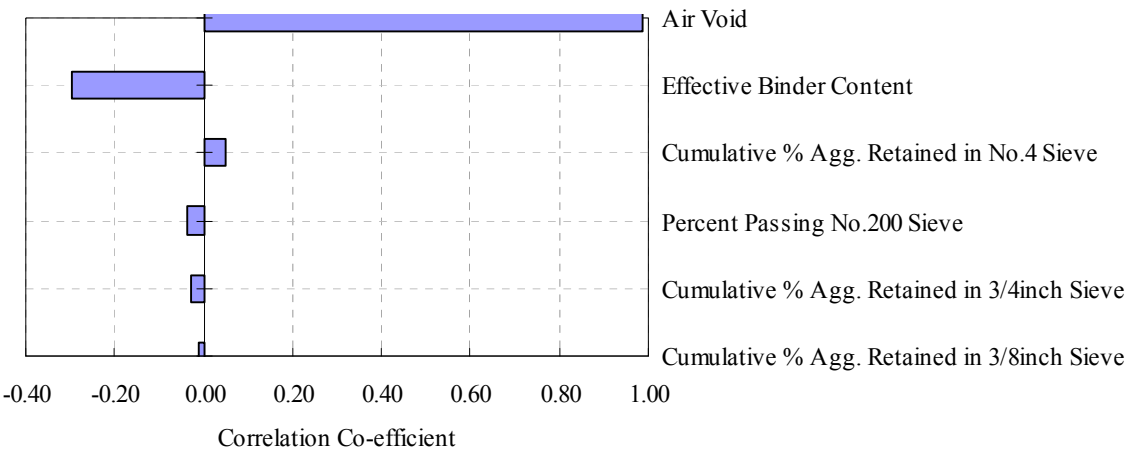

Figure 5. 6 Sensitivity of HMA Material Inputs on Fatigue Cracking

Table 5. 9 Sensitivity of HMA Material Inputs on Fatigue Damage

HMA Material Input	Spearman Correlation Co-efficient, r (Equation 5.1)
Air Void, %	0.99
Effective Binder Content, %	-0.30
Cumulative Aggregate Retained in No.4 sieve, %	0.05
Aggregate Passing No.200 Sieve. %	-0.04
Cumulative Aggregate Retained in 3/4inch sieve, %	-0.03
Cumulative Aggregate Retained in 3/8inch sieve, %	-0.01

For the pavement structure (Section 4.2) considered, the air void content and cumulative aggregate retained on 3/8 inch sieve for the HMA layer are the most and least sensitive variable, respectively, on the type of distress evaluated. To illustrate the relative effect of these two variables on distress prediction and the effectiveness of sensitivity analysis described, the stand-alone application (Section 3.2) was executed for:

- Case A: Mean values of the input variables (as in Table 4.1).
- Case B: Air void content increased from 6.5% to 8% (by one standard deviation). All other variables are kept as in Case A.
- Case C: Cumulative aggregate retained on 3/8 inch sieve is increased from 21% to 23.5% (by one standard deviation). All other variables are kept as in Case A.

Table 5.10 shows the effect of the change in input variable on HMA rutting. It can be seen that an increase in sensitive air void content (r = 0.83) as in case B results in an increase in the predicted HMA rutting depth from 0.562 inch to 0.637 inch (Table 5.10) or an increase of 13.3%. But an increase of insensitive 'Cumulative aggregate retained on 3/8" sieve' (r = -0.11) variable as in case C as decreased the predicted HMA rutting by only 2% from 0.562 inch to 0.551 inch (Table 5.10).

Table 5.11 shows the similar effect of these two variables on fatigue bottom-up cracking. The increase in sensitive air void content (r = 0.99) in case B as almost doubled (95.9%) the predicted cracking from 3.9% to 7.64% (Table 5.11). But the increase in insensitive 'Cumulative aggregate retained on 3/8" sieve' (r = -0.01) as in case C as decreased the predicted cracking by only 1.5% from 3.9% to 3.84% (Table

5.11). Also, it can be observed that the magnitude of Spearman's correlation coefficient is a clear indicator of the effect of the variable on predicted distress.

Table 5.10 Effect of Most and Least Sensitive Variable on HMA Rutting

	Spearman Correlation Coefficient (r) with Rutting	Case A	Case B	Case C
Air void , %	0.83	6.5	8	6.5
Cumulative aggregate retained on 3/8" sieve, %	-0.11	21	21	23.5
other variables as in Table 4.1				
HMA Rutting, inch		0.562	0.637	0.551
Deviation from case A, %		-	13.3	-2.0

Table 5.11 Effect of Most and Least Sensitive Variable on Fatigue Bottom-up Cracking

	Spearman Correlation Coefficient (r) with Fatigue Bottom-up Cracking	Case A	Case B	Case C
Air void, %	0.99	6.5	8	6.5
Cumulative aggregate retained on 3/8" sieve, %	-0.01	21	21	23.5
other variables as in Table 4.1				
Fatigue Bottom-up Cracking		3.9	7.64	3.84
Deviation from case A, %		-	95.9	-1.5

5.5.3 Extreme tail analysis

Reliability analysis computes the predicted distress distribution under the given level of input uncertainty. However, the reliability of pavement performance is related to the spread of this distribution. Therefore, the extreme values in the distribution are critical to improving reliability predictions. In general, the designer must limit the possibility of the occurrence of extreme distress in the pavement, so that the pavement structure could performs its function throughout the design period at higher reliability. Extreme tail analysis is a procedure that can be used to systematically identify uncertain critical input variables that contribute to the tail in the distribution of distress values. Identification of such input variables will assist in effectively reducing the extent of tail in distress distributions ensuring better quality control during construction or the development of better standards by reducing the uncertainty in such inputs.

The procedure of conducting an extreme tail analysis on the distress consists of the following steps (Vose.1997):

Step 1: Arrangement of the predicted distress values in an ascending order from the total simulations.

Step 2: Identification of the extreme distress values and the grouping of their corresponding input values.

Step 3: Calculation of the median of each input in the group.

Step 4: Computation of a normalized variable α for each input as:

$$\alpha = \frac{\left(Median_{Group} - Median_{Total}\right)}{\sigma_{Total}} \tag{5.2}$$

where:

$Median_{Group}$ – Median of the input in the group

$Median_{Total}$ – Median of the input in the total simulations

σ_{Total} - Standard deviation of the input in the total simulations

Step 5: Rank each input variables based on the computed α value.

The extreme values of input variables in the group with $|\alpha| \geq 0.5$ are generally considered to be significant and contribute to the extreme values of predicted distress. A positive significant α value for an input indicates that positive extreme values of the input is one of the possible reasons for positive extreme distress values and the vice versa for the negative significant α.

The result from 4000 Monte Carlo simulations performed in Chapter 4 is used in the extreme tail analysis to identify the set of input variables contributing to extreme distress values. Extreme tail analysis is conducted for each computed distress output. The predicted distress values are arranged in ascending order. For a reliable pavement performance, both left and right tails of the distribution are of interest. The lower 5% of the distress distribution value is taken as left tail and the higher 5% as right tail. The median of the each simulated input variable within left and right tail are computed and the corresponding α value is calculated using Equation 5.2. Table 5.12 and 5.13 summarizes the results of extreme tail analysis for rutting in HMA and fatigue bottom-up cracking, respectively. The results of extreme tail analysis on rutting at the base, sub-

base and sub-grade yielded results similar to that found for HMA rutting. As discussed in the previous section, change in HMA stiffness resulting from the changes in HMA material properties impacts the stresses in the unbound layers in the same manner and consequently their performance.

Table 5.12 Extreme Tail Analysis on HMA Rutting Distribution

HMA Material Input	Overall Median %	Left Tail		Right Tail	
		Median, %	α (Eqn. 5.2)	Median , %	α (Eqn. 5.2)
Air Void, %	6.5	4.14	-1.59	9.10	1.74
Aggregate Passing No.200 Sieve, %	3.0	3.77	0.75	2.13	-0.86
Cumulative Aggregate Retained in No.4 Sieve, %	60.0	57.28	-0.78	61.93	0.55
Cumulative Aggregate Retained in 3/4 inch Sieve, %	4.0	4.96	0.54	3.44	-0.32
Effective Binder Content, %	12.5	12.56	0.11	12.36	-0.29
Cumulative Aggregate Retained in 3/8 inch Sieve, %	21.0	21.52	0.20	20.36	-0.25

Figure 5.7 and 5.8 show the effect of variability in air void content on predicted values of HMA rutting and bottom-up fatigue cracking, respectively. For the given pavement structure, and the HMA rutting distribution obtained from 4000 simulations, the left tail contributes to HMA rutting values less than 0.4667 inch and right tail contributes to HMA rutting more than 0.7133 inch (Figure. 5.7). It is also evident that

high air void content percentage is the primary contributor to extreme values of HMA rutting values. Similar characteristics are observed between air void content and extreme fatigue cracking values (Figure 5.8). The variability in the air void content corresponding to extreme HMA rutting and fatigue cracking are computed through α value of extreme tail analysis.

Table 5.13 Extreme Tail Analysis on Fatigue Cracking Distribution

HMA Material Input	Overall Median %	Left Tail		Right Tail	
		Median, %	α (Eqn. 5.2)	Median , %	α (Eqn. 5.2)
Air Void, %	6.5	3.51	-2.01	9.31	1.89
Effective Binder Content, %	12.5	12.75	0.50	12.12	-0.76
Aggregate Passing No.200 Sieve, %	3.0	2.96	-0.04	2.78	-0.22
Cumulative Aggregate Retained in No.4 Sieve, %	60.0	59.83	-0.05	60.72	0.21
Cumulative Aggregate Retained in 3/8 inch Sieve, %	21.0	20.76	-0.10	21.17	0.07
Cumulative Aggregate Retained in 3/4 inch Sieve, %	4.0	4.20	0.11	3.91	-0.05

The high α value for air void content (Table 5.12 and 5.13) indicates that the extreme variation in air void content is the primary contributor to the extreme values in both rutting and fatigue crack prediction. Thus, an effective quality control on extreme variability in air void content will reduce the uncertainty in distress prediction.

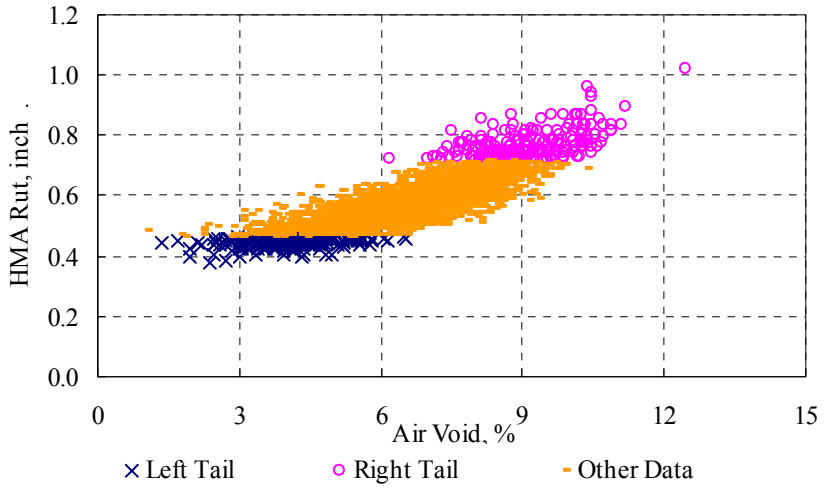

Figure 5.7 Extreme Tail Analysis – Relation between HMA Rutting and Air Void Content

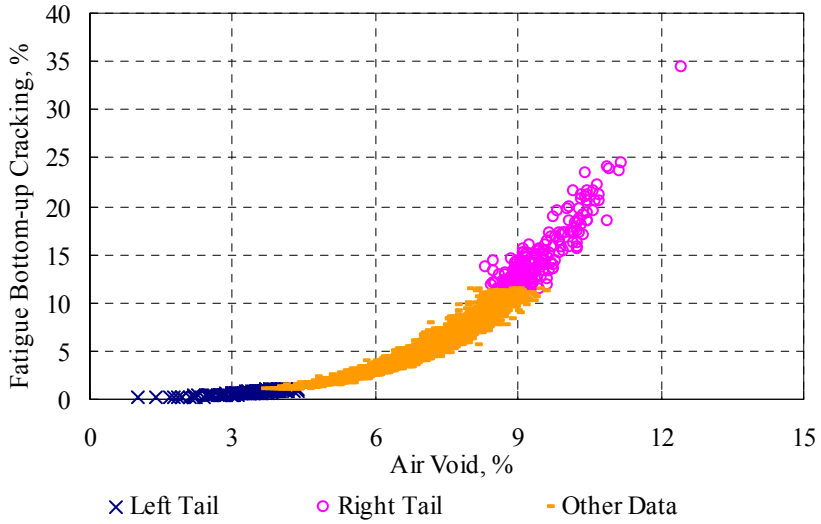

Figure 5. 8 Extreme Tail Analysis – Relation between Fatigue Bottom-up Cracking and Air Void Content

Figure 5.9 shows the relation between effective binder content (V_{be}) and HMA rutting. The effective binder content values corresponding to both right and left tails of predicted HMA rutting covers the entire uncertainty range of the input variable (V_{be}). This is reflected in the α values (0.11 for left tail and -0.29 for right tail) calculated through extreme tail analysis (Table 5.12). Hence, it can be concluded that the extreme values in effective binder content may not contribute to extreme values in HMA rutting.

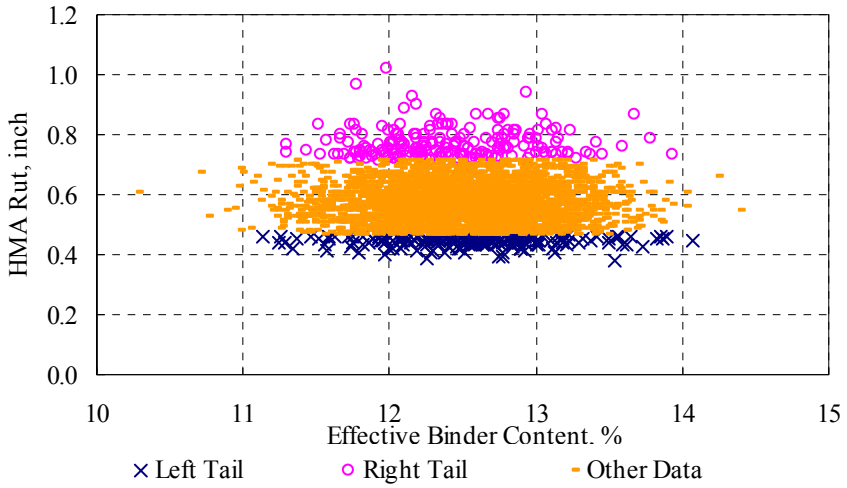

Figure 5.9 Extreme Tail Analysis – Relation between HMA Rutting and Effective Binder Content

Figure 5.10 shows the relation between effective binder content values and corresponding bottom-up fatigue cracking. The variability of effective binder content at right and left tail of predicted distress levels are again quantified in terms of α values (Table 5.13). From the extreme tail analysis, fatigue prediction are pushed to right extreme values when the effective binder content is close to the left extreme values (α = -0.76). Hence, decrease in effective binder content is one of the potential reasons for high fatigue damage prediction. However, the variability in effective binder content is probably not the reason behind the extreme low values (left tail) of fatigue cracking (α = 0.5).

The α value ($|\alpha| > 0.5$) corresponding to aggregate passing No.200 sieve indicates that the HMA rutting (Table 5.12) are affected by its extreme variability. Extreme high values of rutting are possible (α = 0.75) when the variability leads to lower percentages of aggregates passing No.200 sieve values in HMA and vice versa (α = -0.86).

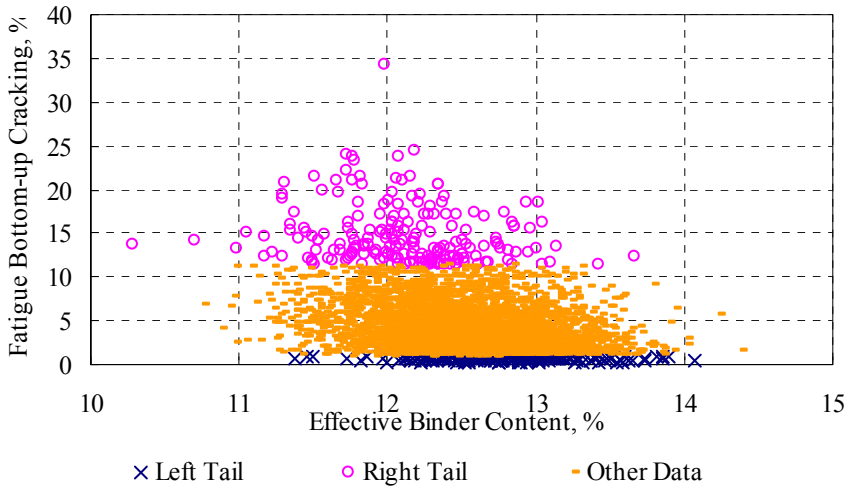

Figure 5.10 Extreme Tail Analysis – Relation between Fatigue Bottom-up Cracking and Effective Binder Content

Cumulative aggregate retained in No.4 sieve is seen to affect the left tail distribution of HMA rutting (Table 5.12). Decrease in aggregates larger than 4.75 mm in the HMA mix will possibly (α = -0.78) lead to lower extreme rutting values, but an increase does not necessarily lead to high extreme rutting values (since $|\alpha| \cong 0.5$). α values less than 0.5 indicate that variability in cumulative aggregate retained in 3/4 inch and 3/8 inch sieve are not a potential contributors to extreme rutting values.

From Table 5.13, all four input variables which represent aggregate gradation (Cumulative aggregate retained in 3/4 inch, 3/8 inch and No.4 sieve and passing No.200 sieve) have α values less than 0.5. Hence, it can be concluded that the aggregate gradation have less effect on extremes of predicted fatigue cracking values.

For the pavement section considered in the study and among the variable considered in the reliability analysis, air void content is the most critical variable that affects both predicted rutting values in each structural layer and fatigue bottom-up

cracking percentage in the HMA layer. The sensitivity analysis here suggest the need for more rigorous methods of determining the air void content in HMA layer (Table 5.8 and Table 5.9). On the other hand, extreme tail analyses suggest the need for better control in variability of HMA air void content. The effective binder content is critical on the fatigue bottom-up cracking; however it is least sensitive on the prediction of rutting in structural layers. Hence, if fatigue bottom-up cracking is the crucial distress in the given pavement design, effective method of determination and variability control are necessary on the effective binder content values.

The aggregate gradation is found to have little effect on predicted fatigue cracking. This may be due to the cold climatic conditions used in the chosen pavement structure. The aggregate gradation plays a critical role on stiffness and deformation of HMA layer during the hot seasons when the load is carried through particle friction. This is one illustration to show the necessity of repeating the sensitivity analysis with change in design conditions.

Quality control effects on distress variability reduction

For the pavement section studied, the results from the extreme tail analyses identified that the air void content in HMA mix is the single most critical variable affecting both HMA rutting and fatigue cracking values and thereby their distribution. Thus, the variability in air void content must be controlled to prevent extreme distress occurring in the pavement. On the contrary, the extreme tail analysis results suggest that among the variables studied the variability in 'cumulative aggregate retained in 3/8 inch sieve' has the least effect on the predicted distress. The following section compares the

effect of controlling the variability of most and least critical variable on distress distribution.

The results of reliability analyses executed with 4000 Monte Carlo simulation are compared for the following three cases:

Case 1: Probabilistic characteristics of the input variables as in Table 4.1

Case 2: Variability in 'air void content' reduced to 1.0% standard deviation from 1.50% used in Case 1. (The probabilistic characteristics of other variables are kept as in Table 4.1).

Case 3: Variability in 'cumulative aggregate retained in 3/8 inch sieve' increased to 4.0% standard deviation from 2.50% used in Case 1. (The probabilistic characteristics of other variables are kept as in Table 4.1).

Table 5.14 summarizes the probabilistic characteristics of the distress distribution obtained from the three cases analyzed above. As expected, the variability in the predicted distress is reduced in Case 2, indicated by the decrease in standard deviation and co-efficient of variation (Table 5.14).

Figure 5.11 (a) and (b) show the frequency and cumulative distribution of HMA rutting, respectively. A similar plot for fatigue cracking distribution is presented in Figure 5.12 (a) and (b). The frequency distribution of the HMA rutting and fatigue cracking distress (Figure 5.11 (a) and Figure 5.12 (a)) shows a narrow distribution for Case 2 (σ = 0.06 inch and 2.235 %) than in Case 1 (σ = 0.078 inch and 3.46 %). The cumulative frequency distribution of the distress (Figure 5.11 (b) and Figure 5.12 (b))

shows that in Case 2 there is less probability of the occurrence of extreme distress values than in Case 1 (i.e. truncated tail). Thus, the designer can design a more reliable pavement without changing the pavement structure if the variability in few critical variables is well controlled. In this study, effective control in variability of air void content can reduce the possibility of extreme distress occurrence in the field.

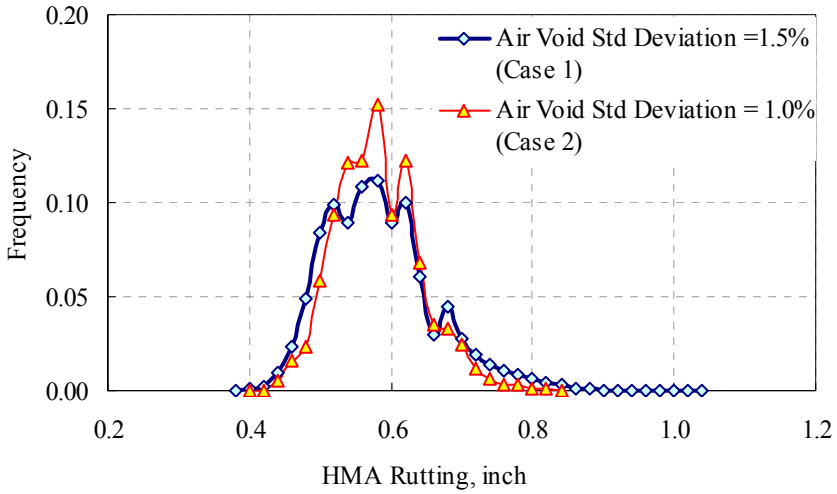

(a) Distribution

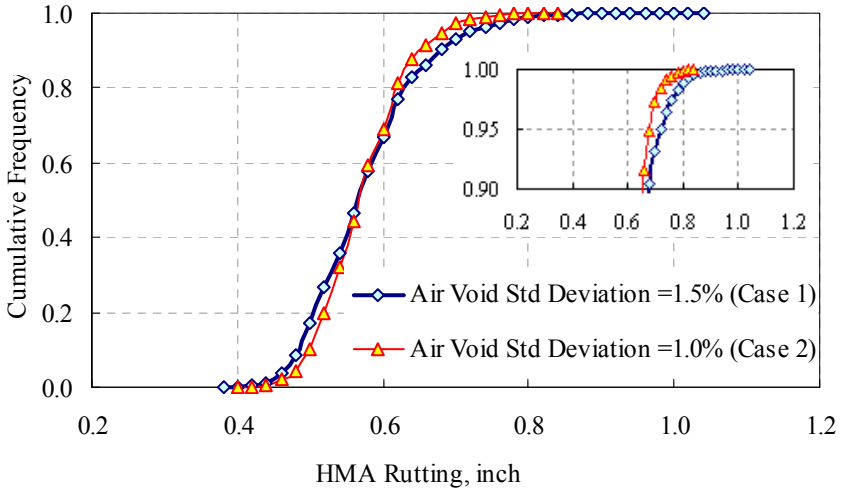

(b) Cumulative Distribution

Figure 5. 11 Effect of Decrease in Sensitive Input Variability on HMA Rutting Distribution

Table 5. 14 Effect of Quality Control on Distress Distribution

Distress	Case 1: Distribution with Probabilistic Characteristic of Table 4.1 (σ_{AV} = 1.5% and $\sigma_{cum3/8ret}$ = 2.5%)			Case 2: Distribution with reduced Air Void Standard Deviation (σ_{AV} = 1.0%)			Case 3: Distribution with increased 'Cumulative % Aggregate Retained in 3/8 inch' Standard Deviation ($\sigma_{cum3/8ret}$ = 4.0%)		
	Standard Deviation	COV %	Distress @ 90% reliability	Standard Deviation	COV %	Distress @ 90% reliability	Standard Deviation	COV %	Distress @ 90% reliability
HMA Rutting, inch	0.078	13.7	0.674	0.060	10.5	0.648	0.079	13.8	0.681
Base Rutting, inch	0.004	4.5	0.087	0.003	3.5	0.086	0.004	4.5	0.087
Sub-Base Rutting, inch	0.003	2.7	0.111	0.002	2.1	0.111	0.003	2.8	0.112
Subgrade Rutting, inch	0.002	1.0	0.223	0.002	0.7	0.222	0.002	1.0	0.223
Total Rutting, inch	0.087	8.9	1.094	0.067	6.8	1.066	0.088	8.9	1.103
Fatigue Bottom-up Cracking. %	3.460	72.1	9.14	2.235	51.2	7.4	3.530	72.7	9.4

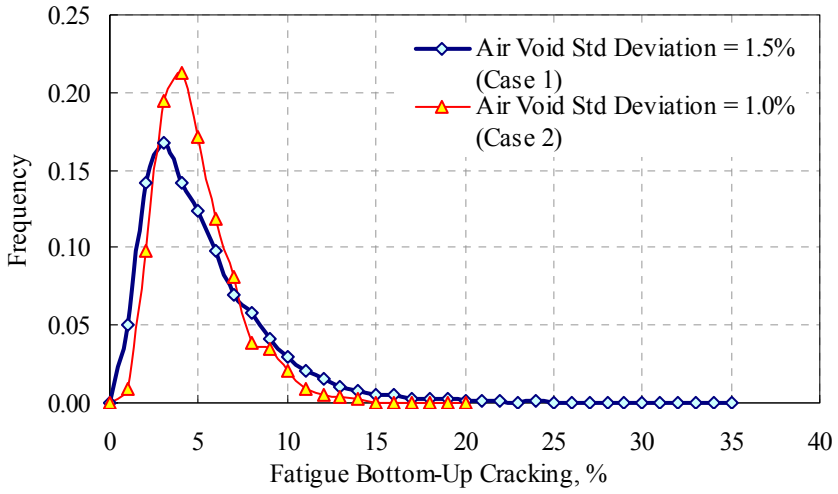

(a) Distribution

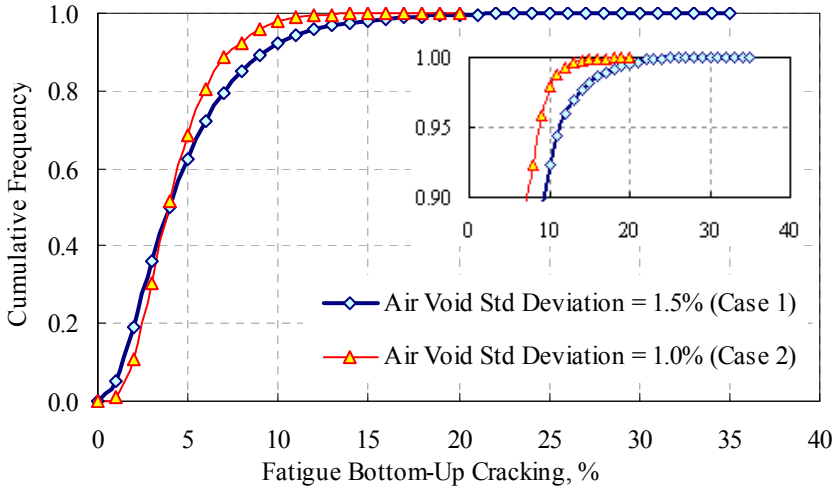

(b) Cumulative Distribution

Figure 5. 12 Effect of Decrease in Sensitive Input Variability on Fatigue Bottom-Up Cracking Distribution

Table 5.14 shows that the probabilistic characteristics of the predicted distress distribution are almost unchanged with the increase in variability of 'cumulative aggregate retained in 3/8 inch sieve' input variable (Case 1 versus Case 3). Figure 5.13 (a) and (b) show the frequency and cumulative distribution of HMA rutting, respectively. A similar plot for fatigue cracking distribution is presented in Figure 5.14 (a) and (b).

The resulting frequency and cumulative distributions from both HMA rutting and fatigue cracking in Case 1 and Case 3 nearly overlaps each other. Thus, the variability in 'cumulative aggregate retained in 3/8 inch sieve' input variable is not the one that contributes to the extreme distress values predicted. Hence the strict quality control of this particular input variable may not be needed.

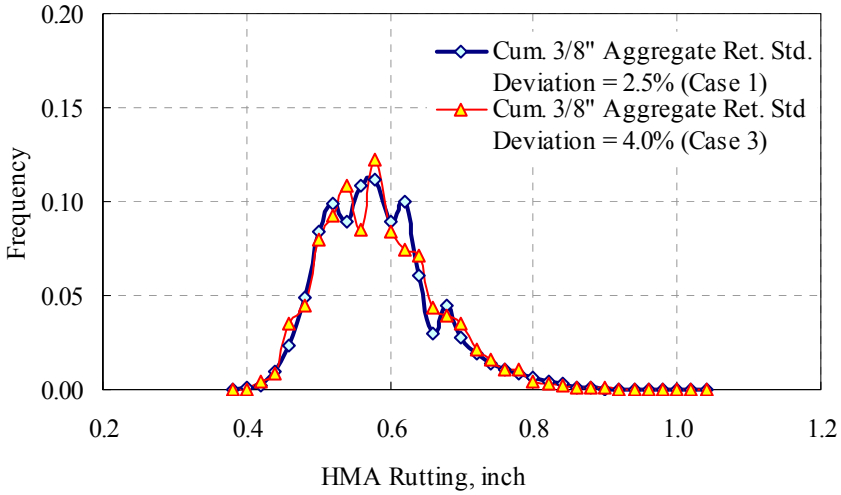

(a) Frequency Distribution

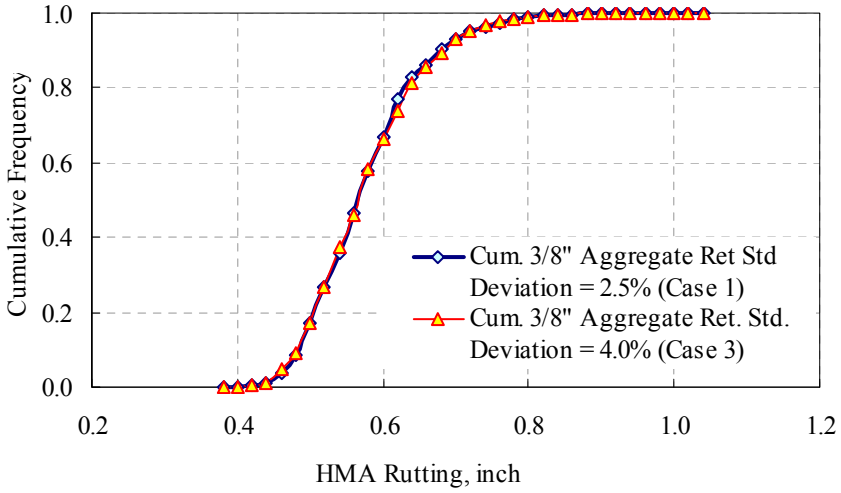

(b) Cumulative Distribution

Figure 5. 13 Effect of Increase in Least Sensitive Input Variability on HMA Rutting Distribution

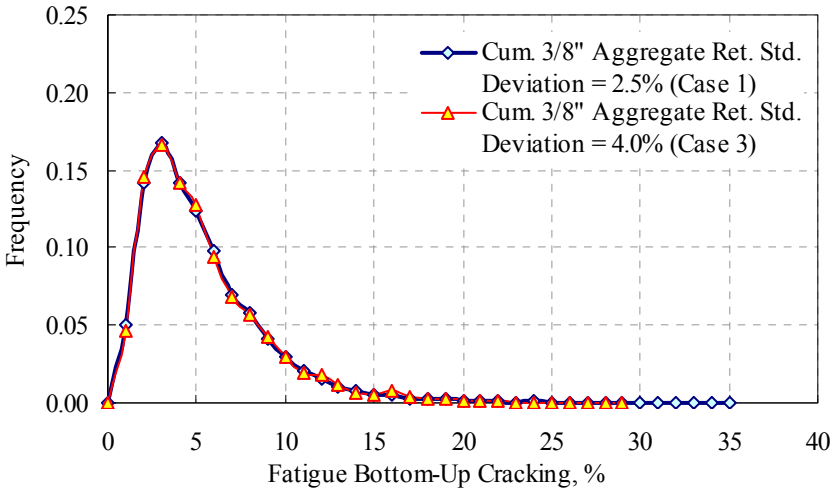

(a) Frequency Distribution

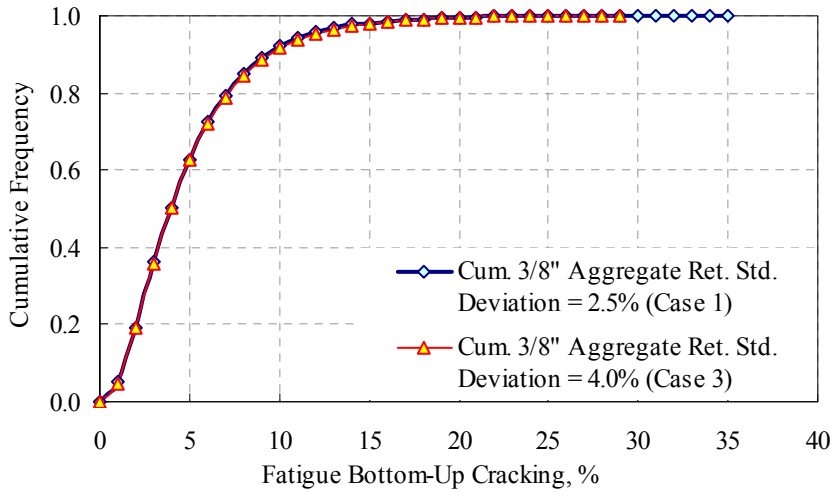

(b) Cumulative Distribution

Figure 5.14 Effect of Increase in Least Sensitive Input Variability on Fatigue Bottom-Up Cracking Distribution

CHAPTER SIX

CONCLUSIONS AND RECOMMENDATIONS FOR FURTHER RESEARCH

This study developed an improved procedure for strain computations and reliability analysis of the Mechanistic-Empirical Pavement Design Guide in the context of flexible pavements. It has proposed improvements to the load-strain interpretations in the MEPDG, and has developed advanced techniques to predict pavement distress reliability. The proposed reliability techniques were validated using a published case study.

The first part of the study investigated the effects of the load-strain linear proportionality assumption made in the MEPDG and the extent of the error incurred in the prediction of pavement rutting. The load-strain linear proportionality assumption holds true only if the contact area remains the same as axle load varies, resulting in similar variation in the contact pressure. In reality, for truck loads of interest, the contact (tire inflation) pressure remains within a narrow range whereas the contact area changes with axle load. This is violated by the load-strain linear proportionality assumption made in the current MEPDG procedure. The analyses conducted here have shown that, for typical traffic load spectra, the linear proportionality assumption may result in significant under prediction of rutting, by over 50% for the four cases analyzed in this study (Section 3.6). However, relaxation of this assumption will result in impractical computing time for routine analyses.

The inaccuracy due to the load-strain linear proportionality assumption was shown to have the most effect on the prediction of HMA rutting and also in fatigue bottom-up cracking of thin HMA overlays. The calibration constants of the distress models obtained from national and local efforts may lessen the effects of this inaccuracy. However, the magnitude of the error incurred indicates that the accuracy of the prediction could be affected significantly when the distribution of the traffic load spectrum deviates from those that were used in the calibration.

A 3-Point approach, where strains were calculated at three reference load levels - selected as 6, 18 and 24 kip single axle loads - and interpolated or extrapolated for other load levels within the traffic load spectrum was developed to avoid this strain linear proportionality assumption. It was shown to predict pavement distress accurately with a much reduced computing time.

The second part of the study developed a new reliability based pavement design procedure. The current reliability method incorporated in the Design Guide (MEPDG) is based upon predetermined standard deviation values obtained from a performance database rather than on those based on the site specific input parameters that induce such uncertainty in distress prediction. The new procedure simulated the effects of uncertainty in HMA material inputs directly in the development of reliability based design analysis of flexible pavements.

A similar reliability effort in the past by Khazanovich et al. (2008) had used repeated execution of MEPDG for each set of simulated input variables. This resulted in eight days of computational time on a personal computer (Khazanovich et al. 2008). Most of this time was incurred as a result of the repeated execution of the inbuilt system

of procedures. In this study, for each set of simulated input variables, the HMA material modulus was extrapolated from corresponding modulus values obtained by execution of MEPDG with mean input values. This avoided the need for repeated execution of EICM and Global aging models (Step 2 and 3 of the design procedure, Section 2.2). In addition, identification of representative layered elastic (LE) structures minimized the required number of JULEA executions involved in reliability analysis. These sets of representative LE structures can replicate all LE structures with negligible loss in accuracy. Critical strain values for LE structures can be obtained from the closest representative LE structure whose dynamic modulus value deviate no more than 1% in any of its sub-layers. The efficiency obtained in incorporation of EICM, Global aging model and structural response computation made the proposed reliability analysis practical. For example, it reduced the computational time of the reliability analysis by the proposed technique for the same pavement structure by Khazanovich et al. (2008) to 25 hours.

The six input variables required for computation of dynamic modulus in the HMA layer at input Level 3 were simulated with the probabilistic characteristics obtained from the Long Term Pavement Performance (FHWA-RD-02-001, 2001) data. The input variables included cumulative aggregate retained in 3/4 inch, 3/8 inch and No. 4 sieve, aggregates passing No. 200 sieve, and air void content and effective binder content in the HMA layer. The Monte Carlo simulation technique was used to simulate these input variables and obtain the probabilistic characteristics of the two basic distresses, rutting and fatigue bottom-up cracking. The stability of the distress distribution from the Monte Carlo simulation method was ensured using a suitable convergence measure.

Based on the pavement structure with the level of variability considered in the HMA material inputs (Section 4.2) the following conclusions can be drawn:

- Pavement rutting values consisted of a normal distribution whereas fatigue bottom-up cracking is of a log-normal distribution.
- The variability of the distress predicted by the developed procedure was less than that predicted by MEPDG. This was expected since MEPDG includes errors in field distress measurement, construction quality, and model bias apart from variability in material inputs whereas the developed procedure included only input variability in HMA material.
- It is noted that the properties of the distress distribution would vary with the type of pavement structure or the magnitude of the variability considered in the input variable.

The computational efficiency and accuracy of techniques such as Monte Carlo and Latin Hypercube simulation methods and Rosenblueth's 2K+1 point estimate method were compared. A minimum of 3000 Monte Carlo simulations were required to obtain stable output distribution characteristics that takes 3.5 days of computational time on a personal computer with a 3 GHz Intel processor and 1GB RAM. Both Latin Hypercube (at 300 simulations) and Rosenblueth's 2K+1 point estimate method compute distress distribution characteristics that were close to the accuracy of Monte Carlo simulation method, but in about a day and 3 hours of computation time, respectively on the same computer.

Latin Hypercube simulation method is found to be an efficient alternate to the computationally intensive Monte Carlo simulation method. The drawback in

Rosenblueth's 2K+1 point estimate method is mainly attributed to its inability to capture the type of distress distribution. Therefore, it is recommended that Latin Hypercube simulation is an effective tool to incorporate input uncertainty in reliability analysis. On the other hand, if the need is to obtain the basic measures of probabilistic characteristics of the distress (such as mean and COV), Rosenblueth's 2K+1 point estimate method can be used with minimal computing time.

The proposed reliability procedure was validated with the pavement structure and uncertainty level reported in Khazanovich et al. (2008). The coefficient of variations for HMA rutting and fatigue bottom-up cracking obtained by the proposed procedures was shown to match well with their results.

Sensitivity analyses are recommended on any new design project to identify key variables and to group them according to their significance in affecting the output. This would enable the designer to put more efforts on the determination of highly significant variables. In the past, sensitivity analyses were primarily carried out by changing a specific variable by some fixed measure (such as the coefficient of variation) while keeping other variables constant. Such analyses do not capture the typical interaction among the different variables in the field and their combined effect on the distress prediction. This study showed that Tornado plots are a powerful means to study the combined effect of different variables and quantify the sensitivity of a specific input variable on distress for the given pavement design. On the other hand, extreme tail analyses captured the extent of effects of variability in input parameter on the variability of predicted distress.

For the pavement structure considered in this study, the air void content in the HMA layer was found to be the most sensitive variable affecting the distress prediction. In addition, its variability is most critical in affecting the prediction of the variability in pavement distress. Better control of variability in air void content in the HMA layer is shown to reduce the overall variability in distress prediction. Effective binder content in the HMA layer is sensitive to fatigue cracking predictions, and its variability has to be controlled to minimize the variability in fatigue bottom-up crack predictions. However, effective binder content or its variability has little effect on rutting prediction and its variability, respectively.

The aggregate gradation and its variability did not have a significant effect on fatigue prediction. However, aggregates finer than 75 μm (passing No.200 sieve) and cumulative aggregates coarser than 4.75 mm (retained on No.4 sieve) and their variability could affect the rutting prediction and its variability.

It is necessary to repeat the sensitivity analysis with any change in pavement design or input. Generalization of the criticality of the variable on distress for different design conditions would lead to erroneous conclusions.

RECOMMENDATIONS FOR FURTHER RESEARCH

The study developed an improved reliability based design procedure for flexible pavements. However, only uncertainties corresponding to HMA material properties were included in the current developed procedure. Though this covers the major part of uncertainty involved in the pavement design, it is recommended to include other design inputs such as variations and uncertainties in traffic loadings, climate, other material

properties, layer thickness and the errors associated with all predictive models incorporated in the design guide. Such a comprehensive reliability approach would require an accurate estimate of variances of the different inputs and prediction models. If not, the results obtained would be completely misleading and erroneous. The sensitivity analyses must be coupled with the reliability analysis in the design procedure. This way, the designers will have a sufficient knowledge of the critical inputs that need to be given additional effort in their determination for the pavement design considered.

Similar reliability based design procedure that can include the input variability should be developed for concrete pavements. The neural network technique used in the rigid pavement design may make the computationally intense simulation technique more practical.

REFERENCES

1. AASHTO T307, American Association of State Highway and Transportation Officials, "Determining the Resilient Modulus of Soil and Aggregate Materials." *AASHTO Provisional Standards*, June 1998.

2. AASHTO T307, American Association of State Highway and Transportation Officials, Resilient modulus of base and subbase materials (soil, gravel, aggregate)." *AASHTO Provisional Standards*, June 1998.

3. Al-Qadi, Imad. "Impact of Wide-Base Tires on Pavement and Trucking Operation" *International Workshop on the Use of Wide-Base Tires*, Turner-Fairbank Highway Research Center, Oct 2007.

4. Alsherri, A., and George, K. P. (1988). "Reliability model for pavement performance." *Journal of Transportation Engineering,* 114(2), 294-306.

5. Ang, A. H. S., and Tang, W. H. (1975). *Probability concepts in engineering planning and design volume I – Basic Principles*. John Wiley and Sons, Inc. New York.

6. Asphalt Institute. (1991). Thickness Design – Asphalt Pavements for Highways and Streets. *Manual Series No.1* (MS-1), Lexington, KY.

7. Ayres, M. (1997) *Development of a Rational Probabilistic Approach for Flexible Pavement Analysis*, Ph.D. Dissertation, University of Maryland, College Park, MD.

8. Ayres, M. and Witczak, M. (1998) "AYMA – A Mechanistic Probabilistic System to Evaluate Flexible Pavement Performance", *Transportation Research Board*, 77th Annual Meeting, Paper No.980738, Washington, D.C.

9. Chou, Yu. T. (1989) "Probabilistic and reliability analysis of asphalt concrete airfield pavements." 5th *International Conference on Structural Safety and Reliability*.

10. Chou, Yu. T. (1990) "Reliability Design Procedures for Flexible Pavements" *Journal of Transportation Engineering*, 116(5) pp.602-614.

11. Darter, M., Khazanovich, L., Tom, Yu., and Mallela, J. (2005) "Reliability analysis of cracking and faulting prediction in the new mechanistic-empirical pavement design procedure." *Transportation Research Record*, n 1936, 150-160.

12. Eschenbach, T.G. (2006) "Technical Note: Constructing Tornado Diagrams with Spreadsheets". *The Engineering Economist,* 51. pp. 195-204.

13. FHWA-RD-02-001, "Assessment of Selected LTPP Material Data Tables and Development of Representative Test Tables", *U.S. Department of Transportation, Federal Highway Administration*, McLean, Virginia, USA 2001.

14. Highway Community EXchange, Design Guide Community of Practice, http://knowledge.fhwa.dot.gov/cops/hcx.nsf/home?openform&Grou

p=NCHRP%201-37A%20(Mechanistic-Empirical)%20Pavement%20Design%20Guide, April, 2005.

15. Haider, S. W., Salama, H.K., Buch, N., and Chatti, K. (2007) "Significant M-E PDG design inputs for jointed plain concrete pavements in Michigan." *MAIREPAV5 - Proceedings of the fifth international conference on maintenance and rehabilitation of pavements and technological control*. Utah, USA.

16. Haldar, A., and Mahadevan. A. (2000) "Reliability Assessment Using Stochastic Finite Element Analysis". John Wiley & Sons, Inc.

17. Hasofer, A. M., and Lind, N. (1974). "An exact and invariant first-order reliability format." *Journal of Engineering Mechanics*, 100 EM1. 111-121.

18. Jiang, Y. J., Selezneva, O., Mladenovic, G., Aref, S., and Darter, M. (2003). "Estimation of pavement layer thickness variability for reliability-based design." *Transportation Research Record*, n 1849, 156-165.

19. JULEA (Jacob Uzan Layered Elastic Analysis) developed by Dr. Jacob Uzan, Technion University, Israel.

20. Jung, F.W., Kher, R., and Phang, W.A. (1975). "A Performance Prediction Subsystem—Flexible Pavements". *Ontario Ministry of Transportation and Communications*, Downsview, Ont., Research Report 200.

21. Kaloush, K. E. and Witczak, M. W. (2000). "Development of a Permanent to Elastic Strain Ratio Model for Asphalt Mixtures". Development of the 2002 Guide for the Design of New and Rehabilitated Pavement Structures. *NCHRP 1-37 A*. Inter Team Technical Report.

22. Khazanovich. L., Wojtkiewicz. S. F. and Velasquez. R. (2008) "MEPDG-RED: A Framework for Reliability Analysis with the Mechanistic-Empirical Pavement Design Procedure" *Transportation Research Board* 87th Annual Meeting, Washington D.C.

23. Killingsworth, B. M., and Zollinger, D. G. (1995). "Sensitivity analysis of input parameters for pavement design and reliability." *Transportation Research Record,* n1482, 111-122.

24. Kim, H. B., and Buch, N. (2003) "Reliability – based pavement design model accounting for inherent variability of design parameters." *82nd Transportation Research Board Annual Meeting*, Washington D.C.

25. Leahy, R.B., Permanent Deformation Characteristics of Asphalt Concrete, Ph.D. Dissertation, *University of Maryland*, College Park, 1989.

26. Lemer, A. C., and Moavenzadeh, F. (1971). "Reliability of highway pavements." *Highway Research Record*, n 36 1-8.

27. Li, N., Haas, R., and Xie, W. C. (1997). "Investigation of relationship between deterministic and probabilistic prediction models in pavement management." *Transportation Research Record*, n1592, 70-79.

28. MEPDG (2007), Mechanistic Empirical Pavement Design Guide, Version 1.003 (Evaluation Copy), *Developed for NCHRP 1-37A and NCHPR 1-40D*, Developed by Applied Research Associates-Transportation and Arizona State University.

29. Melchers, R.E. (2002) "Structural Reliability Analysis and Prediction". John Wiley & Sons.

30. Montano, M. J. R., Koyanagawa, M., and Fukuda, T. (1989) "Evaluation of service life of concrete pavement by Monte Carlo simulation." *Doboku Gakkai Rombun-Hokokushu /Proceedings of the Japan Society of Civil Engineers*, n 402 pt 5-10, 161-167.

31. NCHRP (2004), National Cooperative Highway Research Program, "Guide for Mechanistic-Empirical Design of New and Rehabilitated Pavement Structures." *NCHRP Project 1-37A* Final Report, Washington, D.C. (2004).

32. NCHRP 1-28A, National Cooperative Highway Research Program, Resilient Modulus of Unstabilized Aggregate Base and Subgrade Materials, Washington, D.C.

33. Nowak, A. S., and Collins, K. (2000) "Reliability of Structures". *McGraw-Hill* Publisher.

34. Park, D., Fernando, E., and Leidy, J. (2005) "Evaluation of Predicted Pavement Response with Measured Tire Contact Stresses", *Transportation Research Record*: No. 1919, Washington DC., pp 160 – 170.

35. Phoon, K. K., Quek, S. T., Chow, Y. K., and Lee, S. L. (1990). "Reliability analysis of pile settlement". *Journal of Geotechnical Engineering*, 116(11), 1717-1735.

36. Rosenblueth, E. (1975), "Point Estimates for Probability Moments". In Proceedings National Academic of Science, USA. 72(10):3812-3814.

37. Sues, R. H., Lua, Y. J., Dass, S. M., and Murfee, J. (1993). "Reliability-based analysis and design of flexible airfield pavements." *Airport Pavement Innovations Theory to Practice*, 76-89.

38. Timm, D.H., Newcomb, D.E., and Galambos, T.V. (2000). "Incorporation of reliability into mechanistic-empirical pavement design." *Transportation Research Record* n1730, 73-80.

39. Tseng, K. and Lytton, R. (1989) "Prediction of Permanent Deformation in Flexible Pavement Materials". Implication of Aggregates in the Design, Construction, and Performance of Flexible Pavements, *ASTM STP 1016*, ASTM, pp. 154-172.

40. Val, D.V., and Melchers, E. (1997). "Reliability of deteriorating RC slab bridges." *Journal of Structural Engineering,* 123(12), 1638-1644.

41. Vose, D. (1997) "Quantitative Risk Analysis: A Guide to Monte Carlo Simulation Modelling". *John Wiley & Sons*.

Appendix A

IDENTIFICATION OF REPRESENTATIVE LAYERED ELASTIC STRUCTURE - Sample Calculation

This appendix explains the procedure developed to identify the representative LE structure with sample calculation. Table A-1 contains typical modulus values for a LE structure with 16 sub-layers. Let us consider Table A-1 as the database DB1 (n = 10) generated after stage 3 of the reliability analysis (computation of aged dynamic modulus for simulated material inputs). The objective of the efficiency scheme is to identify the representative LE structure. The procedure generates two databases DB2 and DB3. Database DB2 contains only the representative LE structures. Database DB3 contains all the LE structures in the DB1 along with the ID corresponding to the representative LE structure in DB2, with which it matches to less than 1% accuracy.

Step 1: The first LE structure is always representative, hence copy it to the databases DB2 and DB3 (Table A-2 and Table A-3 respectively). m = 1

Step 2: $$Deviation(j,z) = abs\left(\frac{E_{DB}(j,z) - E_n(i,z)}{E_n(i,z)}\right) * 100$$

i = 2; j = 1; z =1;

From Table A-1 $E_n(i, z) = 2415000$

and Table A-2 $E_{DB}(j, z) = 2350000$

$$Deviation(1,1) = abs\left(\frac{2350000 - 2415000}{2415000}\right) * 100 = 2.7$$

Step 3: The above step is repeated for all the sub-layers and the result is summarized in Table A-4. The maximum deviation is 44.6% (Table A-4)

Step 4: Repeat Step 2 and 3 for m LE structures in DB2. There is only one LE structure in DB2 at this stage.

Step 5: The minimum deviation is 44.6% which is greater than 1%. Hence $E_n(2, z)$ is appended to DB2 (Table A-2). m= 1+1 = 2. Also, append $E_n(2, z)$ to DB3 with ID m (Table A-3).

Step 6: Step 2 to 5 is repeated for n (=10) LE structures in DB1 (Table A-1)

The LE structure $E_n(6, z)$ (i = 6)in the database DB1 has two representative LE structures (j = 2, 4) in DB2 with deviation less than 1%. Step 5 identifies the minimum deviation, 0.6% and identifies the LE structure $E_n(6, z)$ with ID of E_{DB} (4, z), i.e., 4 (Table A-3).

Table A-1 Sample Database DB1 Generated in Stage 3 of the Reliability Procedure

Layered Elastic Structure ID	Sub layer															
	1	2	3	4	5	6	7	8	9	10	11	12	13	14	15	16
1	2350000	2056000	1779000	1530000	1360000	1180000	53080	52680	43910	41670	40080	38890	8656	9831	14200	8352
2	2415000	2347000	2283000	2226000	2185000	2129000	42640	49320	43530	42250	40690	39500	8555	9672	14050	8338
3	2415000	2347000	2283000	2226000	2185000	2129000	42640	49320	43530	42250	40690	39500	8555	9672	14050	8338
4	2099000	1905000	1742000	1621000	1540000	1466000	42640	49320	43530	42250	40690	39500	8555	9672	14050	8338
5	2448000	2376000	2284000	2226000	2185000	2129000	42640	49320	43900	42500	41000	39820	8512	9599	13950	8338
6	2435000	2367000	2283000	2213000	2185000	2129000	42640	49320	43850	42490	40920	39820	8512	9599	13950	8338
7	2415000	2347000	2283000	2213000	2132000	2021000	53080	52680	50460	57040	42780	39820	8512	9599	13950	8338
8	2085000	1912000	1818000	1768000	1770000	1777000	42640	49320	50460	57040	42780	39820	8512	9599	13950	8338
9	2415000	2347000	2283000	2226000	2185000	2129000	53080	52680	43530	42250	38860	40660	8454	9483	13750	8323
10	2415000	2347000	2283000	2226000	2185000	2129000	53500	52680	43530	42250	38860	40660	8454	9483	13750	8323

Table A-2 Sample Database DB2 Generated in Stage 4 of the Reliability Procedure

Layered Elastic Structure ID	Sub layer															
	1	2	3	4	5	6	7	8	9	10	11	12	13	14	15	16
1	2350000	2056000	1779000	1530000	1360000	1180000	53080	52680	43910	41670	40080	38890	8656	9831	14200	8352
2	2415000	2347000	2283000	2226000	2185000	2129000	42640	49320	43530	42250	40690	39500	8555	9672	14050	8338
3	2099000	1905000	1742000	1621000	1540000	1466000	42640	49320	43530	42250	40690	39500	8555	9672	14050	8338
4	2448000	2376000	2284000	2226000	2185000	2129000	42640	49320	43900	42500	41000	39820	8512	9599	13950	8338
5	2415000	2347000	2283000	2213000	2132000	2021000	53080	52680	50460	57040	42780	39820	8512	9599	13950	8338
6	2085000	1912000	1818000	1768000	1770000	1777000	42640	49320	50460	57040	42780	39820	8512	9599	13950	8338
7	2415000	2347000	2283000	2226000	2185000	2129000	53080	52680	43530	42250	38860	40660	8454	9483	13750	8323

Table A-3 Sample Database DB3 Generated in Stage 4 of the Reliability Procedure

Layered Elastic Structure ID	Sub layer															
	1	2	3	4	5	6	7	8	9	10	11	12	13	14	15	16
1	2350000	2056000	1779000	1530000	1360000	1180000	53080	52680	43910	41670	40080	38890	8656	9831	14200	8352
2	2415000	2347000	2283000	2226000	2185000	2129000	42640	49320	43530	42250	40690	39500	8555	9672	14050	8338
2	2415000	2347000	2283000	2226000	2185000	2129000	42640	49320	43530	42250	40690	39500	8555	9672	14050	8338
3	2099000	1905000	1742000	1621000	1540000	1466000	42640	49320	43530	42250	40690	39500	8555	9672	14050	8338
4	2448000	2376000	2284000	2226000	2185000	2129000	42640	49320	43900	42500	41000	39820	8512	9599	13950	8338
4	2435000	2367000	2283000	2213000	2185000	2129000	42640	49320	43850	42490	40920	39820	8512	9599	13950	8338
5	2415000	2347000	2283000	2213000	2132000	2021000	53080	52680	50460	57040	42780	39820	8512	9599	13950	8338
6	2085000	1912000	1818000	1768000	1770000	1777000	42640	49320	50460	57040	42780	39820	8512	9599	13950	8338
7	2415000	2347000	2283000	2226000	2185000	2129000	53080	52680	43530	42250	38860	40660	8454	9483	13750	8323
7	2415000	2347000	2283000	2226000	2185000	2129000	53500	52680	43530	42250	38860	40660	8454	9483	13750	8323

Table A-4 Deviation from the Representative Layered Elastic Structure

	Deviation between corresponding sub-layer modulus																Maximum Deviation
	1	2	3	4	5	6	7	8	9	10	11	12	13	14	15	16	
Check DB1-ID 2																	
With DB2-ID 1	2.7	12.4	22.1	31.3	37.8	44.6	24.5	6.8	0.9	1.4	1.5	1.5	1.2	1.6	1.1	0.2	**44.6**
Check DB1-ID 3																	
With DB2-ID 1	2.7	12.4	22.1	31.3	37.8	44.6	24.5	6.8	0.9	1.4	1.5	1.5	1.2	1.6	1.1	0.2	**44.6**
With DB2-ID 2	0.0	0.0	0.0	0.0	0.0	0.0	0.0	0.0	0.0	0.0	0.0	0.0	0.0	0.0	0.0	0.0	**0.0**
Check DB1-ID 4																	
With DB2-ID 1	12.0	7.9	2.1	5.6	11.7	19.5	24.5	6.8	0.9	1.4	1.5	1.5	1.2	1.6	1.1	0.2	**24.5**
With DB2-ID 2	15.1	23.2	31.1	37.3	41.9	45.2	0.0	0.0	0.0	0.0	0.0	0.0	0.0	0.0	0.0	0.0	**45.2**
Check DB1-ID 5																	
With DB2-ID 1	4.0	13.5	22.1	31.3	37.8	44.6	24.5	6.8	0.0	2.0	2.2	2.3	1.7	2.4	1.8	0.2	**44.6**
With DB2-ID 2	1.3	1.2	0.0	0.0	0.0	0.0	0.0	0.0	0.8	0.6	0.8	0.8	0.5	0.8	0.7	0.0	**1.3**
With DB2-ID 3	14.3	19.8	23.7	27.2	29.5	31.1	0.0	0.0	0.8	0.6	0.8	0.8	0.5	0.8	0.7	0.0	**31.1**
Check DB1-ID 6																	
With DB2-ID 1	3.5	13.1	22.1	30.9	37.8	44.6	24.5	6.8	0.1	1.9	2.1	2.3	1.7	2.4	1.8	0.2	**44.6**
With DB2-ID 2	0.8	0.8	0.0	0.6	0.0	0.0	0.0	0.0	0.7	0.6	0.6	0.8	0.5	0.8	0.7	0.0	**0.8**
With DB2-ID 3	13.8	19.5	23.7	26.8	29.5	31.1	0.0	0.0	0.7	0.6	0.6	0.8	0.5	0.8	0.7	0.0	**31.1**
With DB2-ID 4	0.5	0.4	0.0	0.6	0.0	0.0	0.0	0.0	0.1	0.0	0.2	0.0	0.0	0.0	0.0	0.0	**0.6**
Check DB1-ID 7																	
With DB2-ID 1	2.7	12.4	22.1	30.9	36.2	41.6	0.0	0.0	13.0	26.9	6.3	2.3	1.7	2.4	1.8	0.2	**41.6**
With DB2-ID 2	0.0	0.0	0.0	0.6	2.5	5.3	19.7	6.4	13.7	25.9	4.9	0.8	0.5	0.8	0.7	0.0	**25.9**
With DB2-ID 3	13.1	18.8	23.7	26.8	27.8	27.5	19.7	6.4	13.7	25.9	4.9	0.8	0.5	0.8	0.7	0.0	**27.8**
With DB2-ID 4	1.4	1.2	0.0	0.6	2.5	5.3	19.7	6.4	13.0	25.5	4.2	0.0	0.0	0.0	0.0	0.0	**25.5**

Check DB1-ID 8																	
With DB2-ID 1	12.7	7.5	2.1	13.5	23.2	33.6	24.5	6.8	13.0	26.9	6.3	2.3	1.7	2.4	1.8	0.2	**33.6**
With DB2-ID 2	15.8	22.8	25.6	25.9	23.4	19.8	0.0	0.0	13.7	25.9	4.9	0.8	0.5	0.8	0.7	0.0	**25.9**
With DB2-ID 3	0.7	0.4	4.2	8.3	13.0	17.5	0.0	0.0	13.7	25.9	4.9	0.8	0.5	0.8	0.7	0.0	**25.9**
With DB2-ID 4	17.4	24.3	25.6	25.9	23.4	19.8	0.0	0.0	13.0	25.5	4.2	0.0	0.0	0.0	0.0	0.0	**25.9**
With DB2-ID 5	15.8	22.8	25.6	25.2	20.5	13.7	24.5	6.8	0.0	0.0	0.0	0.0	0.0	0.0	0.0	0.0	**25.6**
Check DB1-ID 9																	
With DB2-ID 1	2.7	12.4	22.1	31.3	37.8	44.6	0.0	0.0	0.9	1.4	3.1	4.4	2.4	3.7	3.3	0.3	**44.6**
With DB2-ID 2	0.0	0.0	0.0	0.0	0.0	0.0	19.7	6.4	0.0	0.0	4.7	2.9	1.2	2.0	2.2	0.2	**19.7**
With DB2-ID 3	13.1	18.8	23.7	27.2	29.5	31.1	19.7	6.4	0.0	0.0	4.7	2.9	1.2	2.0	2.2	0.2	**31.1**
With DB2-ID 4	1.4	1.2	0.0	0.0	0.0	0.0	19.7	6.4	0.8	0.6	5.5	2.1	0.7	1.2	1.5	0.2	**19.7**
With DB2-ID 5	0.0	0.0	0.0	0.6	2.4	5.1	0.0	0.0	15.9	35.0	10.1	2.1	0.7	1.2	1.5	0.2	**35.0**
With DB2-ID 6	13.7	18.5	20.4	20.6	19.0	16.5	19.7	6.4	15.9	35.0	10.1	2.1	0.7	1.2	1.5	0.2	**35.0**
Check DB1-ID 10																	
With DB2-ID 1	2.7	12.4	22.1	31.3	37.8	44.6	0.8	0.0	0.9	1.4	3.1	4.4	2.4	3.7	3.3	0.3	**44.6**
With DB2-ID 2	0.0	0.0	0.0	0.0	0.0	0.0	20.3	6.4	0.0	0.0	4.7	2.9	1.2	2.0	2.2	0.2	**20.3**
With DB2-ID 3	13.1	18.8	23.7	27.2	29.5	31.1	20.3	6.4	0.0	0.0	4.7	2.9	1.2	2.0	2.2	0.2	**31.1**
With DB2-ID 4	1.4	1.2	0.0	0.0	0.0	0.0	20.3	6.4	0.8	0.6	5.5	2.1	0.7	1.2	1.5	0.2	**20.3**
With DB2-ID 5	0.0	0.0	0.0	0.6	2.4	5.1	0.8	0.0	15.9	35.0	10.1	2.1	0.7	1.2	1.5	0.2	**35.0**
With DB2-ID 6	13.7	18.5	20.4	20.6	19.0	16.5	20.3	6.4	15.9	35.0	10.1	2.1	0.7	1.2	1.5	0.2	**35.0**
With DB2-ID 7	0.0	0.0	0.0	0.0	0.0	0.0	0.8	0.0	0.0	0.0	0.0	0.0	0.0	0.0	0.0	0.0	**0.8**

APPENDIX B

RANK ORDER CORRELATION METHOD

This appendix shows a sample computation procedure for 'Rank order correlation' that is used in the generation of Tornado plots. In this example, the sensitivity of the HMA air void content on rutting is computed through correlation coefficient. A sample of 20 air void values used in the simulation is shown in Table B.1. The corresponding rutting predicted in HMA layer by the design procedure is also summarized. The rank of air void and rutting (relative position of the value) is determined based on the 20 simulated values. The difference in ranks is computed for 20 simulations (Table B.1)

Spearman's rank order correlation coefficient is calculated using Equation 5.1 as

$$r = 1 - \left(\frac{6\sum (\Delta R)^2}{n\left(n^2 - 1\right)} \right) = 1 - \left(\frac{6 * 169}{20\left(20^2 - 1\right)} \right) = 0.8729$$

Based on the 20 simulation, air void content in HMA layer has positive correlation of 0.8729 with HMA rutting. A high positive correlation implies the necessity of quality control over mix air void content to avert high degree of HMA rutting.

Table B. 1 Spearman's Rank Order Correlation

No	Air Void, %	HMA Rutting, Inch	Rank of Air Void (R_1)	Rank of HMA Rutting (R_2)	Difference in Ranks $\Delta R^2 = (R_1-R_2)^2$
1	6.5	0.5952	12	12	0
2	8	0.6570	20	18	4
3	5.55	0.5498	5	4	1
4	6.5	0.5744	12	10	4
5	6.37	0.6173	11	13	4
6	7.62	0.6379	18	17	1
7	6.29	0.5589	10	6	16
8	7.49	0.6175	17	14	9
9	5.23	0.5599	2	7	25
10	5.31	0.5243	3	3	0
11	6.17	0.6175	8	14	36
12	7.84	0.6705	19	20	1
13	6.54	0.6268	14	16	4
14	6.11	0.5617	7	8	1
15	5.11	0.4736	1	1	0
16	7.06	0.5746	16	11	25
17	6.18	0.5499	9	5	16
18	5.4	0.5069	4	2	4
19	6.9	0.6570	15	18	9
20	6.01	0.5743	6	9	9
				Sum of Difference	169